TISSUE REGENERATION IN COMPOSITE INJURY MODELS OF LIMB TRAUMA

A Dissertation
Presented to
The Academic Faculty

by

Brent A. Uhrig

In Partial Fulfillment
of the Requirements for the Degree
Doctor of Philosophy in Bioengineering

Georgia Institute of Technology
August 2013

TISSUE REGENERATION IN COMPOSITE INJURY MODELS OF LIMB TRAUMA

Approved by:

Dr. Robert E. Guldberg, Advisor
School of Mechanical Engineering
Georgia Institute of Technology

Dr. W. Robert Taylor
School of Medicine
Emory University

Dr. Ravi V. Bellamkonda
Department of Biomedical Engineering
Georgia Institute of Technology

Dr. Johnna S. Temenoff
Department of Biomedical Engineering
Georgia Institute of Technology

Dr. Shawn R. Gilbert
School of Medicine
University of Alabama at Birmingham

Date Approved: June 17, 2013

To my family

ACKNOWLEDGEMENTS

When I reflect on the last five years and the decisions that led me to pursue this Ph.D. in the first place, I cannot with the benefits of hindsight say that I would absolutely travel the same path. That said, I cannot say for sure that I would do things differently, either. Regardless, this process has been an incredible learning experience. I learned a lot about myself; I learned a lot about friendships and relationships; I somehow managed to learn things about my wonderful family that I hadn't in the 24 years prior to coming to Atlanta. I even learned a bit about scientific research along the way.

I want to gratefully acknowledge anyone and everyone who assisted me in this journey, no matter how small the contribution. I cannot even begin to enumerate all the names, but my sincerest thanks are extended to every individual who in some way helped propel me to the completion of this degree.

First and foremost, I need to thank my thesis advisor, Dr. Robert E. Guldberg. I came to Georgia Tech with every intention of working for Bob, and told him as much when I arrived on campus in the fall of 2008. Thankfully, he saw enough potential in me to take me on despite the fact that I had not really even thought about a cell since high school freshman biology. He then stuck with me through that first year when on any number of days he could have taken a look at the obnoxious neck-beard I insisted on growing, silently shook his head, and decided that this just wasn't going to work out. The growth I have experienced as a researcher since first joining the lab is due in no small part to Bob. He was a calm, thoughtful mentor who provided a constant steadying force while I did my best to navigate the ups and downs of doctoral research; on more

than one occasion, he probably believed in me and my work more than I did myself. His ability to give insightful, critical analysis without crossing the boundary to personal criticism was a key to keeping my project moving forward on more than one occasion. Now, as my time in the lab draws to a close, Bob has been incredibly supportive and proactive in trying to help me with career development, even as I struggle to figure out what exactly I want that next step to be. Finally, there has never been a question as to whether Bob cares about my personal well-being, not just my productivity as a student, and for that I am truly grateful.

I also wish to thank each of my committee members for their essential roles in this project. Dr. Taylor gave valuable input on the project, especially aspects related to vascular growth, and reinforced the importance of precise word choice for explaining my rationale and results. Dr Bellamkonda was an important collaborator on the bone and nerve model, and made sure I always kept the big picture questions in mind. Dr. Temenoff challenged me to always be clear about the specific scientific question I was trying to address. Dr. Gilbert provided unique perspective and useful input from an orthopaedic clinician who also values and participates in basic science research. All of these individuals were generous with their time and expertise despite their incredibly demanding schedules. Through their insightful comments and probing questions, both this project and my abilities as a researcher were able to achieve potential they otherwise would not have.

In some form or fashion, all of the educators I've encountered throughout my life contributed to this degree. For a professional group that never really receives their

deserved credit, I offer my deepest gratitude here. Especially in (the incredibly unlikely) case any of them stumble across this document one day.

This work certainly would not have been possible without the contributions, past and present, of my fellow Guldberg lab members. No one truly enjoys days spent in the OR suite, but they do have a funny way of building bonds and instilling a collaborative spirit with the group in a way few other things can. Also, ORS conferences will likely be some of the best "work" trips I ever take, due in large part to my tremendous labmates. Hazel Stevens and Angela Lin deserve special recognition for everything they do for the lab. If either is ever in need of a reminder of just how important they are to the group, I will be more than happy to send heaps of praise their way. Hazel does a tremendous job keeping the lab running smoothly, was instrumental in the latter aspects of my project, and her wit is one-of-a-kind. Conversations with her were one of the little joys of day-to-day lab work. I still hold out hope that her claim to not enjoy Queen or The Rolling Stones is some sort of cruel jape. Angela is one of the world experts on micro-CT and provided immeasurable technical help at numerous points in my project. I have a suspicion that she may not have been my biggest fan in the early days, but I now count her amongst my closest friends. Fry parties, lobster boils, Candlerwood/Cabbagewood races, and Bourbon Street are among the many Angela related memories I will cherish. She is also the reason I will always remember that "winter is coming" and "the enemy's gate is down." Vivian Johnson deserves thanks for always managing to squeeze me into Bob's schedule on short notice and never seeming remotely annoyed by my requests. I need to thank Ken Dupont and Yash Kolambkar for all the help they provided when they were on the way out the door and I was just arriving, as much of their work paved the

way for my own. I have no doubt there were numerous times when they were annoyed with my nagging questions, but were always generous with their time and advice, and remain so to this day. Joel Boerckel was perhaps the labmate most essential to my project, providing enormous help for 3 solid years, and I enjoyed the reciprocal assistant roles we each took in the other's work. Joel possesses a great mind for research, and was always eager to make conversation on anything from science to bicycles to life in general. Nick Willett has been a tremendous asset to the lab and picked up where Joel left off by providing significant contribution to the latter parts of this project. Nick was incredibly generous with his time and very supportive of me as a researcher and an individual, for which I am incredibly grateful. Also, if ever in the need of travel companions for a two week jaunt through central Europe, he and his bride-to-be, Amber Hudson, are top notch. Chris Dosier … where does one even begin? Chris is undoubtedly one of the smartest people I know and also one of the most unique. His ability to deliver sound scientific input in the most non-PC way possible is likely unmatched (as is his ability to apply Top Gun quotes to any real life situation – sorry, Dave). His sense of humor also ensured that every day at work was different from the last. Jason Wang has been with me all 5 years in the lab, and provided good company for many of the long hours in the CT room. Jessica O'Neal Green and Mela Johnson Carroll were great labmates in my early years, and even better kickball teammates. Alice Li has been a terrific co-investigator in the composite injury research group, and I have all the confidence in the world in her as the torch bearer of that group going forward. Tanu Thote and Lauren Priddy have been excellent additions to the lab and were solid back row officemates who made sure that I removed my headphones and engaged my

neighbors in conversation at least a couple times each day (until I moved to the office and resumed my hermit ways). Laxmi Krishnan, David Reece, and Marian Hettiaratchi have always been willing to help with surgeries, and contributed thought-provoking questions and useful input on my research. Tamim Diab, Liqin Xie, Taran Lundgren, Shamus (SHAMUS!!) Moran, Yazdan Raji, and Chelsea Fechter also deserve thanks for the assistance they provided in various aspects of this project. The future of the lab also appears to be in very capable hands with Brennan Torstrick, Albert Cheng, and Giuliana Salazar-Noratto. Again, my absolute sincerest thanks to all of my fellow Guldbergers for making this Ph.D. possible. I wish every one of you absolutely nothing but the best in all of your future endeavors, which undoubtedly will be enormously successful.

One final labmate acknowledgement is in order, but will fall woefully short on these pages. I cannot even begin to express how truly amazing and special Ashley Allen is, or adequately thank her for her consistently positive disposition, devoted friendship, the love and support she provided me, and all of the countless ways she bettered my world, so I won't embarrass either one of us in attempting to do so.

My wing 2D/lair colleagues deserve many thanks as well for contributing useful scientific discussion, encouraging useful non-scientific discussion, commiserating when experiments had utterly failed, and in general, just promoting a terrific work environment. I also owe an incredible amount of gratitude to Dr. Laura O'Farrell, Kim Benjamin, and the PRL staff. Dr. O'Farrell provided essential input at several points of my project and training in many areas vital to its completion. The PRL staff is such an important part of the IBB in facilitating the *in vivo* work done and making our jobs as researchers infinitely easier. I want to also thank the IBB staff, including Aqua Asberry,

Floyd Wood, James Godard, Alyceson Andrews, Karen Cannon, Allen Echols, and Meg McDevitt, all of whom provided great help to me at one point or another.

Two research collaborators deserve specific recognition for their technical contributions to this thesis – Isaac Clements and Natalia Landázuri. Isaac was essential for the experimental execution of all things neuro, and without Natalia's expertise, adaptation of the ischemia surgery technique would have been much more difficult and time consuming.

Lest I give the impression that my time at Georgia Tech was all work and no play, I also developed some phenomenal friendships that will continue to endure long after my time here is done. Dave Dumbauld and Kelly Erby Dumbauld are exceptional people and hands down two of the greatest friends I will ever know. In many ways, I was practically their full-grown child – they fed me, planned my weekend activities, took me to visit grandparents, and ultimately, ushered me through some of the darkest days I've known. This all despite the fact that on more than one occasion I was invited over for social football watching, only to sit in the back of the room watching a different game with headphones on [insert guilty face here]. So many of my favorite Atlanta memories are Dumbauld-related, and I look forward to all Larryville ones yet to come. Vince Fiore and Alison Douglas filled in admirably following Dave and Kelly's departure from 8th & Argonne. Vince and I have been fast friends since I came to his rescue on the BBUGS rafting trip our first month in Atlanta. Vince's dedication to his research is truly admirable, his passion for living-it-up infectious, and his support of me unwavering. Alison is quick to offer libations, eager to extend invitations, and always a willing listener; she has been a terrific influence on Vince, and a great friend to me. Jeremy Lim

is an incredibly dedicated friend, whom I could count on for anything from grabbing a beer, to hashing out personal issues, performing *a cappela* Beastie Boys karaoke, or just playing catch in the park. A constant companion at sporting events, even the biggest gaffe during our friendship (miles of unnecessary walking on and around the Auburn University campus) produced a memorable moment – the round mound of rebound, Sir Charles! Ted Lee is a truly unique individual who possesses a terrific mind for science, a remarkable knack for befriending nearly anyone and everyone, and a *modus operandi* of letting the good times roll (bottles in the club). Were motivating happy hour excursions at all analogous to Voltron assembly, Ted would undoubtedly be the head. Although unbeknownst to me, I nearly sabotaged my friendship with the wonderful Kate Wilson before it even began. Thankfully, when afforded a second chance, I found a great friend in the teleworker extraordinaire/board game aficionado who truly excels at pointed discussion of "feelings" and the art of giving hugs. Not to be forgotten is the Murray Hill crew of Scott Robinson and Rich Carpenedo (and all affiliated parties). Rich, long lost to the Great White North, taught me about cycling in Atlanta and about drinking in Atlanta … and then how to successfully pair the two. Scrob is an unrivaled story teller, who introduced me to the glories of Patak cured meats, tank tops, and the refined pairing of scotch, steak, and bad sci-fi movies. Sean Coyer and Shetal Shah brought The Blue Frog into my life (uh, thanks for that, I guess), and I was incredibly honored to be present for their nuptials, an event so impressive and entertaining that it will forever temper my expectations when attending future weddings. Ed Phelps and Devon Headen are all around good dudes, and continuously humble me in research and cycling capabilities, respectively. Tim Petrie befriended me early on, and brought me into the BBUGS

intramural sports fold, where I developed friendships with Andrés Bratt-Leal, JP Rabbah, Jay Sy, Matt Magnusson, Nathan Hotaling, Randy Ankeny, Chris Edens, and Eric Ping. Other folks who contributed to good times in Atlanta include Chris Lee, Katie Pitz, Song Seto, Jonathan Suever, Jen Lei, Ian Campbell, Cindy Bower, Julia Henkels, and Mel Li.

I need to also thank my non-Atlanta friends for the roles they have played in getting me to this point. Specifically, The Roo – Neil, DB, Tim, Ferrel, Matt, Ross, RJ, Dan, and Jeff – for being the greatest, funniest, most unique group of friends I could ask for. Several of them have been my closest friends for over half of my 29 years, and I consider them brothers in every sense of the word. There was many a day that the Roo thread boosted my spirits when research was trying its best to keep me down. It's been an absolute pleasure to have them all along on this ride. My close friend Zack Rabold deserves thanks for all the support, encouragement, and advice he has provided for many years. Though our friendship took a tortuous path at times, the two of us share innumerable fond memories, and Zack has long believed in my ability to achieve great things (in short, he might say "I been knowin'").

My family deserves more thanks than I could ever convey here. Absolutely none of this would have been possible without my incredible parents: Earlene Uhrig and Rod Uhrig. They are two of the strongest people I will ever meet and are walking, talking examples of persevering through adversity. They have taught me so, so much, and continue to do so on a weekly basis. The value of hard work; to always give my best effort; to believe in myself; to passionately live my life and pursue my dreams; to be steadfast in my convictions; to be curious but practice patience; to treat people with integrity and respect; to be kind and compassionate; and perhaps above all else, to remain

loyal, honest, and keep my word. My Grandma Stuart also deserves special thanks for the immeasurable impact she has had on my life. She is far and away one of the most inspirational and loving people I will ever know. I consider her one of the greatest blessings I will ever receive. My aunts, uncles, cousins, etc. provided continuous love and support throughout this endeavor, and served up constant reminders to continuously refine my ability to talk about research with people from outside of the field. These individuals molded me into the man I am today. I strive to do my best every single day to make them all proud.

Finally, endless thanks go to my brother, Brian, for being my absolute best friend in this world and unequivocally the greatest sibling anyone could ever hope for. We have partnered on an incredible journey that began 29 years ago when sharing a womb, with many a moment of pure, unbridled happiness, but certainly our fair share of trials and tribulations. Through broken noses and broken bones, broken spirits and broken hearts, we've endured together. I know that no matter what the circumstance, when all the chips are down, there is, at minimum, one person in this world who will always, always be in my corner. Thank you, bro. I can't imagine doing this thing called life without you.

TABLE OF CONTENTS

LIST OF TABLES

LIST OF FIGURES

LIST OF SYMBOLS AND ABBREVIATIONS

2D	two dimensional
3D	three dimensional
ANG	angiopoietin
ACTA2 (SMAA)	smooth muscle alpha-actin
ANOVA	analysis of variance
BD	bone defect
BDNF	brain-derived neurotrophic factor
BMP	bone morphogenetic protein
cDNA	complementary deoxyribonucleic acid
CGRP	calcitonin gene-related peptide
CNAP	compound nerve action potential
CNS	central nervous system
CSF	colony stimulating factor
COL1A1	collagen, type 1, alpha 1
ECM	extracellular matrix
FGF	fibroblast growth factor
FGFR	fibroblast growth factor receptor
H&E	hematoxylin & eosin
HIF	hypoxia-inducible transcription factor
HLI	hind limb ischemia
IGF	insulin-like growth factor
IL	interleukin
LDPI	laser Doppler perfusion imaging

MCP-1 (CCL-2)	monocyte chemotactic protein-1
pMOI	polar moment of inertia
Micro-CT	microcomputed tomography
MMP	matrix metalloproteinase
mRNA	messenger ribonucleic acid
NGF	nerve growth factor
OPN	osteopontin
OSX	osterix
PCL	poly(ε-caprolactone)
PDGF	platelet derived growth factor
PNS	peripheral nervous system
qRT-PCR	real-time reverse transcription polymerase chain reaction
RANKL	receptor activator of nuclear factor kappa-B ligand
rhBMP-2	recombinant human bone morphogenetic protein-2
ROI	region of interest
RUNX2	runt-related transcription factor 2
SEM	standard error of the mean
SMC	smooth muscle cell
TE/RM	tissue engineering/regenerative medicine
TGF-β	transforming growth factor beta
TNF-α	tumor necrosis factor alpha
VEGF	vascular endothelial growth factor
VEGFR	vascular endothelia growth factor receptor
VOI	volume of interest

SUMMARY

Severe extremity trauma often involves significant damage to multiple tissue types, including bones, skeletal muscles, peripheral nerves, and blood vessels. Such injuries present unique challenges for reconstruction, and improving structural and functional outcomes of intervention remains a pressing, unmet clinical need. While tissue engineering/regenerative medicine (TE/RM) therapeutics offer promising potential to overcome the status quo limitations of surgical reconstruction, very few products have transitioned to clinical practice. Improving treatment options will likely require advancing our understanding of the biological interactions occurring in the repair of damaged tissues.

Bone tissue is known to be innervated and highly vascularized, and both tissue types are involved in normal bone physiology. However, the degree to which these tissue relationships influence the repair of large, multi-tissue defects remains unknown. Accordingly, the goal of this thesis was to investigate tissue regeneration in two novel composite injury models. First, we characterized interactions in a composite bone and nerve injury model where a segmental bone defect was combined with a peripheral nerve gap. Our results indicated that although tissue regeneration was not impaired, the composite injury group experienced a marked functional deficit in the operated limb compared to single-tissue injury. Second, we developed a model of composite bone and vascular extremity trauma by combining a critically-sized segmental bone defect with surgically-induced hind limb ischemia to evaluate the effects on BMP-2-mediated bone repair. Interestingly, our results demonstrated a stimulatory effect of the recovery

response to ischemia on bone regeneration. Finally, we investigated early vascular growth and gene expression as potential mechanisms coupling the response to ischemia with bone defect repair. Although the response to ischemia promoted robust vascular growth in the thigh, it did not directly augment vascularization at the site of bone regeneration. In addition, the stimulatory effects of ischemia on bone regeneration could not be explained by gene expression alone based on the genes and time points investigated.

Taken together, this thesis presents pioneering work on a new thrust of TE/RM research – tissue regeneration in models of composite injury. This work has provided new insights on the complexity of composite tissue repair, specifically in regard to the relationship between vascular tissue growth and bone healing. Going forward, successful leverage of models of composite tissue injuries will provide valuable test beds for screening new technologies, advance the understanding of tissue repair biology, and ultimately, may produce new therapeutic interventions for limb salvage and reconstruction that improve outcomes for extremity trauma patients.

CHAPTER 1

SPECIFIC AIMS

Introduction

Severe extremity trauma resulting in significant injury to multiple tissues, including bone, skeletal muscle, nerve, and vasculature, presents a multitude of clinical challenges that often cannot be managed with conventional reconstruction techniques. Furthermore, due to the complex nature of these injuries, a lack of consensus exists for surgical intervention strategies (Yazar *et al.*, 2004; DeFranco and Lawton, 2006; Nauth *et al.*, 2011). Multi-stage treatment is routinely required in these cases, and patients are often encumbered with diminished long-term function even if limb salvage and reconstruction are successful (Bosse *et al.*, 2002; MacKenzie *et al.*, 2005).

Autologous tissue grafting remains the clinical gold standard for many tissue defect reconstruction procedures, including those for large bone defects, peripheral nerve gaps, and blood vessel repair. In nearly all cases, these procedures face limitations due to the volume of tissue available for grafting and the associated morbidity at the donor site. The field of tissue engineering and regenerative medicine (TE/RM) has emerged with potential strategies to overcome the unmet clinical needs of reconstruction, but to date, few products are commercially available. Considerable investigation is ongoing in tissue engineering and regenerative medicine therapeutics to improve reconstruction outcomes; however, the vast majority of musculoskeletal trauma models employed for testing therapeutics consist of single-tissue defects. Such models have an undeniable place as TE/RM research tools, but possess only limited utility for investigating therapeutic

strategies for the repair of large, multi-tissue defects. Furthermore, they offer little potential for insight into endogenous interactions between healing tissues.

Bone tissue is known to be innervated and highly vascularized, and both tissue types are involved in physiological bone processes. Neuronal regulatory pathways have been implicated in fracture healing and also in homeostatic metabolism. Additionally, bone repair is known to be tightly coupled to angiogenesis, and local blood supply is essential to maintain viable bone tissue. However, the degree to which these tissue relationships influence the repair of large, multi-tissue defects remains unknown. Accordingly, the *overall objective* of this project was to develop two novel composite injury models of limb trauma and investigate the effects of composite injury on tissue regeneration. This was done in support of the *long-term goal* of improved engineering of TE/RM therapeutics by advancing our understanding of interactions in composite tissue repair. The *central hypothesis* of this work was that composite tissue trauma results in perturbed healing responses with effects on tissue regeneration and functional restoration. We approached this objective through the following specific aims:

Specific Aim I

Develop a composite limb injury model of severe bone and peripheral nerve trauma and assess the effects of concomitant injury on bone and nerve regeneration.

Extremity trauma resulting in extensive skeletal damage often involves injury to surrounding tissues including peripheral nerves. Our working hypothesis was that composite injury affects bone regeneration and limb function compared to bone injury alone. To test this hypothesis, we developed a rat model of composite lower limb bone and nerve injury featuring quantitative functional outcome measures. The composite

injury model consisted of an 8 mm mid-femoral bone defect and a 14 mm sciatic nerve gap, both of which have been demonstrated to be critically-sized, and single-injury groups were used for comparison. We characterized the healing response in the composite injury model to biomaterials-based therapeutics previously demonstrated to show promise in well-established, single-tissue injury models. Quantitative outcome measures were used to assess both bone regeneration and peripheral nerve regeneration, as well as overall limb function. Secondarily, we studied morphology and mechanical properties of ipsilateral and contralateral femora to test the hypothesis that the nerve injury induces an adaptive response in intact femora. The results of this aim are discussed in Chapter 3.

Specific Aim II

Evaluate the effects of hind limb ischemia on rhBMP-2-mediated segmental bone defect repair in a composite injury model of severe lower limb bone and vascular trauma.

Bone repair is known to be tightly coupled to angiogenesis, and concomitant vascular insults present clinical complications for fracture and bone defect healing. Based on reported clinical and experimental observations on the importance of vascular networks in bone repair, we hypothesized that concomitant hind limb ischemia impairs bone regeneration compared to bone injury alone. To test this hypothesis, we developed a rat model of composite lower limb bone and vascular trauma to discern how hind limb ischemia affects the BMP-2-mediated segmental bone defect repair process. The composite injury model consisted of a critically-sized 8 mm mid-femoral bone defect in combination with surgical excision of the femoral artery and vein. Bone repair was

investigated at both bridging and non-bridging doses of rhBMP-2. Traditional radiography, micro-CT, and histology techniques were used to evaluate bone healing, and mechanical testing was used to assess functional restoration. Quantitative, anatomical evaluation of vascular tissue networks was performed using contrast-enhanced micro-CT angiography. The outcomes of this aim are discussed in Chapter 4.

Specific Aim III

Determine the effects of hind limb ischemia on early vascular growth and gene expression in rhBMP-2-mediated segmental bone defect repair.

Early vascular network growth and biological signaling cascades are critical in the process of bone repair. Our working hypothesis was that the injury response to hind limb ischemia produces changes in early vascular tissue growth and/or gene expression compared to bone injury alone. Such changes might help to explain the enhanced bone regeneration response observed in Aim II. Histology provided qualitative assessment of early bone regeneration and vascular growth. Changes in blood flow were assessed using laser Doppler perfusion imaging and contrast-enhanced micro-CT angiography was used for quantitative evaluation of vascular morphology. Comparison of gene expression was performed in both the defect region and adductor muscle tissue using quantitative real-time reverse transcription polymerase chain reaction (qRT-PCR). The outcomes of this aim are discussed in Chapter 5.

Significance

Extremity trauma remains the predominant combat casualty for U.S. armed forces members in ongoing military conflicts, a continuation of historical trends. Explosive

munitions are the primary mechanism for these injuries (Owens *et al.*, 2007; Owens *et al.*, 2008), resulting in penetrating blast wounds with large zones of injury that encompass multiple tissue types, and, notably, a high incidence of bone and soft tissue trauma (Owens *et al.*, 2007). High-energy trauma incidents, such as motor vehicle collisions, produce an additional civilian patient population. Although passenger survival in these incidents has increased with improved engineering of safety features, severe extremity trauma remains common (Burgess *et al.*, 1995; Richter *et al.*, 2005).

A variety of potential therapeutic strategies to circumvent the status quo reconstruction limitations are under investigation throughout the field of tissue engineering and regenerative medicine. However, current animal models of musculoskeletal trauma used in evaluating emerging technologies typically consist of critically-sized, single-tissue defects. Such models are vital research tools, but possess only limited utility for investigating therapeutic strategies for multi-tissue repair and offer little potential for insight into endogenous interactions in healing tissues. Developing effective TE/RM therapies and successful translation to clinical practice will first require establishing rigorous, well-characterized pre-clinical models with quantitative outcome measures of functional restoration to use as test beds for evaluating emerging technologies. Accordingly, there exists a need for challenging animal models of composite tissue injury.

The work described herein is *significant* because it presents the pioneering research on a platform of small animal test-bed models of composite limb injury which will provide a foundation for benchmarking new technologies. Additionally, it has advanced our understanding of endogenous interactions that occur during repair of bone

& nerve or bone & vascular injuries. Specifically, this work has suggested additional complexity to the coupling of bone repair with vascular growth/remodeling. Ultimately, elucidating such interactions is a critical step toward better management of extremity trauma patients in the present, and will open the door for future development of novel therapeutics designed to leverage combinatorial or synergistic tissue repair and regeneration to achieve better functional outcomes for patients.

CHAPTER 2

LITERATURE REVIEW

Bone Structure and Development

Bone is unique in many ways, not the least of which is that it is both a tissue and an organ. Bones provide a multitude of physiological functions that include protection of internal organs, providing a support structure that allows for locomotion, serving as a homeostatic mineral repository, and housing the activities of hematopoiesis. At an anatomical level, bones are often classified as long bones, short bones, or flat bones. Long bones, such as the femur, are the most relevant to this thesis, and are often divided into three anatomical sections base on their geometry and the type of bone structure present: diaphysis, methaphysis, and epiphysis. The diaphysis is the tube-shaped shaft of long bones composed primarily of cortical (compact) bone. The epiphysis is located at the ends of long bones, and the metaphysis is located between the diaphysis and epiphysis. The growth plate (physis) provides a physical boundary between the metaphysis and epiphysis. Both the metaphysis and epiphysis are composed primarily of trabecular (cancellous) bone with a thin shell of cortical bone. At a structural level, cortical and trabecular bone have distinct differences. Cortical bone is densely organized with very little macroscopic spaces (less than 10% porosity), whereas trabecular bone is organized as a network of interconnecting plates and rods with considerable macroscopic voids (30-90% porosity). These structural dissimilarities allow for specialized homeostatic and mechanical functions (Miller *et al.*, 2007).

Regardless of the structure presented, bone tissue has the same compositional constituents: bone matrix and bone cells. Bone matrix is the primary component of bone

tissue and is comprised of inorganic mineral (60-70% of the tissue) and organic matrix material (20-25% of the tissue). The inorganic mineral is primarily in the form of hydroxyapatite, a calcium phosphate apatite with molecular composition $Ca_{10}(PO_4)_6(OH)_2$. The organic matrix component is predominantly Type I collagen (~90%), with noncollagenous proteins (such as osteopontin, osteocalcin, bone sialoprotein, etc.) and proteoglycans making up the remainder. Bone matrix also contains a small amount of embedded growth factors inclusive of, but not limited to, members of the BMP, TGF-β, IGF, and FGF families. Three primary cell types make up the cellular constituent of bone tissue: osteblasts, osteoclasts, and osteocytes. Osteoblasts are bone forming cells responsible for laying down new matrix, whereas osteoclasts are bone resorbing cells. Osteoblast and osteoclast activity is reciprocally coupled in the regulatory process of bone remodeling. Osteocytes are the most common cell type in bone tissue, and are derived from terminally differentiated osteoblasts that became embedded in the bone matrix. Osteocytes reside in the lacunae of bone tissue and each possess numerous cell processes that extend outward in the canaliculi where they connect with neighboring osteocytes at gap junctions. The primary function of osteocytes is thought to be intercellular signaling for homeostatic bone maintenance and adaptation (Miller *et al.*, 2007).

Developmental skeletogenesis occurs through two distinct physiological pathways termed endochondral and intramembranous ossification. Endochondral bone formation is the primary developmental pathway for long bones and consists of a cartilaginous skeletal anlage that is subsequently remodeled and replaced by bone in a process coupled to angiogenic blood vessel invasion (Gerber *et al.*, 1999). Intramembranous bone

formation is the common developmental process for flat bones of the skeleton. In contrast to endochondral ossification, intramembranous bone formation does not proceed through a cartilage intermediate, instead resulting from the direct differentiation of mesenchymal progenitor cell condensations to osteoblasts.

Irrespective of the developmental pathway, the resulting bone tissue is primary woven bone. This initial tissue has no clear collagen or mineral organization, and is subsequently removed and replaced by highly organized llamelar (secondary) bone in the bone remodeling process. Woven bone is formed more rapidly, and is less mineralized than its lamellar counterpart, likely to allow for easier remodeling. While lamellar bone is formed more slowly, the organizational structure provides the necessary mechanical properties for functional bone tissue. (Miller *et al.*, 2007)

Bone Healing and Regeneration

Bone repair is a unique postnatal healing response whereby bone tissue is regenerated in the absence of scar tissue formation. The exact mechanisms of bone regeneration involve a complex spatial and temporal coordination of multiple cellular and molecular contributors in physiological processes that, in part, recapitulate embryonic skeletogenesis (Ferguson *et al.*, 1999). As in development, bone healing involves a combination of both endochondral and intramembranous ossification pathways. In general, bone healing proceeds through the three overlapping hallmark stages of wound healing: inflammation, repair, and remodeling.

The inflammation stage encompasses the initial injury, hematoma formation, inflammatory cell invasion and inflammatory cytokine signaling (Gerstenfeld *et al.*, 2003). The importance of inflammation in initiating bone repair has been recently

reviewed (Mountziaris and Mikos, 2008; Kolar *et al.*, 2010), with formation of the hematoma having been shown to be a critical step in the healing process (Grundnes and Reikeras, 1993; Kolar *et al.*, 2010), as it possesses both osteogenic (Mizuno *et al.*, 1990) and angiogenic (Street *et al.*, 2000) potential. The invading inflammatory cell types are inclusive of polymorphonuclear cells, platelets, macrophages, and lymphocytes that coordinate and secrete a variety of cytokines and growth factors necessary for the proper cascade of morphogenetic events. Amongst these secreted factors, tumor necrosis factor-α (TNF-α) has demonstrated a particularly important role (Gerstenfeld *et al.*, 2001; Gerstenfeld *et al.*, 2003). Other factors involved are inclusive of interleukins-1 and -6 (IL-1 and IL-6), receptor activator of nuclear factor kappa-B ligand (RANKL), macrophage colony stimulating factor (M-CSF), multiple chemokines including monocyte chemotactic protein-1 (MCP-1/CCL-2), transforming growth factor-β (TGF-β), several bone morphogenetic proteins (BMPs), platelet derived growth factor (PDGF), vascular endothelial growth factor (VEGF), and fibroblast growth factor-2 (FGF-2/bFGF). Together, the secreted factors facilitate on the ongoing mediation of inflammation and initiate the recruitment of osteoprogenitors and uncommitted mesenchymal stem cells that will actively participate in bone repair (Gerstenfeld *et al.*, 2003; Schindeler *et al.*, 2008; Pape *et al.*, 2010).

The distinct processes involved in the reparative stage of bone healing are largely dictated by the degree of stability at the site of injury (Le *et al.*, 2001). In rare instances of anatomical restoration with rigid fixation producing negligible interfragmentary strain, primary bone healing can occur as the cortex attempts to directly re-establish itself (Einhorn, 1998). More classically, bone repair proceeds through what is known as

secondary bone healing, consisting of sequential sub-stages of soft and hard callus formation (Einhorn, 1998; Gerstenfeld *et al.*, 2003). The early hallmarks of this repair process include intramembranous ossification at the periosteal surface, as well as chondrocyte synthesis of the cartilaginous soft callus. The function of the soft callus is to provide the requisite initial mechanical stability for fracture repair, but it will also ultimately serve as a scaffold for the bony callus to follow. Upon completion of the soft callus, chondrocytes undergo hypertrophy and the calcification of the callus takes place (Einhorn, 1998; Schindeler *et al.*, 2008). This mechanically stable, calcified callus then becomes a target for vascular ingrowth in a coordinated process that involves matrix metalloproteinase (MMP)-driven extracellular matrix remodeling and angiogenic vessel growth. MMP-9, MMP-13, and VEGF are all critical mediators of the vascular invasion portion of endochondral ossification (Ferguson *et al.*, 1999; Gerber *et al.*, 1999; Colnot *et al.*, 2003). Coupled to vascular ingrowth is the formation of the bony callus by osteoblasts in which primary woven bone is laid down to replace the cartilage callus. The exact source of osteoprogenitors/chondroprogenitors that direct bone regeneration remains unclear, and potential contributors are thought to arise from the surrounding soft tissue, bone marrow space, and periosteum (Einhorn, 1998), with the latter being of particular importance (Ushiku *et al.*, 2010; Yu *et al.*, 2010). Other hypotheses include the contribution of circulating progenitor cells (Matsumoto *et al.*, 2008) or a perivascular source of osteoprogenitor cells (Towler, 2007; Crisan *et al.*, 2008; Caplan and Correa, 2011). Coordination of the cellular and molecular processes of bone repair is spatially and temporally regulated by a broad array of growth factors, cytokines, systemic regulators, and extracellular matrix proteins (Deschaseaux *et al.*, 2009; Kempen *et al.*,

2010). Although a complex symphony of signals directs postnatal bone repair, BMP-2 has specifically been identified as an indispensible molecule in this process (Tsuji *et al.*, 2006).

Ultimately, bone healing culminates in the remodeling stage as the anatomical and mechanical properties of the bone are restored. In a nearly identical cellular process to developmental bone formation and homeostatic adaptation, bone resorption performed by osteoclasts is coupled to the deposition of highly-organized secondary llamelar bone by osteoblasts (Gerstenfeld *et al.*, 2003; Schindeler *et al.*, 2008).

Neuronal Interactions in Bone Repair

The innervation of the skeletal system has long been established, both clinically and experimentally (Hurrell, 1937; Sherman, 1963); however, the anatomical distribution is yet to be thoroughly characterized and the physiological implications of innervation remains incompletely understood. In general, the periosteum is densely innervated, and nerves predominantly enter bones alongside arterial blood supply, after which they branch to Haversian canals, bone marrow, and even mineralized bone tissue (Serre *et al.*, 1999; Mach *et al.*, 2002). While the number of nerve fibers in bone may not be numerous, they are thought to provide two specific regulatory roles: 1) mediators of mechanical forces in bone and 2) a source of trophic factors necessary for bone form and function (Masi, 2012).

Nerve growth factor (NGF), a neurotrophin modulating sensory and sympathetic pathways, has been shown to be present in developing skeletal tissues (Frenkel *et al.*, 1990). A growing body of work continues to elucidate neurotransmitter and neuropeptide signaling pathways in the skeletal system and a neuronal arm contributing

to the regulation of bone modeling and remodeling (Imai and Matsusue, 2002; Spencer *et al.*, 2004; Elefteriou, 2008). Notably, Ducy *et al*. demonstrated a leptin-mediated central nervous system control of bone mass (Ducy *et al.*, 2000). In addition, others have reported a neural contribution in the regulation of functional adaptation to loading (Sample *et al.*, 2008), at least partially mediated via the sympathetic nervous system (Kondo *et al.*, 2005; Nagao *et al.*, 2011). Furthermore, the neuropathy-induced reduction in bone mineral density is not strictly a result of reduced load bearing (Whiteside *et al.*, 2006).

During fracture healing, regenerating nerve fibers have experimentally been shown to be present in the hematoma at early stages, followed by presence in the fracture callus, periosteum, fibrocartilage, and ultimately new woven bone at later time points (Li *et al.*, 2001). Immunological characterization of tissue samples from non-infected, human diaphyseal fractures that experienced delayed or nonunion revealed a virtually non-existent presence of peripheral nerve fibers (Santavirta *et al.*, 1992). Furthermore, clinical observation of enhanced osteogenic activity in fracture patients with head injuries provides anecdotal evidence for the role of the nervous system in bone physiology (Perkins and Skirving, 1987; Spencer, 1987; Garland, 1988). However, it remains controversial whether this increase in osteogenesis is an actual acceleration of fracture healing, or rather, a form of heterotopic ossification (Kushwaha and Garland, 1998; Morley *et al.*, 2005).

Existing Models of Composite Bone and Nerve Injury

While increasing effort is being devoted to investigating the complexity of cross-talk between the nervous and skeletal systems, interactions in instances of composite

bone and nerve injuries have largely been left unexplored. Among the experiments that have been performed, the primary model employed has been disrupted innervation in tibial fracture healing by way of sciatic nerve transection. Aro *et al.* studied the effect of sciatic nerve transection, spinal cord transection, or both on tibial fracture healing in a rat model (Aro *et al.*, 1981). Weight bearing controls (fracture alone) and non-weight bearing controls (fracture with hip dislocations) were included. Groups with disrupted innervation displayed more frequent fracture union at early time points, but possessed noticeably less dense calluses than control groups. By the study end point, all fractures had achieved union; however, irregularities in shape and/or density were reported for fracture calluses with denervation. While tensile testing of specimens indicated greater load to failure at early time points for fracture groups with disrupted innervation compared to control groups, this method of loading is of minimal physiological relevance. In a subsequent study, Aro again used transection of the sciatic nerve to further study the effect of nerve injury on fracture healing and callus formation in the rat (Aro, 1985). In this study, no attempt was made to control for unequal weight bearing in groups with or without nerve injury. In confirmation of previous findings, radiographs and histology indicated more rapid bridging in fractures with nerve transection, but smaller, less dense calluses. A smaller amount of collagenous matrix was also reported for denervated fracture calluses compared to controls.

Nordsletten *et al.* also used a rat model to study the effect of sciatic nerve resection on tibial fracture healing, but included cast-immobilization of the fractured limbs to control for differences in weight bearing between denervated animals and controls (Nordsletten *et al.*, 1994). Larger fracture calluses were reported for the nerve

resection group compared to controls. In fact, radiographs of control fractures indicated very little callus formation. Furthermore, nerve resection fractures possessed significantly higher bone mineral content. The larger, more mineralized nerve resection fracture calluses did not demonstrate better mechanical properties, however, when evaluated in three-point bending. A parallel experiment from these authors using histological techniques to study the growth of neural fibers into fracture calluses in this model corroborated the observed radiographic results (Hukkanen *et al.*, 1995). In a follow-up to this study, Madsen *et al.* investigated fracture healing and callus innervation after resection of both the sciatic and femoral nerves (Madsen *et al.*, 1998). Again, cast-immobilization was used to control for differences in weight bearing. When assessed radiographically, calluses from the nerve resection group were larger than controls. Immunostaining of the fracture callus for nerve fibers and neuropeptides indicated the pattern of innervation is altered following nerve resection, but total denervation is not experienced. Mechanical testing of the femora in three-point bending demonstrated decreased mechanical properties for nerve resection fractures. These results suggest that maturation of the fracture callus may be dependent on the innervation status of the bone.

The discrepancies in callus formation and bone healing results for fractures with sciatic nerve transection from seemingly similar surgical models may be explained by differences in fixation stability. All experiments used intramedullary nailing for internal fixation; however, Nordsletten *et al.* (Nordsletten *et al.*, 1994), Hukkanen *et al.* (Hukkanen *et al.*, 1995), and Madsen *et al.* (Madsen *et al.*, 1998) attempted to control for unequal weight bearing between groups by immobilizing fractured limbs in casts, whereas the work from Aro *et al.* (Aro *et al.*, 1981; Aro, 1985) allowed for weight

bearing on fractured limbs. Although, cast-immobilization may prevent unequal load bearing during ambulation, it also precludes functional mechanical stimulation of the healing fracture, a factor known to influence bone modeling and remodeling. Thus, it is possible that cast-immobilized control fractures were stable enough to proceed through primary fracture healing, which would explain the absence of callus formation. If true, this may suggest modulation of fracture healing via sensory innervation feedback on fracture stability. Consideration should also be given to the physiological loading imparted by skeletal muscle. While immobilization can attempt to tease out effects of load bearing, it cannot account for disruption of the resting muscle tone in the lower limb as a result of nerve transection.

While sciatic nerve transection in combination with tibial fracture is the predominant composite bone and nerve injury model found in the literature, other models have been described. Frymoyer and Pope used a rat model of fibular fractures absent fixation to study the effect of sciatic nerve resection on healing (Frymoyer and Pope, 1977). No attempt was made to control for possible differences in weight bearing due to sciatic nerve injury. Histological scoring of fracture healing was performed at multiple time points, with no observed differences except in one instance, at which time fractures from the sciatic nerve injury group displayed better healing than controls. Differences in mechanical properties from tensile testing of samples were reported, with denervated fractures outperforming controls, but are of questionable relevance to physiological loading conditions. Others have taken an additional step with this model and investigated the effect of sciatic nerve transection on fibular fracture healing including the surgical removal of periosteal neural mechanoreceptors located in the distal portion of the rat

fibula (Aro *et al.*, 1985). In relative agreement with Frymoyer and Pope, this study found that fibular fracture healing proceeded undisturbed by transection of the sciatic nerve. However, surgical stripping of mechanoreceptors was associated with fracture nonunion that, at times, became atrophic. Inclusion of sciatic nerve transection exacerbated this effect, with all fractures going on to atrophic nonunion. Histological analysis of atrophic fragments indicated they were active sites of osteoclastic bone resorption. Interestingly, two control samples with stripped mechanoreceptors and intact sciatic nerves presented hypertrophic nonunions in the distal fibula, visible as early as one month post-surgery. No such instances were observed in intact control fibulae with stripped mechanoreceptors and transected sciatic nerves, but thinner appearance was noted, potentially attributable to altered weight bearing in response to the sciatic nerve injury. Recently, Apel *et al*. used neurotoxin injection at the cortex of the femur to model fracture healing in instances of local sensory denervation (Apel *et al.*, 2009). Intramedullary rods were used for fixation, and no attempt was made to control for weight bearing in this model. Sensory denervation resulted in decreased type I and II collagen deposition during early fracture healing, but an eventual increase in the size of the fracture callus when evaluated histologically and via microcomputed tomography. Despite larger fracture calluses, sensory-denervated samples failed at lower loads in three-point bending.

Although not specifically a composite limb injury model, Boes *et al*. recently investigated experimental fracture healing with associated traumatic brain injury in a reproducible rat model (Boes *et al.*, 2006). To do so, a standard closed femoral fracture with intramedullary fixation was combined with a model of traumatic brain injury produced from an impact acceleration system. The brain-injury group demonstrated

smaller fracture calluses with increased torsional stiffness compared to fracture alone, which may suggest enhanced progression through the remodeling stage of fracture healing. Further, to investigate possible systemic mitogenic differences between groups, serum collected at euthanasia was used to supplement in vitro cell culture media. Increased proliferation was observed in a mesenchymal stem cell line when supplemented with serum from the brain-injury group compared to serum from the fracture-only group, but enhanced proliferation was not observed in osteoblastic or fibroblastic cell lines.

Mechanisms of Bone and Nerve Interaction

Several potential means of interaction between bones and the nervous system exist, including a regulatory arm in bone metabolism and neuropeptide/neurotransmitter signaling pathways (Fig. 2.1).

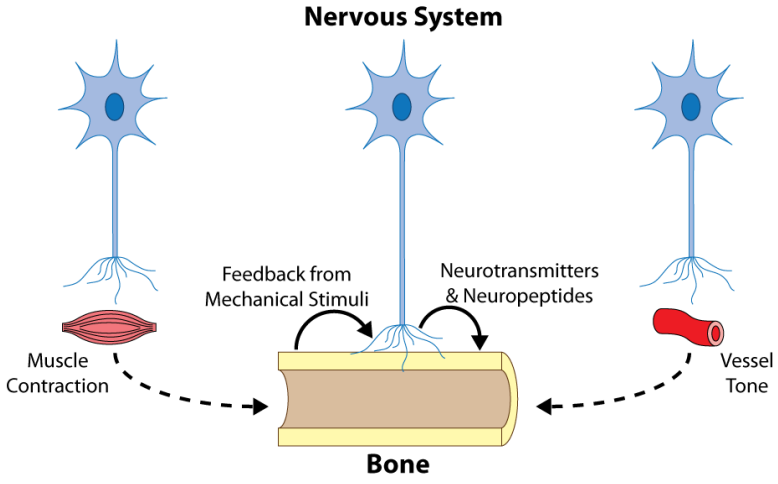

Figure 2.1. Mechanisms of interaction between bone and the nervous system. Neurotransmitter and neuropeptides offer pathways for direct signaling, and the nervous system has a regulatory role in loading-induced bone metabolism. Indirect interactions (shown with dotted lines) are also exerted via nervous system control of muscle contractions and blood vessel tone.

Given the relative paucity of research in this area to date, the cellular and molecular mechanisms involved are far from completely understood, though. Several studies have implicated sensory neuropeptide calcitonin gene-related peptide (CGRP) as a potential mechanism to exert a neural influence on bone repair. CGRP-immunoreactive sensory fibers are known to innervate normal bone tissue (Bjurholm *et al.*, 1988; Hukkanen *et al.*, 1993; Mach *et al.*, 2002). Additionally, CGRP-immunoreactive fibers are reported to sprout and proliferate in bone tissue during normal fracture healing (Hukkanen *et al.*, 1993), but exhibit a reduced presence in tibial fracture healing when innervation to the lower limb has been disrupted by sciatic nerve resection (Hukkanen *et al.*, 1995). Modulation of skeletal repair by CGRP could occur directly, as CGRP has been shown to have osteogenic capacity *in vitro*, with CGRP-supplemented media increasing bone forming colonies in a dose-dependent manner (Bernard and Shih, 1990), and *in vivo*, as CGRP expression in osteoblasts gives way to a skeletal phenotype with increased bone density in mice (Ballica *et al.*, 1999). The influence may also be exerted in an indirect route through the vasculature given the potent vasodilator action of CGRP (Brain *et al.*, 1985) and its ability to stimulate endothelial cell proliferation (Haegerstrand *et al.*, 1990).

Neurotrophins NGF, brain-derived neurotrophic factor (BDNF), and and neurotrophin-3 (NT-3), as well as their receptors, have been shown to be expressed at both protein and gene expression levels in bone forming cells during murine rib fracture healing, suggesting potential autocrine and paracrine regulatory functions in bone repair (Asaumi *et al.*, 2000). Local delivery of NGF at the fracture site via mini-osmotic pump has also been suggested to accelerate the rate of repair of rib fracture healing in a rat model, and was associated with increased concentrations of catecholamines epinephrine

and norepinephrine in the callus (Grills *et al.*, 1997). Another potential mediator of neural-osseous crosstalk in bone repair is neuropeptide Y (NPY). The NPY signaling axis exerts strong control on bone metabolism through the G-protein coupled receptors Y1 (via PNS) and Y2 (via CNS), primarily thought to occur via negative regulation of osteoblast activity (Shi and Baldock, 2012). Involvement of NPY in fracture repair and remodeling has also recently been proposed, however, the exact role remains undetermined (Long *et al.*, 2010).

An effect of denervation on fracture healing may also be modulated indirectly by changes in blood perfusion and hemodynamics in the surrounding skeletal muscle. Previously, transection of the sciatic or femoral nerves was shown to result in transient hyperemia in the muscles of the hind limb (Midrio *et al.*, 1968). Others have reported that denervation of a muscle flap produces an acute increase in arteriole diameters and a more sustained increase in perfused capillaries compared to innervated controls (Siemionow *et al.*, 1994). An increase in blood flow in the bones of the lower leg have also been associated with transection of the sciatic nerve (Shim *et al.*, 1966). The coupling of tissue blood perfusion in response to nerve injuries is most likely explained, at least in part, by sympathetic nervous system control of vascular tone.

Vascular Interactions in Bone Repair

Although the importance of blood vessels in skeletal system physiology has been documented for well over 200 years (Haller, 1763; Hunter, 1794), complexities in this relationship continue to be discovered. Healthy bones are highly vascularized, with long bones receiving blood supply from the intramedullary nutrient artery (or arteries), arteries in the periosteum, and metaphyseal and epiphyseal arteries that enter near bone ends.

Branching of these arterial sources, such as the supply to Volkmann's canals, is abundant and complex, with significant anastomosis. During skeletal development, blood vessel invasion is a critical step in the conversion of the cartilage intermediate to bone in the endochondral bone formation process (Ferguson *et al.*, 1999; Gerber *et al.*, 1999; Kronenberg, 2003). Postnatal skeletal repair is also tightly coupled to, and dependent on, vascular supply and angiogenesis (Glowacki, 1998; Carano and Filvaroff, 2003). Sufficient vascular supply is imperative for bone healing due to its physiological role in oxygen and nutrient transport, but it also serves as a conduit for migrating inflammatory and progenitor cells as well as soluble factors. In addition, disrupted blood perfusion may have potential consequences for local cell fate in the region of bone repair (Muschler *et al.*, 2004). Clinical risk factors for delayed or nonunion fracture healing include diminished blood supply (Einhorn, 1995) and concomitant vascular injury (Dickson *et al.*, 1994; Brinker and Bailey, 1997). Furthermore, lower limb fractures with vascular injuries are associated with higher rates of amputation (Glass *et al.*, 2009).

Existing Models of Composite Bone and Vascular Injury

Despite the established links between vasculature and bone healing, few models of composite bone and vascular injuries are found in the literature. Kase *et al*. incorporated transient, acute hindlimb ischemia (via tourniquet and microvascular clip application) in a rat tibial fracture model to investigate how bone healing was affected (Kase *et al.*, 1998). Interestingly, no differences in fracture healing were found radiographically or in three-point bending mechanical testing. Labeled microspheres were used to evaluate blood perfusion to the tibia and surrounding muscles, with no differences found between ischemic and control groups. While surprising, the lack of

differences observed in bone healing may be due to insufficient ischemia produced by the transient, acute ischemia-reperfusion procedure, or the lack of quantitative outcome measures of tissue composition at the fracture site. In a mouse model, Lu *et al*. found that ischemia induced by resection of the femoral artery impaired healing of non-stabilized tibial fractures (Lu *et al.*, 2007). At early time points, reduced blood vessels were present in and around fractures in ischemic legs. Ischemic fractures also displayed decreased cell proliferation, increased cell death, and delayed chondrocyte maturation at early time points. Fracture calluses in ischemic limbs were smaller than controls, and possessed less bone and cartilage. Nearly all ischemic fractures failed to achieve bony bridging, whereas all control fractures proceeded normally to bridging.

While few studies have used definitive models of composite bone and vascular injuries, a significant amount of work has focused on the intimate relationship between angiogenesis and bone repair. Most relevant to this chapter is the research incorporating interventions to impair angiogenesis in an effort to determine what effect this decoupling has on bone repair. Street *et al*. used murine models for femoral fracture healing and tibial cortical defects to demonstrate that inhibition of angiogenesis will disrupt endochondral and intramembranous bone repair, respectively (Street *et al.*, 2002). In fracture repair, angiogenesis was shown to be a mediator of both soft callus formation and calcification of the hard callus. In cortical defects, where repair proceeds primarily through intramembranous ossification, the effects of angiogenesis inhibition were more prominent at early time points than later. Similar results have been reported by Hausman *et al*. in a rat femoral fracture model, where administration of a pharmaceutical angiogenesis inhibitor impaired both the endochondral and intramembranous osteogenic

pathways (Hausman *et al.*, 2001). Fractures in the treatment group developed little to no bony callus, displayed minimal periosteal woven bone formation, and typically proceeded to nonunion. Additionally, the treatment group fractures demonstrated decreased mechanical properties compared to control fractures when tested in torsion. Wan *et al*. used a transgenic mouse model to impair angiogenesis at the level of gene expression during distraction osteogenesis in the tibia (Wan *et al.*, 2008). Compared to wild-type controls, the transgenic mice displayed decreased vascularity in the distraction region and subsequent reduction in bone regeneration. Administration of a pharmaceutical angiogenesis inhibitor (the same as that used by Hausman *et al*.) was used by Fang *et al*. in a mandibular distraction osteogenesis model in rats to investigate the effect on bone regeneration (Fang *et al.*, 2005). Once again, inhibition of angiogenesis was shown to preclude successful bone formation in the distraction region, giving way to fibrous scar tissue. Although this study did not use a limb injury model, it reported the particularly interesting finding that both an osteogenic mechanical environment and angiogenic gene expression are necessary conditions for the formation of a vascular network to support bone regeneration, and that either stimuli alone is insufficient.

An ability of the mechanical environment to influence formation of vascular networks, and ultimately bone healing, has been reported by several investigators. Wallace *et al*. investigated the difference between rigid or semi-rigid axial fixation stiffness in an ovine tibial osteotomy model with external fixation (Wallace *et al.*, 1994). The semi-rigid fixation group experienced transiently increased micromovement at the osteotomy site and increased corticomedullary blood flow compared to rigid fixation. While differences in blood flow or interfragmentary movement did not persist at later

time points, differences were apparent in the morphology of healing bones, as the semi-rigid group displayed increased callus perimeter and cross-sectional area with decreased cortical porosity. In a similar design, Lienau *et al*. used external fixators of rigid or semi-rigid bending stiffness in an ovine tibial osteotomy model to study vascularization and tissue differentiation (Lienau *et al.*, 2005). Larger interfragmentary movement was observed in the semi-rigid group at early time points, and was accompanied by an initially reduced number of blood vessels compared to rigid fixation. Differences in callus size and tissue composition at later time points were indicative of semi-rigid fixation leading to delayed healing.

The effects of interfragmentary movement on vascularity reported by Lienau *et al*. (Lienau *et al.*, 2005) are in contrast to those previously reported by Wallace *et al*. (Wallace *et al.*, 1994). Clearly, altering fixation bending stiffness as opposed to axial stiffness may be the source of the discrepancy. It may also be in part due to a difference in evaluation methods and the regions analyzed. Wallace *et al*. measured blood flow to the bone 10 mm proximally and distally to the osteotomy based on the accumulation of systemically delivered labeled microspheres, whereas Lienau *et al*. histomorphometrically quantified blood vessels in the region that extended only 6 mm proximally and distally. Additionally, Wallace *et al*. were unable to distinguish whether the increase in blood flow was due to increased perfusion to existing vessels, new vessel formation, or a combination of both.

Boerckel *et al*. used a critically-sized rat femoral defect model and contrast-enhanced 3-D vascular imaging to demonstrate an effect of the timing of load initiation on vascular growth and remodeling during bone repair (Boerckel *et al.*, 2011). Whereas

application of early axial mechanical loading resulted in decreased vascularity in the defect and attenuated bone regeneration compared to unloaded controls, delayed loading enhanced bone regeneration and was associated with apparent vascular remodeling, exhibiting a decrease in the number of small vessels and an increase in the number of large vessels. When taken together with the ovine model studies, the evidence for an effect of mechanical loading on blood vessel network formation and bone healing is both compelling and complex. If applied too soon or in excess, mechanical loading has the potential to disrupt vascular ingrowth and negatively influence bone healing, whereas when applied with the appropriate timing and magnitude, mechanical signals can have stimulatory effects.

Mechanisms of Bone and Vascular Tissue Interaction

Means of interaction between bones and vascular tissue networks extend beyond the physiological supply of oxygen and nutrients, as the vessels also serve as a conduit for soluble vactors and cellular exchange (Fig. 2.2).

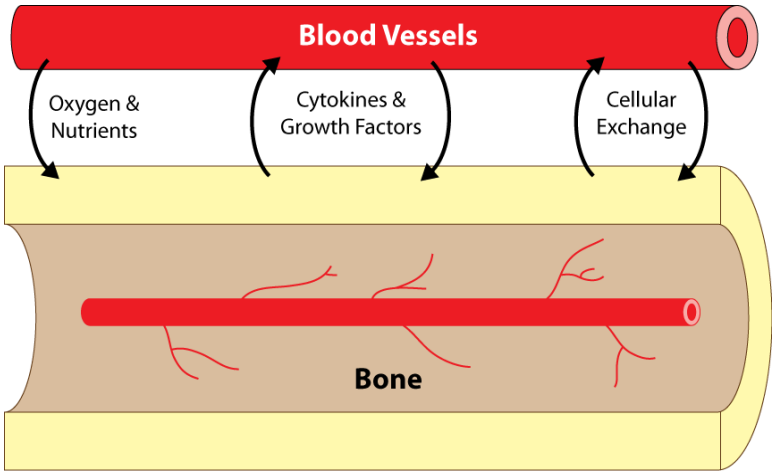

Figure 2.2. Mechanisms of interaction between bone and blood vessels. In addition to providing oxygen and nutrients, blood vessels provide a conduit for transport of soluble factors and cellular exchange.

The molecular coupling of angiogenesis and osteogenesis by a "vascular stimulating factor" was first proposed by Trueta in 1963 (Trueta, 1963). Since then, a variety of growth factor and cytokine molecular players have been implicated, including members of the transforming growth factor beta (TGF-β), bone morphogenetic protein (BMP), platelet-derived growth factor (PDGF), vascular endothelial growth factor (VEGF), fibroblast growth factor (FGF), and insulin-like growth factor (IGF) families, as well as systemic regulators (e.g., vitamin D and parathyroid hormone) (Carano and Filvaroff, 2003; Kempen *et al.*, 2010). Of these, VEGF has been perhaps the most thoroughly studied. VEGF-mediated angiogenesis is an essential component for coordinating conversion of cartilaginous anlage to bone during endochondral bone formation in skeletal development (Ferguson *et al.*, 1999; Gerber *et al.*, 1999). Endogenous VEGF is also necessary for normal bone healing in both intramembranous and endochondral ossification, and delivery of exogenous VEGF enhances fracture and segmental bone defect repair (Street *et al.*, 2002). This contribution to bone repair is, at least in part, controlled at the gene expression level by hypoxia-inducible transcription factor one alpha (HIF-1α), an angiogenic transcription factor under inhibitory control in normoxic conditions. During skeletal development, the HIF-1α/VEGF pathway couples angiogenesis and osteogenesis (Wang *et al.*, 2007; Araldi and Schipani, 2010). HIF-1α is also a mediator of postnatal skeletal repair, as constitutively active osteoblast HIF-1α via genetic mutation was shown to enhance angiogenesis and bone regeneration in a VEGF-dependent process, whereas osteoblast-specific knock out of the HIF-1α gene resulted in impaired angiogenesis and bone regeneration (Wan *et al.*, 2008). Furthermore, pharmacological small molecule activation of HIF-1α has been shown to effectively

augment vascularity and bone repair in models of fracture healing (Shen *et al.*, 2009), distraction osteogenesis (Wan *et al.*, 2008), and segmental defect repair (Stewart *et al.*, 2011).

Another important source of molecular cross-talk between bone and vasculature is provided by members of the BMP family of proteins. Given their osteoinductive capacity (Urist, 1965), BMPs play a vital role in osteogenesis; however, they also provide an important contribution in the angiogenesis-osteogenesis interaction by stimulating osteoblast VEGF production and increasing blood vessel formation (Deckers *et al.*, 2002; Zhang *et al.*, 2009). VEGF may also up-regulate BMP-2 expression in vascular tissues via paracrine loops (Bouletreau *et al.*, 2002; Matsubara *et al.*, 2012) and/or act through direct binding with osteoblast VEGF receptors (Deckers *et al.*, 2000; Clarkin and Gerstenfeld, 2013). BMPs may also act directly on endothelial progenitor cells to promote angiogenesis (Smadja *et al.*, 2008). Furthermore, sequential co-delivery of exogenous VEGF followed by BMP-2 was reported to enhance bone formation (Kempen *et al.*, 2009), whereas delivery of stem cells engineered to co-express VEGF and BMP-4 demonstrated synergistic enhancement of bone regeneration in a calvarial defect model (Peng *et al.*, 2002). In a follow-up to previous work in a mouse model of ischemic tibial fractures (Lu *et al.*, 2007), rhBMP-7 treatment appeared sufficient to overcome the limitations of diminished blood supply, providing enhanced healing in fractures that would otherwise proceed to delayed or nonunion (Lu *et al.*, 2010).

Beyond osteogenic-angiogenic coupling, interactions from traditional mechanisms of arteriogenic blood vessel growth are also plausible contributors to bone regeneration. Indeed, it was recently shown that during distraction osteogenesis,

arteriogenic vessel growth in the surrounding skeletal muscle envelope precedes angiogenic vessel growth in the regenerating space (Morgan *et al.*, 2012). The extracellular matrix protein osteopontin (OPN) is significantly up-regulated in response to HLI (Lyle *et al.*, 2012), plays a definitive role in collateral vessel development and recovery from ischemia (Duvall *et al.*, 2008), and is involved in regulating several aspects of fracture healing (Duvall *et al.*, 2007). Other growth factors thought to be associated with arteriogenesis such as platelet derived growth factor (PDGF), transforming growth factor-β (TGF-β), fibroblast growth factor-2 (FGF-2) (Buschmann *et al.*, 2003), have also been implicated in bone regeneration (Kempen *et al.*, 2010), and provide additional posssible means of molecular cross-talk in these processes. At a cellular level, monocyte/macrophage invasion plays a significant role in collateral vessel growth following arterial occlusion (Arras *et al.*, 1998), and macrophages may possess a capacity for osteoinductive signaling through BMP-2 secretion (Champagne *et al.*, 2002). Vascular smooth muscle cells (SMC) also play a critical cellular role in arteriogenic vessel remodeling, with phenotypic changes and proliferation initiating early in the process (Schaper and Scholz, 2003). Cell populations expressing smooth muscle alpha-actin (SMAA) that actively participate in bone repair are thought to arise from a perivascular or myofibroblast lineage (Kinner *et al.*, 2002; Kalajzic *et al.*, 2008). Additionally, SMCs are considered at least partially responsible for vascular tissue calcification (Trion and van der Laarse, 2004), potentially in a process also involving macrophages (Trion and van der Laarse, 2004; Ikeda *et al.*, 2012). Pericytes, a mural cell "relative" of vascular SMCs more commonly associated with the microvessels, could also

conceivably play some role as a perivascular source of osteoprogenitor cells (Towler, 2007; Crisan *et al.*, 2008; Caplan and Correa, 2011).

Postnatal Vascular Growth

Blood vessels provide several essential physiological functions including oxygen and nutrient transport, as well as serving as a conduit for circulating cells and soluble factors. The essential components of blood vessels are endothelial cells which form the vessel lumen, mural cells that provide vessel stability (pericytes for capillaries, vascular SMCs for arteries and veins), the basement membrane, and extracellular matrix. Postnatal vascular growth occurs predominantly through two distinct processes: angiogenesis and arteriogenesis (Carmeliet, 2000). Whereas angiogenesis is defined as the sprouting of new capillaries from preexisting ones, arteriogenesis consists of the development of collateral vessels via the growth and remodeling of preexisting arterioles (Schaper and Scholz, 2003). A third process, vasculogenesis, consists of the *de novo* formation of vessels by way of angioblast mobilization and differentiation, but its contributions to vascular growth beyond embryonic development remain controversial. Given the dissimilar process definitions, it is unsurprising that the mechanisms responsible for angiogenesis and arteriogenesis appear to be largely distinct.

Angiogenesis

The physiological trigger initiating sprouting angiogenesis is tissue ischemia. Initial steps in angiogenesis include vasodilation of existing vessels, an increase in vascular permeability, and degradation of the surrounding extracellular matrix. The basement membrane degradation is performed primarily by members of the MMP family, and is an essential step in the sprouting process to allow for the migration of proliferating

endothelial cells referred to as the tip cell (Carmeliet, 2000). New sprouts are then driven by environmental cues to resolve tissue oxygen demands. Molecular players directing sprouting angiogenesis are multiple, including VEGFs and their receptors, FGFs, placental growth factor (PlGF), and angiopoietins (ANG-1 and ANG-2), of which VEGF is known to be a critical mediator (Carmeliet, 2000; Isner, 2000; Spyridopoulos *et al.*, 2002). Endogenous VEGF is essential for successful capillary sprouting in ischemic tissue (Couffinhal *et al.*, 1998), and delivery of exogenous VEGF has been reported to provide some degree of therapeutic benefit in animal models of limb ischemia (Takeshita *et al.*, 1994). The upregulation of VEGF production in response to tissue ischemia is mediated by hypoxia-inducible transcription factors (HIFs) (Levy *et al.*, 1995; Forsythe *et al.*, 1996). HIFs are constitutively expressed, but under normoxic conditions are marked for degradation based on the oxygen-sensing mechanisms of prolyl hydroxylases (PHDs). When oxygen tension decreases and hypoxia persists, the activity of PHDs becomes impaired allowing for accumulation of HIF-1α and the resultant downstream VEGF expression (Bruick and McKnight, 2001; Schipani *et al.*, 2009). While angiogenesis has an undeniable place as a postnatal vascular growth process, it remains controversial as to what degree therapeutic angiogenesis alone can compensate for increased flow demands required in instances of peripheral and cardiac ischemia (Isner, 2000; Schaper and Scholz, 2003).

Arteriogenesis

In contrast to the ischemic trigger for angiogenesis, arteriogenesis is thought to be brought on by the increased fluid shear stress experienced by arterioles as they attempt to compensate for greater flow demands (Ito *et al.*, 1997; Schaper and Scholz, 2003). As

with angiogenesis, the precise mechanisms of arteriogenesis include a myriad of molecular and cellular components. Initially, the increase in fluid shear stress results in an "activated" endothelium, prompting the production of endothelial nitric oxide synthase (eNOS) and MCP-1, as well as upregulation of endothelial ICAM-1 and VCAM expression (Scholz *et al.*, 2000; Cai and Schaper, 2008). These signals combine to promote circulating monocyte extravasation into the vessel wall which initiates remodeling. Unsurprisingly, monocytes have been shown to play a significant role in the cellular response during collateral vessel growth (Arras *et al.*, 1998). Furthermore, targeted disruption of the MCP-1 receptor, C-C chemokine receptor type 2 (CCR2) will impair arterial occlusion-induced collateral artery growth (Heil *et al.*, 2004), and delivery of exogenous MCP-1 has been shown to enhance arteriogenesis (Ito *et al.*, 1997).

Although monocytes/macrophages are required for initiation of remodeling, vascular SMCs do most of the heavy lifting of arteriogenesis. Vascular SMCs display a high level of plasticity in arteriogenesis and undergo a transition on their phenotypic continuum from contractile to synthetic (Cai and Schaper, 2008). In this synthetic phenotype, SMCs become much more proliferative and increase production of extra cellular proteins such as collagens, osteopontin, MMPs, and growth factors (Rensen *et al.*, 2007; Beamish *et al.*, 2010). Degradation of the vessel basement membrane and ECM by MMPs, including MMP-9, is an important event allowing for SMC proliferation and arteriogenesis. Monocytes and macrophages are the likely source of initial MMP production, with continued secretion from synthetic SMCs (Cai and Schaper, 2008). Also of significance in arteriogenesis is the ECM protein osteopontin. Monocytes/macrophages, endothelial cells, and SMCs are all capable of synthesizing

osteopontin (O'Brien *et al.*, 1994), and it has been demonstrated to possess a definitive biological role in the arteriogenic recovery from hind limb ischemia (Duvall *et al.*, 2008). Other cell types thought to perhaps play a role in arteriogenesis are bone marrow-derived cells, but primarily through paracrine activity as they have not been shown to incorporate into the remodeling vessels (Heil and Schaper, 2004).

To date, there are few growth factors that have been identified as possessing a dominant regulatory role in arteriogenesis, with many of the most likely candidates proving nonessential (Buschmann *et al.*, 2003; Cai and Schaper, 2008). While the importance of VEGF in angiogenesis is undisputed, its role in arteriogenesis is less clear. Deindl *et al.* reported that femoral artery occlusion-induced arteriogenesis was not associated with increased VEGF or hypoxia-inducible genes (*HIF-1α, LDH A*) (Deindl *et al.*, 2001). Furthermore, any increase in expression of VEGF and FGF-2 appears very limited following induction of hind limb ischemia in the rat (Luo *et al.*, 2002). Targeted deletion of the *Fgf-2* was shown to have no effect on recovery from hind limb ischemia in a murine model (Sullivan *et al.*, 2002), and double knockout of *Fgf-1* and *Fgf-2* genes produced only mild phenotypic differences (Miller *et al.*, 2000). Interestingly, while it has been shown that while mRNA levels of FGF-1 and FGF-2 are relatively unchanged after arterial occlusion, application of a chemical agent that inhibits FGF receptor binding does impair arteriogenesis (Deindl *et al.*, 2003). Angiopoietin-2 has been shown to be involved in mediating inflammation and arteriogenesis during recovery from hind limb ischemia (Tressel *et al.*, 2008). Other growth factors with incompletely understood roles in arteriogenesis include granulocyte-macrophage colony-stimulating factor (GM-CSF) (Schaper and Scholz, 2003) and PDGF (Cao *et al.*, 2003; Wu *et al.*, 2010).

CHAPTER 3

CHARACTERIZATION OF A COMPOSITE INJURY MODEL OF SEVERE LOWER LIMB BONE AND NERVE TRAUMA[a]

Abstract

Severe extremity trauma often results in large zones of injury comprising multiple types of tissue and presents many clinical challenges for reconstruction. Considerable investigation is ongoing in tissue engineering and regenerative medicine therapeutics to improve reconstruction outcomes; however, the vast majority of musculoskeletal trauma models employed for testing the therapeutics consist of single-tissue defects, offering limited utility for investigating strategies for multi-tissue repair. Here we present the first model of composite lower limb bone and nerve injury, characterized by comparison to well-established, single-tissue injury models using biomaterials-based technologies previously demonstrated to show promise in those models. Quantitative functional outcome measures were incorporated to facilitate assessment of new technologies to promote structural and functional limb salvage following severe extremity trauma. Nerve injury induced significant changes in the morphology and mechanical properties of intact bones. However, BMP-mediated segmental bone regeneration was not significantly impaired by concomitant nerve injury as evaluated via radiographs, microcomputed tomography (micro-CT), and biomechanical testing. Nor was nerve regeneration

---

[a] Portions of this chapter were adapted from Uhrig BA, Clements IP, Boerckel JD, Huebsch N, Bellamkonda RV, Guldberg RE. Characterization of a composite injury model of severe lower limb bone and nerve trauma. J Tissue Eng Regen Med. 2012; [Epub ahead of print].

significantly impaired by bone injury when evaluated via histology and electrophysiology. Despite the similar tissue regeneration observed, the composite injury group experienced a marked functional deficit in the operated limb compared to either of the single-tissue injury groups as determined by quantitative, automated CatWalk gait analysis. As a whole, this work presents a challenging, clinically-relevant model of severe extremity trauma to bone and nerve tissue, and emphasizes the need to incorporate quantitative functional outcome measures to benchmark tissue engineering therapies.

Introduction

Severe extremity trauma resulting in significant injury to multiple tissues – including bone, skeletal muscle, nerve, and vasculature – presents a multitude of clinical challenges that often cannot be treated with conventional reconstruction techniques. Furthermore, a lack of consensus exists for surgical intervention strategies (Yazar *et al.*, 2004; DeFranco and Lawton, 2006). Even if limb salvage and reconstruction is successful, the complex nature of the injuries often requires multi-stage treatment and results in diminished long-term function (Bosse *et al.*, 2002; MacKenzie *et al.*, 2005).

Historically, extremity injuries have been the predominant combat wound for members of US armed forces. This trend has continued in the ongoing conflicts in Iraq and Afghanistan, with the primary combat casualty mechanism being explosive munitions (Owens *et al.*, 2007; Owens *et al.*, 2008). These penetrating blast wounds result in large deficits to multiple tissue types in the extremities, and yield a high incidence of bone and soft tissue trauma (Owens *et al.*, 2007). In addition to comprising the largest number of combat casualties, extremity injuries present the greatest demand for medical resources, account for the most number of disabilities, and project as the

highest incurred future disability costs (Masini *et al.*, 2009). The civilian sector contributes an additional patient population from high-energy trauma incidents, such as motor vehicle collisions. Engineering of improved safety features for automobiles has increased passenger survival in these incidents, though many still sustain severe extremity trauma (Burgess *et al.*, 1995; Richter *et al.*, 2005). The consequences of extremity injuries are well documented, and encumber patients with profound functional disabilities and financial burden (Holbrook *et al.*, 1999; Bosse *et al.*, 2002; MacKenzie *et al.*, 2005; MacKenzie *et al.*, 2007).

Currently, autograft procedures are the clinical gold standard of care for both large bone defects and long peripheral nerve gaps. In both cases, these procedures face limitations due to the volume of tissue available for grafting and the associated morbidity at the donor site. Nerve autograft procedures are associated with additional drawbacks given the functional loss experienced at the donor site and possible modality mismatch between the donor and repaired nerves. A variety of potential therapeutic strategies to circumvent such limitations are under investigation throughout the field of tissue engineering and regenerative medicine. However, current animal models of musculoskeletal trauma used in evaluating emerging technologies typically consist of critically-sized, single-tissue defects, which offer limited utility for investigating therapeutic strategies for multi-tissue repair. Accordingly, there exists a need for challenging animal models of composite tissue injury. Moreover, such models would allow investigators to probe for endogenous interactions that may occur in the healing response for multiple tissue defects. Elucidating such interactions would open the door for development of novel therapeutics to leverage combinatorial or synergistic tissue

repair and regeneration. Therefore, the goal of this study was to develop a rat model of composite lower limb bone and nerve injury featuring quantitative functional outcome measures to facilitate assessment of new technologies to promote structural and functional limb salvage following severe extremity trauma. To do so, we characterized the healing response in the selected composite injury model to biomaterials-based therapeutics previously demonstrated to show promise in well-established, single-tissue injury models (Clements *et al.*, 2009; Kolambkar *et al.*, 2011).

Materials and Methods

Nanofiber Mesh Tube and Nerve Guidance Channel Fabrication

Perforated nanofiber mesh tubes were created as previously described (Kolambkar *et al.*, 2011). Briefly, a 12% (m/v) polymer solution was created by dissolving poly(ε-caprolactone) (PCL) pellets (Sigma-Aldrich, St. Louis, MO) in a 90:10 volume ratio of hexaflouro-2-propanol:dimethylformamide (Sigma-Aldrich). The solution was electrospun onto a static collector to obtain nanofiber mesh sheets. Rectangular sections were manually cut from the sheets and then patterned with 1 mm diameter perforations. Sheets were then glued into tubes of approximately 4.5 mm diameter and 12 mm length with a medical grade UV/visible light curing adhesive (1187-M, Dymax, Torrington, CT). Mesh tubes were sterilized via 100% ethanol evaporation and then re-hydrated with sequential sterile phosphate buffered saline (PBS) washes.

Thin-film-enhanced nerve guidance channels were fabricated as previously described (Kim *et al.*, 2008; Clements *et al.*, 2009). Briefly, aligned films of electrospun poly(acrylonitrile-co-methylacrylate, random copolymer, 4 mol% methylacrylate) (PAN–MA) fibers were created through an electrospinning process. 2.2 mm x 14 mm sheets of

aligned thin-films were manually cut with a razor blade for incorporation within polysulfone tubes (17 mm length, 1.6 mm inner diameter, 2.2 mm outer diameter, 50 kDa molecular weight cutoff, Koch Membrane Systems, Willmington, MA). The polysulfone tubes were first halved lengthwise into two longitudinal sections, and a single aligned thin-film was fixed within the interior length of one of the sections before reattaching the sections with a medical grade UV light curing adhesive (Dymax). Significantly, due to the negligible thickness of each thin-film, a minimal percentage of luminal cross-sectional area is occupied by scaffolding. The channels were sterilized by overnight incubation under UV light followed by immersion in 70% ethanol for 30 min. This process was immediately followed by two 20 min washes in sterilized deionized water and a final wash in sterile PBS. The channels were then stored in sterile PBS until surgery.

Preparation of rhBMP-2-containing Alginate Hydrogel

Sterile syringes of pre-gelled, recombinant human bone morphogenetic protein 2 (rhBMP-2)-containing alginate were prepared as previously described (Kolambkar *et al.*, 2011). Irradiated RGD-functionalized alginate (Alsberg *et al.*, 2003) was reconstituted in αMEM (Invitrogen, Carlsbad, CA). Lyophilized rhBMP-2 (R&D Systems, Minneapolis, MN) was reconstituted in 0.1% rat serum albumin (Sigma-Aldrich) in 4 mM HCl according to manufacturer instructions, and then mixed with the RGD-alginate solution to obtain a final solution of 2% alginate (m/v) containing 10 μg/ml rhBMP-2. The rhBMP-2-containing alginate solution was cross-linked via rapid mixing with a calcium sulfate (Sigma-Aldrich) solution. The syringes were stored at 4 °C overnight for use in surgery the following day.

Surgical Procedure

Thirteen-week-old female Lewis rats (Charles River Labs, Wilmington, MA) were anesthetized via isoflurane inhalation and received unilateral surgeries on right hind limbs comprising three experimental groups: bone injury (BI, n=9), nerve injury (NI, n=8), and composite bone and nerve injury (CI, n=8). The bone injury was a critically-sized 8 mm mid-femoral bone defect, created using a previously described surgical technique and stabilized by custom-made modular internal fixation plates (Oest *et al.*, 2007). Treatment was based on a hybrid growth factor delivery system recently described by Kolambkar and colleagues (Kolambkar *et al.*, 2011). Briefly, an electrospun poly(ε-caprolactone) (PCL) nanofiber mesh tube was placed into each bone defect region such that it overlapped at the endswith native bone tissue. A treatment dose of 2 μg rhBMP-2 was delivered in 200 μl of 2% (wt) RGD-functionalized alginate hydrogel (Alsberg *et al.*, 2003) that was injected into the tube lumen. The nerve injury was a 14 mm sciatic nerve gap, and was created using a previously described surgical technique (Kim *et al.*, 2008). Treatment consisted of implanting a 17 mm nerve guidance channel containing a single thin-film of electrospun poly(acrylonitrile-co-methylacrylate, random copolymer, 4 mol% methylacrylate) (PAN–MA) with aligned-fiber topography (Clements *et al.*, 2009). Proximal and distal nerve stumps were sutured 1.5 mm into each end of the channel to yield a 14 mm nerve gap. The composite injury consisted of both the bone defect and nerve gap, and treatment was a combination of the single injury methods. Un-operated, age-matched animals served as intact tissue controls (n=6). For pain relief, animals received subcutaneous injections of buprenorphine upon recovery from anesthesia and again every 8 hours for the first 72 post-operative hours. Animals

were housed in a temperature and humidity controlled environment, maintained on a 12:12 hour light/dark cycle, and allowed access to food and water *ad libitum*. All procedures were reviewed and approved by the Georgia Institute of Technology Institutional Animal Care and Use Committee and the United States Army Medical Research and Materiel Command Animal Care and Use Review Office.

Gait Analysis

Quantitative, computerized gait analysis was performed using CatWalk equipment and software (CatWalk 7.1, Noldus Information Technology, The Netherlands), technology originally detailed by Hamers *et al*. (Hamers *et al.*, 2001). The system has been previously used to assess functional deficit in spinal cord (Koopmans *et al.*, 2005) and sciatic nerve injury (Deumens *et al.*, 2007; Bozkurt *et al.*, 2008; Bozkurt *et al.*, 2011) animal models, as well as models of traumatic brain injury (Wang *et al.*, 2011), neurological disorders (Vandeputte *et al.*, 2010), and osteoarthritis (Ferland *et al.*, 2011). One week prior to data acquisition (two weeks prior to surgery), animals were run on the CatWalk system for acclimation and training. Pre-injury baseline data was acquired one week prior to surgery, and data acquisition was again performed 4, 8, 12, and 16 weeks post-surgery. Only uninterrupted runs were included for analysis. Three runs were analyzed per animal per time point whenever possible.

In Vivo Radiographs and Microcomputed Tomography

To qualitatively assess longitudinal bone regeneration and defect bridging, two-dimensional *in vivo* radiographs (Faxitron MX-20 Digital, Faxitron X-ray Corp., Wheeling, IL) were taken at 2, 4, 8, 12, and 16 weeks post-surgery. Radiographs were acquired at an exposure time of 15 s and an energy of 25 kV. Bony bridging, defined as

continuous bone spanning the defect region, was evaluated in the radiographs by two blinded investigators. In instances of disagreement, a third blinded investigator provided resolution.

At 4, 8, 12, and 16 weeks post-surgery, animals were anesthetized via isoflurane inhalation and *in vivo* microcomputed tomography (micro-CT) scans (vivaCT 40, Scanco Medical, Brüttisellen, Switzerland) were performed to quantitatively assess three-dimensional bone regeneration in the defect. Defects were scanned with an applied electric potential of 55 kVp, a current of 109 μA, and an isometric voxel size of 38 μm. The volume of interest (VOI) for *in vivo* scan analysis spanned a constant length of 5.43 mm (143 slices) at the center of each defect. To segment new mineral formation in the VOI, a global threshold corresponding to 50% of the native cortical bone density was applied. Additional post-mortem micro-CT analysis was performed after harvest and is detailed below.

Electrophysiology

In order to assess the extent of peripheral nerve regeneration, electrophysiological testing was performed as previously described (Clements *et al.*, 2009). Each animal was deeply anesthetized via inhaled isoflurane, and the site of nerve injury was re-exposed and kept moistened with mineral oil warmed to 37 °C. Portions of the sciatic nerve, approximately 15 mm proximal and distal to the ends of the nerve guidance channel, were freed from the surrounding tissue, and fitted with stainless steel bipolar hook electrodes. The distally positioned pair of electrodes, which was attached to a stimulator (Model S88, Grass Technologies, West Warwick, RI) and stimulus isolation unit (Model SIU5B, Grass Technologies), was used to stimulate the regenerated nerve with 0.1 to 0.5

ms square pulses of variable amplitude applied at a rate of 1 Hz. The evoked compound nerve action potentials (CNAPs) were recorded from the proximal pair of electrodes, amplified (Gain=1000), bandpass filtered (10–5000 Hz, Model 1700, A-M Systems, Sequim, WA), and digitally sampled (25 kS/s, Multichannel Systems DAQ card). The recordings were averaged up to 200 times, using a trigger signal provided by the stimulator, and the latencies of the onset of the evoked CNAPs were determined off-line. The precise distances between stimulating and recording electrodes were measured and divided by the latencies to calculate the conduction velocity of the CNAPs through the regenerated nerves. Qualitative assessment of whether regenerating axons crossed the injury gap and functionally reinnervated lower leg musculature was performed by observing contraction of the appropriate muscles in response to stimulation of the proximal nerve segment. These observations were performed before and after crushing the regenerated nerve distal to the site of stimulation.

Ex Vivo Microcomputed Tomography

After euthanasia (16 weeks post-surgery), femora were harvested for *ex vivo* μCT analysis and mechanical testing. Explanted femora were placed in 15ml conicals with phosphate buffered saline and oriented to the z-axis of scanning. Scans were performed with an applied electric potential of 55 kVp, a current of 109 μA, and an isometric voxel size of 21 μm. The *ex vivo* VOI consisted of a 6.99 mm (333 slices) region at the center of each defect. For segmentation of new mineral formation, a global threshold corresponding to 50% of native cortical bone density was applied.

Additionally, geometry and morphology of intact, unoperated femora were assessed for mid-diaphyseal cortical bone and epiphyseal trabecular bone. The cortical

bone VOI was a 2.96 mm (141 slices) region of the mid-diaphysis centered at the midpoint of each femur. A global threshold for cortical bone was determined via inspection and applied for segmentation. The entire epiphyseal trabecular bone compartment, extending from the distal end of the growth plate to divergence of the condyles, was contoured using an automatic algorithm adapted from Buie *et al*.(Buie *et al.*, 2007) Contours were all visually inspected for accuracy and manually adjusted as necessary. The trabecular bone VOI consisted of a 0.67 mm (32 slices) region at the center of each epiphyseal compartment. A global threshold for trabecular bone was determined by visual inspection and applied for segmentation. For all micro-CT analysis, a Gaussian filter was used for noise suppression ($\sigma = 1.2$ and support = 2 for all analyses except trabecular bone, which used $\sigma = 0.8$ and support = 1).

Biomechanical Testing

Femora were biomechanically tested to failure in torsion immediately following *ex vivo* micro-CT scans using a previously described protocol (Oest *et al.*, 2007). Briefly, excess soft tissue was carefully removed from the sample, the ends were potted into blocks with Wood's metal (Alfa Aesar, Wood Hill, MA), and the fixation plate was removed. Potted samples were mounted in torsion fixtures on a Bose ElectroForce system (ELF 3220, Bose EnduraTEC, Minnetonka, MN) and rotated through failure at a ramp rate of 3°/s, with rotation and torque data recorded. For each sample, failure strength and torsional stiffness (given by the maximum torque experienced and the slope of the line fit to the linear region of the torque-rotation curve, respectively) were determined.

Histomorphometry

2 mm-long sections of regenerated nerve were removed from the center of each guidance channel and from approximately the same region in intact sciatic nerves. These explants were fixed overnight with 1% osmium tetroxide in PBS. Samples were then washed with PBS, dehydrated in a graded ethanol series, and embedded in LX112 resin (Ladd Research Industries, Inc., Burlington, VT). Transverse 1 µm-thick sections were slide-mounted and stained with toluidine blue to visualize myelinated axons. Bright field microscopy (Nikon mEclipse 80i, Japan) was used to obtain high power (40x) photomicrographs of mounted nerve cross-sections. Mosaic images were compiled using a Neurolucida Plus software system (MBF Bioscience, Williston, VT) coupled to a mechanized stage and camera (MicroFireTM, Optronics, Goleta, CA). Histomorphometric parameters were obtained from these mosaic images using Image-Pro Plus software (Media Cybernetics, Inc., Bethesda, MD). Axon counts were performed by manually counting subsets of the entire axonal population and applying the density for the counted area to the whole area of nerve. Manual counts were performed on 10-25% of the total nerve area from each cross-section.

Data Presentation and Statistical Analysis

All data are presented as mean ± standard error of the mean (SEM). *In vivo* µCT data were analyzed for differences between groups using unpaired t-tests at each time point. One-factor analysis of variance (ANOVA), with pairwise comparisons made by Tukey's *post hoc* test, or unpaired t-tests were used for analyzing end point data, as appropriate. CatWalk data are expressed as a ratio between ipsilateral and contralateral hind paws. CatWalk data were analyzed by ANOVA with repeated measures to evaluate overall differences based on group, time, and the interaction of the two. Cross-sectional,

one-factor ANOVA was used for comparisons amongst groups at each time point. Paired t-tests with Bonferroni correction were used to make within-group comparisons of post-surgical time points to pre-injury baseline values. A significance level of 0.05 was used for all analyses. Statistical analysis was performed in Minitab 15 (Minitab, State College, PA) or SPSS Statistics 19 (IBM, Somers, NY).

Results

All operated animals tolerated surgical procedures and recovered well. One animal in the bone injury group was excluded from analysis due to abscess formation in the defect. An additional animal from this group was lost due to anesthesia complications during the week 8 *in vivo* micro-CT scan. One animal from each of the nerve injury and composite injury groups developed pododermatitis on the operated limb and were excluded from CatWalk analysis.

Bone Regeneration Radiography and Micro-CT Analysis

Longitudinal radiographs revealed a qualitatively similar bone healing response in the composite injury group compared to the bone injury group (Fig. 3.1). Bridging rates were comparable for the two groups. In the bone injury group, six of eight samples had bridged by week 4, and all but one sample had bridged by week 12, with the exception going on to non-union. In the composite injury group, 7 of 8 samples had bridged by week 4, and all samples had bridged by week 12. Three-dimensional micro-CT reconstructions confirmed these results (Fig. 3.2A). No quantitative differences were observed between groups at any *in vivo* time point in terms of the volume of mineral formation (Fig. 3.2B) or the mean mineral density (data not shown). Both groups

exhibited similar trends for increasing mineral volume and mean density over time. *Ex vivo* quantitative analysis also revealed no differences between groups (data not shown).

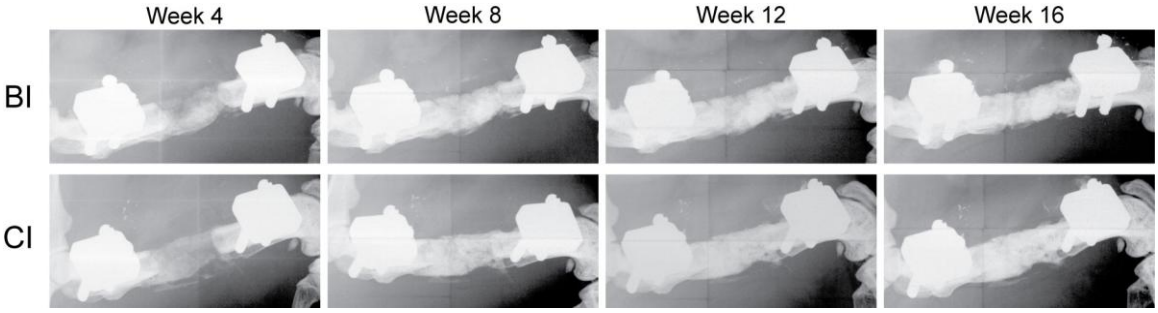

Figure 3.1. Radiographic evaluation of bone healing. Representative 2-D radiographs for bone injury and composite injury groups.

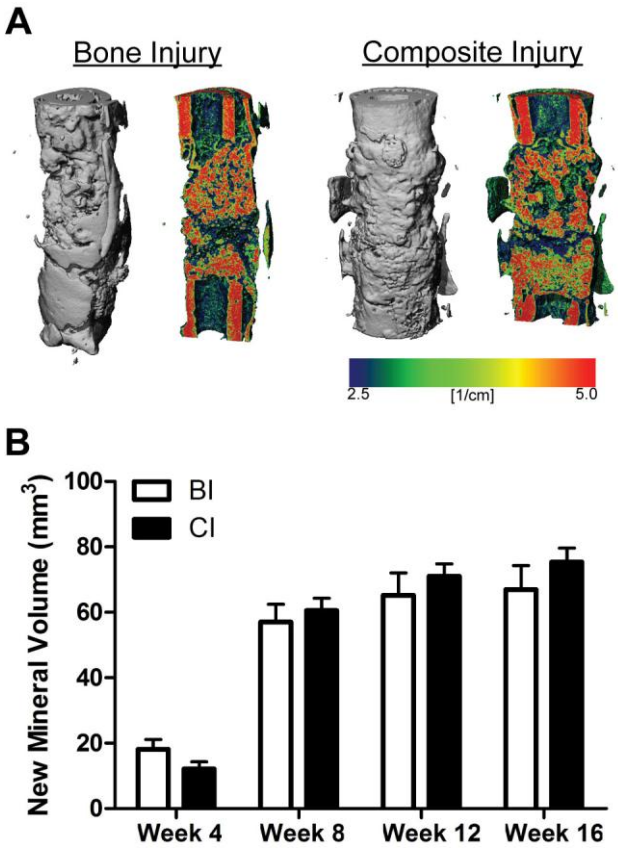

Figure 3.2. Quantitative micro-CT analysis of bone regeneration. (A) Representative 3-D reconstructions of *ex vivo* scans and cross-sections with density mapping. Native cortical bone ends have been included for orientation. (B) Longitudinal quantification of new mineral volume in the defect region from *in vivo* scans. n = 7-8 per group per time point.

Intact Femora Micro-CT Analysis

Ex vivo analysis of intact femora yielded several notable results. Intact ipsilateral femora from the nerve injury group were analyzed to evaluate the effect of the sciatic nerve injury on adaptation in the femur. The mid-diaphyseal region of these femora demonstrated lower polar moment inertia, total cross-sectional area, cortical bone cross-sectional area, cortical bone thickness, and cortical bone density compared to controls (Fig. 3.3). Medullary cavity cross-sectional area was not significantly different (Fig. 3.3). Epiphyseal trabecular bone from these femora exhibited a significantly lower bone volume fraction compared to controls, and a decrease in mean density that did not reach significance (Fig. 3.4).

The intact contralateral femora from each group were also assessed to determine whether adaptation in the mid-diaphysis or distal femur had occurred. In analysis of mid-diaphyseal cortical bone, the composite injury group demonstrated a significantly increased polar moment of inertia, cortical bone cross-sectional area, and cortical bone thickness compared to controls (Fig. 3.5). A trend toward increased total cross-sectional area was noted ($p = 0.107$); no difference was detected for medullary cavity cross-sectional area (Fig. 3.5). Epiphyseal trabecular bone from the bone injury and composite injury groups exhibited greater bone volume fraction values than those in the nerve injury group and controls, but only trended toward significance versus controls (Fig. 3.6). Mean density also appeared increased for the bone injury and composite injury groups compared to the nerve injury group and controls, but did not reach statistical significance.

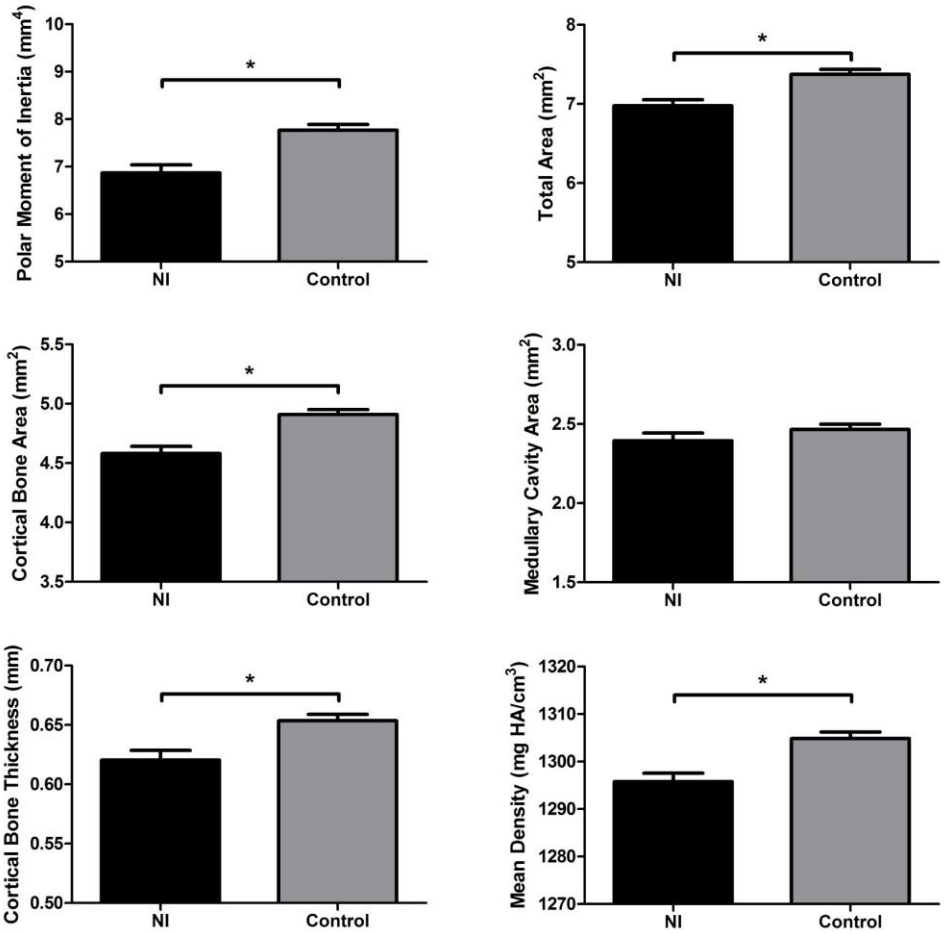

Figure 3.3. Micro-CT analysis of mid-diaphyseal cortical bone in ipsilateral intact femora from the nerve injury group. * = significantly different as indicated ($p < 0.005$). n = 8+ per group.

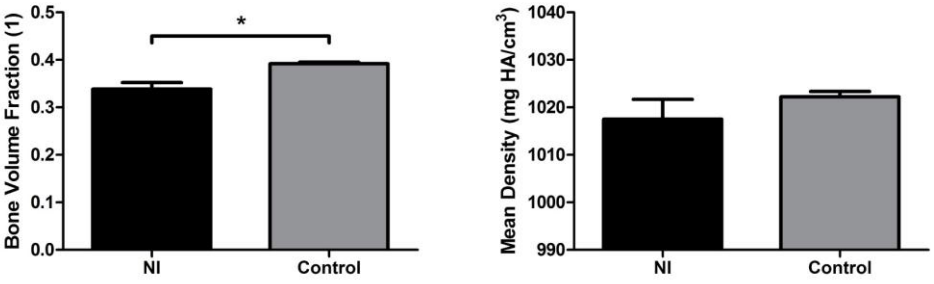

Figure 3.4. Micro-CT analysis of epiphyseal trabecular bone in ipsilateral intact femora from the nerve injury group. * = significantly different as indicated ($p < 0.0005$). n = 8+ per group.

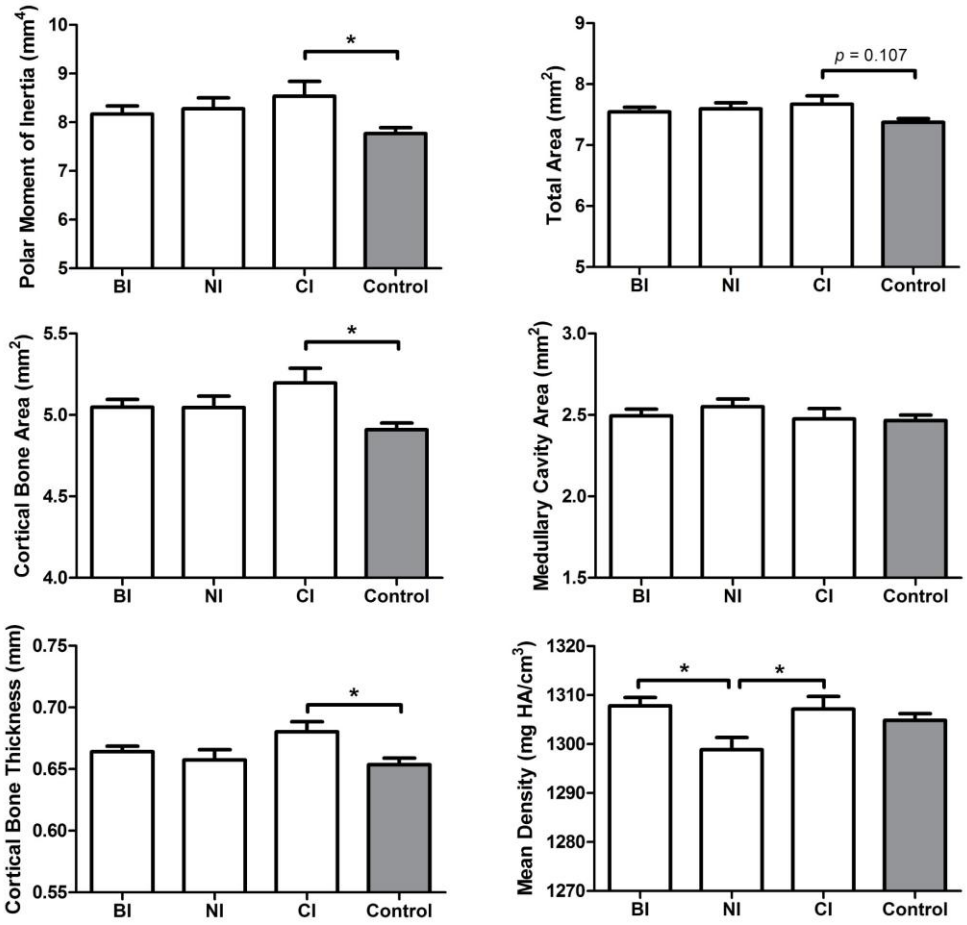

Figure 3.5. Micro-CT analysis of mid-diaphyseal cortical bone in contralateral intact femora. * = significantly different as indicated ($p < 0.05$). n = 7-8 for BI, NI, and CI. n = 12 for Control.

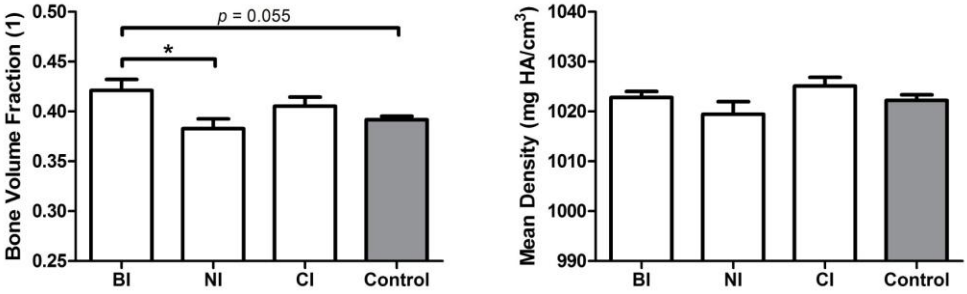

Figure 3.6. Micro-CT analysis of epiphyseal trabecular bone in contralateral intact femora. * = significantly different as indicated ($p < 0.05$). n = 7-8 for BI, NI, and CI. n = 12 for Control.

Biomechanical Testing

No differences were detected between bone injury and composite injury groups for maximum torque at failure, and both groups failed at significantly lower torque than intact controls (12.1% and 17.0% of controls, respectively) and intact ipsilateral femora from the nerve injury group (Fig. 3.7A). Intact ipsilateral femora from the nerve injury group also exhibited lower torque at failure than the control group (83.5% of controls, Fig. 3.7A). Torsional stiffness data presented slightly different results. The bone injury group exhibited significantly lower stiffness than the composite injury group, and both had lower stiffness than controls and ipsilateral nerve injury group femora (Fig. 3.7B). Differences in torsional stiffness were not significant between the ipsilateral nerve injury femora and controls (Fig. 3.7B). Intact contralateral femora from the composite injury group demonstrated a trend toward increased torque at failure ($p = 0.118$) compared to controls; no differences in torsional stiffness were observed (Fig. 3.8).

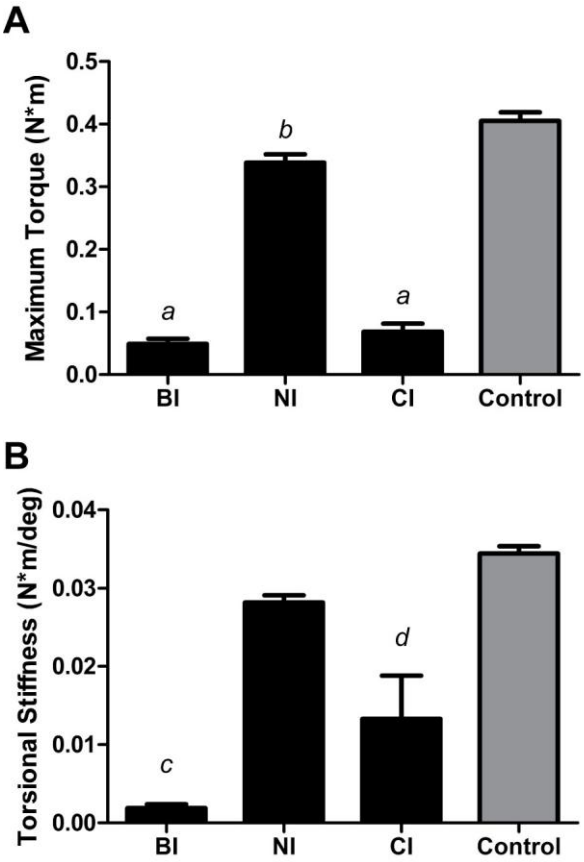

Figure 3.7. Biomechanical properties for functional assessment of regenerated bone tissue. (A) Maximum torque at failure. a = significant vs. NI and Control ($p < 0.0001$). b = significant vs. Control ($p < 0.005$). (B) Torsional stiffness. c = significant vs. NI, CI, and Control ($p < 0.05$). d = significant vs. NI and Control ($p < 0.005$). n = 7-8 for BI, NI, and CI. n = 12 for Control.

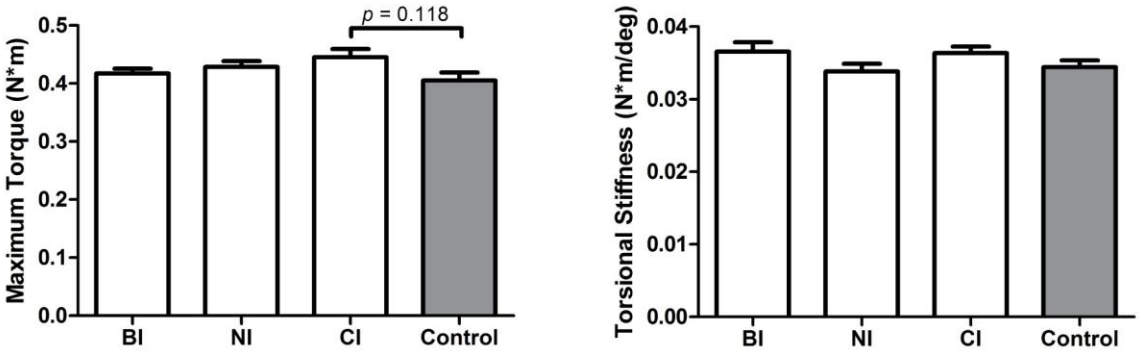

Figure 3.8. Mechanical properties of contralateral intact femora. n = 7-8 for BI, NI, and CI. n = 12 for Control.

Nerve Regeneration Histology

Regenerating nerves in nerve injury and composite injury groups appeared to have much smaller overall cross-sectional area in comparison to intact controls, in addition to possessing smaller, more densely organized myelinated axons. However, nerve injury and composite injury group sections did not appear markedly different (Fig. 3.9). Intact ipsilateral sciatic nerves from the bone injury group appeared qualitatively similar in morphology to intact controls (Fig. 3.9). Histomorphometric parameters were investigated to further probe for semi-quantitative differences in the regenerating nerves. No differences were observed between the nerve injury and composite injury groups for nerve cross-sectional area, axon density, or total axon count. Confirming qualitative observations, both groups had significantly less cross-sectional area, greater axon density, and fewer total axons compared to intact controls (Fig. 3.10).

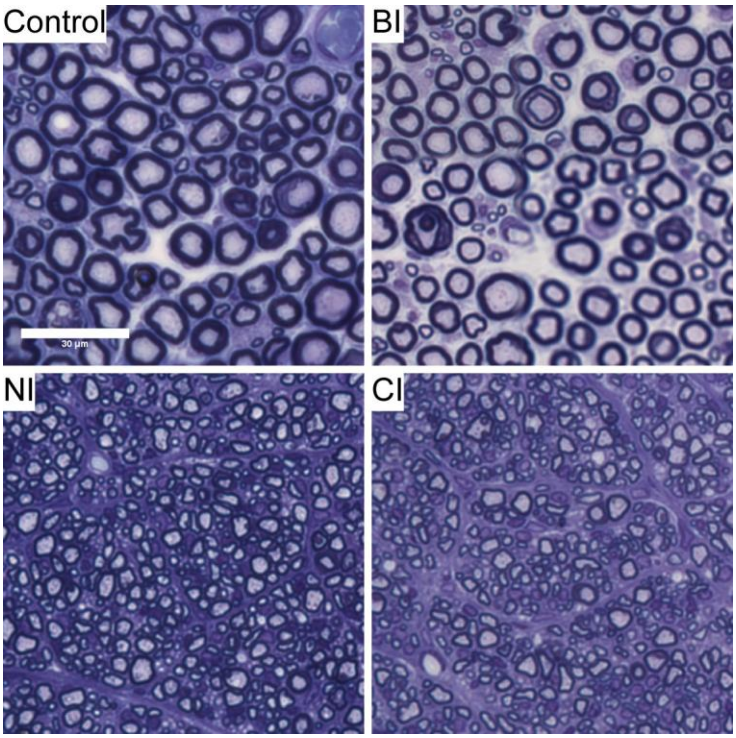

Figure 3.9. Histological assessment of nerve regeneration. Representative high-power fields (40x) from slide-mounted cross-sections of intact control sciatic nerves (Control, BI) and regenerating nerves in guidance channels (NI, CI) stained with toluidine blue to visualize myelinated axons. Scale bar = 30 µm.

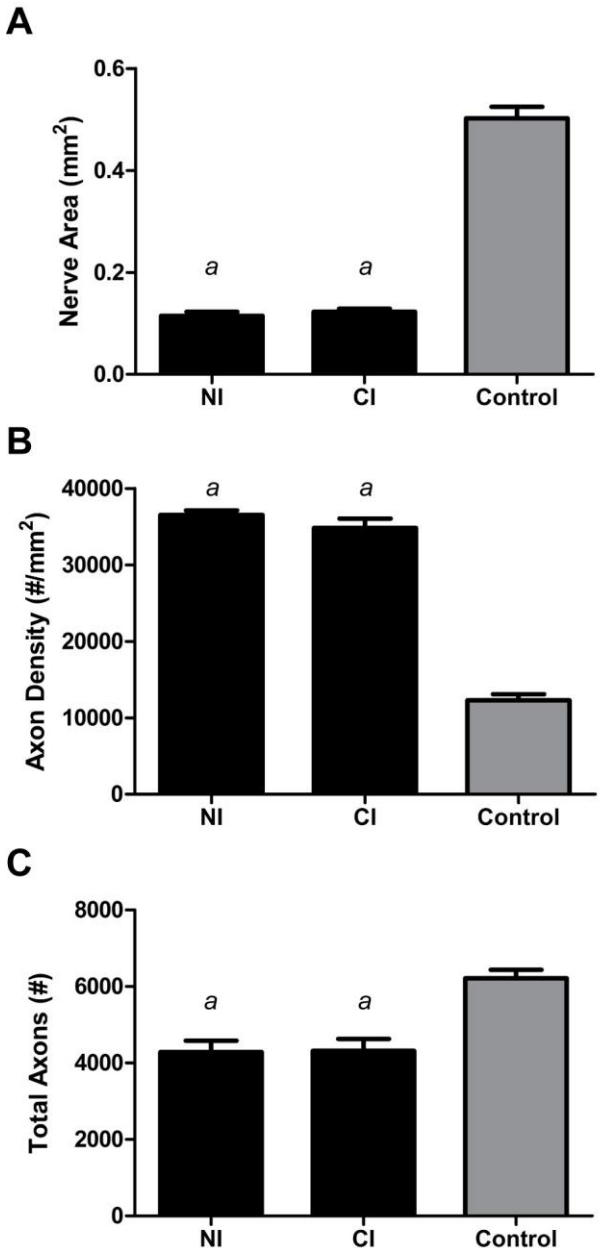

Figure 3.10. Histomorphometric analysis of nerve regeneration. (A) Total nerve tissue cross-sectional area. (B) Cross-section axon density. (C) Total number of axons in cross-sectional area. a = significant vs. Control ($p < 0.0005$). n = 8 per group.

Electrophysiology

Contractions of lower leg musculature were observed for all animals in the composite injury and nerve injury groups upon stimulation of the sciatic nerve proximal to the nerve guidance channel. No quantitative differences in evoked CNAP conduction velocity were found between the nerve injury and composite injury groups; however, both groups demonstrated significantly slower velocities compared to controls, achieving only 34% of the control nerve conduction velocity (Fig. 3.11).

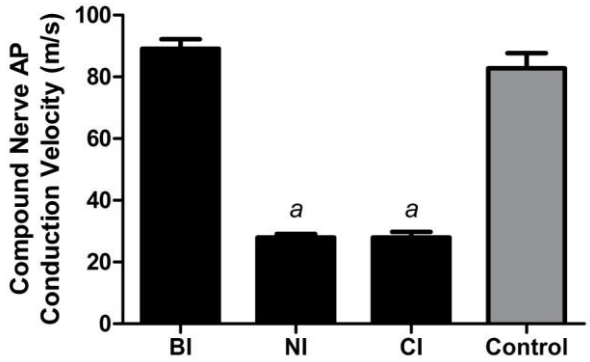

Figure 3.11. Electrophysiological determination of compound nerve action potential conductance velocity for functional assessment of regenerated nerve tissue. a = significant vs. BI and Control ($p < 0.0001$). n = 8 for NI and CI. n = 4 for BI and Control.

Gait Analysis

Quantitative gait analysis indicated that the composite injury group experienced significantly impaired limb function compared to either single-injury group. Hind paw duty cycle was investigated as a dynamic gait parameter indicative of favoring one limb versus another, with significant differences observed amongst groups. Duty cycle is calculated per step cycle as the ratio of the time a paw is in contact with the floor to the

total time of the step cycle. The nerve injury group exhibited a decrease compared to the bone injury group, whereas the composite injury group showed a decrease compared to both (Fig. 3.12A), an indication that the composite injury group spent less time weight-bearing on the injured limb compared to either single-injury group, instead favoring the contralateral limb. No groups demonstrated significant change in duty cycle over time. Hind paw print area was also used to investigate the degree of functional deficit associated with each injury model. Again, differences were observed amongst groups, but these difference varied with time post-surgery (Fig. 3.12B). In general, the nerve injury and composite injury groups had significantly lower hind paw print area ratios compared to the bone injury group. While significantly different at week 4, differences in print area ratio were not found between the nerve injury and composite injury groups at subsequent time points. Compared to pre-injury baseline measurements, all groups demonstrated a significant decrease in duty cycle and print area at week 4 that remained significant through week 16.

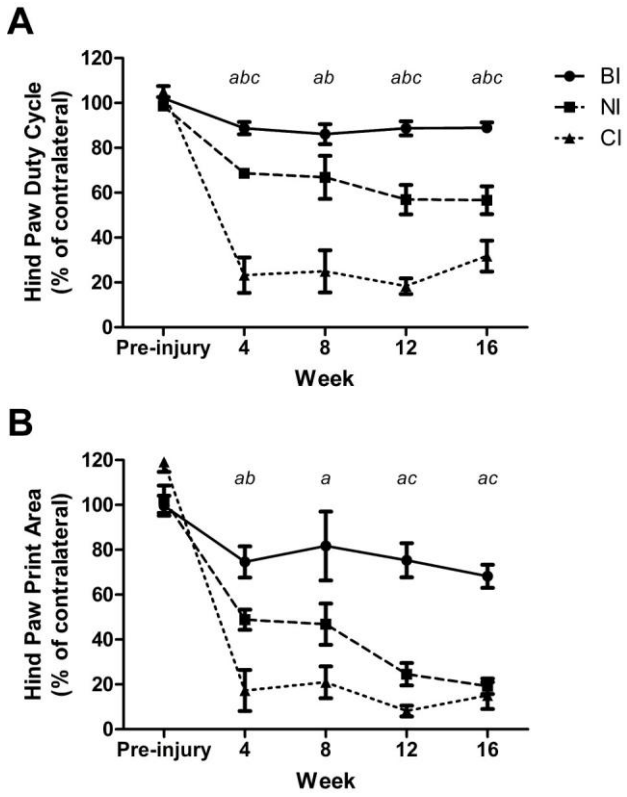

Figure 3.12. CatWalk gait analysis of limb function for parameters (A) Hind Paw Duty Cycle and (B) Hind Paw Print Area. All data represented as percent of contralateral hind paw. a = BI vs. CI significant within time point ($p < 0.05$). b = NI vs. CI significant within time point ($p < 0.05$). c = BI vs. NI significant within time point ($p < 0.05$). n = 7 per group per time point.

Discussion

To our knowledge, this study is the first to describe a rat composite injury model of severe lower limb bone and nerve trauma. Characterization of the model was performed using biomaterials-based therapeutics previously demonstrated to show promise in well-established, single-tissue injury models. Outcome parameters investigated tissue regeneration, morphological skeletal changes in the uninjured contralateral limb, and quantitative functional assessments. The latter included an evaluation of overall limb function in addition to traditional measures of individual tissue function. Interestingly, bone regeneration in the femoral defect was not significantly impaired by concomitant injury to the sciatic nerve, nor was nerve regeneration significantly impaired by bone injury. Nonetheless, despite the similar tissue regeneration observed, the composite injury group experienced a marked functional deficit in the operated limb compared to either of the single-tissue injury groups.

Although treatment resulted in consistent bridging of the defects, mechanical properties were much lower than those of intact controls. This result is attributable to the relatively low dose of rhBMP-2 (2 μg), which was chosen to limit the possibility of masking potential interactions in the healing response. Previously, Kolambkar *et al.* demonstrated that this hybrid delivery system is capable of restoring intact bone mechanical properties at a 5 μg rhBMP-2 dose (Kolambkar *et al.*, 2011). With no treatment, or vehicle alone, these defects will not heal and will progress to non-union (Oest *et al.*, 2007; Kolambkar *et al.*, 2011). Comparison of the mechanical properties between the bone injury and composite injury groups indicated no differences in the failure torque of regenerated new bone; however, the composite injury group

demonstrated greater stiffness. The latter result does not appear consequential, though, given the lack of increase in failure torque and the fact that the mean stiffness value is still only 38.7% of controls. Although there were marked differences in functional use of the operated limb between the bone injury and composite injury groups, we have little reason to believe local mechanical stimuli at healing defects were different, as much of the ambulatory load is shielded by fixation hardware (Boerckel *et al.*, 2011). Furthermore, while sciatic nerve resection would disrupt resting muscle tone in the lower leg, it would unlikely have much effect on upper leg muscle tone.

The observed decreases in mid-diaphyseal cortical bone and epiphyseal trabecular bone, as well as the decrease in failure torque, for intact ipsilateral femora in the nerve injury group are likely attributed to disuse-induced remodeling (or lack of modeling) associated with sciatic nerve resection (Robling *et al.*, 2006). Similarly, the significant increases observed in cortical bone morphology in contralateral femora from the composite injury group are likely explained by an adaptive response resulting from the demonstrated functional deficit in the injured limb. Duty cycle data clearly indicated that this group favored the contralateral limb during ambulation, and this increased weight bearing manifested itself as increased polar moment of inertia, total cross-sectional area, cortical bone cross-sectional area, and cortical bone thickness in the femur mid-diaphysis. Although changes in mid-diaphyseal cortical bone morphology were significant, the increase is failure torque trended toward, but did not quite reach, significance. These results are likely reconciled with solid mechanics theory (Boerckel *et al.*, 2011). Failure torque is a function of the minimum polar moment of inertia, whereas the μCT morphology values are only representative of the mean values in the mid-diaphysis. The

increases, although not all statistically significant, in epiphyseal bone volume fraction and mineral density in the bone injury and composite injury groups could be attributable to a systemic response to the bone injury in these groups, the osteogenic intervention, or some combination of the two. The disparity in trends between the mid-diaphysis and distal femur results may be a function of the physiological loading experienced during ambulation in the rat.

Qualitative electrophysiology indicated that all treated nerve gaps achieved some degree of functional reinnervation, with lower leg muscle contractures observed upon stimulation of the sciatic nerve proximal to the repaired gap. Regenerated nerve tissue, however, exhibited less cross-sectional area than normal sciatic nerve, and demonstrated significantly slower conduction velocities, the latter at least partially attributable to the former (Rushton, 1951). Unsurprisingly, the regenerating axons appeared smaller in diameter and possessed greater area density than those in native tissue. These results are in accordance with reports that the early stage of peripheral nerve repair is characterized by an increase in the number and density of nerve fibers as regenerating axons sprout, and these axons are smaller in diameter compared to normal nerves. Over time, regenerated axons undergo a selective pruning process, and values for axon number and density return to more normal values with an accompanying increase in average diameter (Mackinnon *et al.*, 1991). Although unable to restore fully-functional nerve tissue in the 16-week time frame, these conduits still provide a therapeutic response. Previous work has demonstrated that empty constructs are insufficient for nerve regeneration (Dodla and Bellamkonda, 2008; Kim *et al.*, 2008), and that the aligned nanofiber topography improves healing compared to random orientation (Kim *et al.*, 2008).

The exact mechanism responsible for the marked functional deficit observed in the composite injury group is unknown. This response may simply be a result of bone trauma compounding the loss of innervation to the lower leg. Presence of the fixation hardware may also augment the muscle contractures observed in sciatic nerve resection and contribute to an increased functional deficit. The time course for full functional restoration may also be longer than the 16 weeks of healing allotted in this study. The decrease in functional measures over time in the nerve injury group was another interesting result from this data. These observations may be partially explained by previous work that demonstrated slowly retreating mechanical allodynia following sensory recovery in a sciatic nerve crush model (Vogelaar *et al.*, 2004). Muscle contractures in the lower limb associated with sciatic nerve transection may also contribute if they progress in severity over time. It would be an oversight to not consider the role of a physical therapy protocol (or lack thereof) in assessing functional outcomes following extremity trauma. Physical therapy is a vital component in the rehabilitation and recovery process for human patients. In this study, the lack of a physical therapy protocol may be at least partially responsible for the persistent functional deficit; however, implementation of a standardized protocol for rats would present a multitude of logistical hurdles.

Although our primary motivation in this study was developing a small animal test bed model of limb trauma that was more clinically-relevant than traditional single-tissue models, we recognize the additional potential for composite injury models to facilitate investigation of endogenous cellular and molecular interactions that may occur in the healing response of multiple-tissue defects. Identification of such interactions could

stimulate research for innovative therapeutics to leverage combinatorial, or even synergistic, tissue repair and regeneration. Previous work has demonstrated a neural component in several aspects of bone physiology (Imai and Matsusue, 2002; Spencer *et al.*, 2004; Elefteriou, 2008). Specifically, Sample *et al.* recently demonstrated a neural contribution in the regulation of functional adaptation to loading (Sample *et al.*, 2008), and Whiteside *et al.* showed that neuropathy-induced reduction in bone mineral density is not strictly a result of reduced weight bearing on the affected limb (Whiteside *et al.*, 2006). More closely related to the research covered here, sciatic nerve resection has experimentally been shown to influence fracture healing in the tibia, yielding a larger, less dense fracture callus with diminished mechanical properties (Nordsletten *et al.*, 1994; Madsen *et al.*, 1998). Although these studies immobilized the fractured limb to prevent unequal loading for groups with or without sciatic nerve resection, disruption of resting muscle tone associated with nerve injury may have imparted differing local mechanical stimuli. Subsequent studies in the same model have implicated sensory neuropeptide calcitonin gene-related peptide (CGRP) in the impaired healing response. CGRP-immunoreactive sensory fibers are known to innervate normal bone (Bjurholm *et al.*, 1988; Mach *et al.*, 2002), have been shown to sprout and proliferate in normal fracture healing (Hukkanen *et al.*, 1993), but are reduced in tibial fracture healing disrupted by sciatic nerve resection (Hukkanen *et al.*, 1995). The specific mechanism of this response may be the potent vasodilator action of CGRP (Brain *et al.*, 1985), and its ability to stimulate endothelial cell proliferation (Haegerstrand *et al.*, 1990). Additionally, CGRP has been shown to have osteogenic capacity *in vitro* (Bernard and Shih, 1990) and *in vivo* (Ballica *et al.*, 1999).

In this study, no clear healing interactions between bone and nerve tissue were observed, which may be a consequence of the model design. Given the close anatomical proximity of the sciatic nerve and the femur (the former running just posterior to the latter in the musculature of the hamstrings), it is susceptible to injury in instances of lower extremity trauma that damage the femur. This relationship made it a logical choice for a trauma model. From a functional perspective, though, the two are not as closely related. The primary function of the sciatic nerve is to innervate the lower leg and foot. This inability for direct signaling between the femur and sciatic nerve injury sites is a potential explanation for the lack of observed healing response interactions. It may be necessary to disrupt the specific nerves responsible for innervation of the injured bone in order to observe a neuronal influence on bone healing. In support of this idea, a recent study showed that chemically-induced local sensory denervation was associated with impaired healing of femur fractures by way of a larger, less dense fracture callus, with a significantly decreased failure load (Apel *et al.*, 2009). Alternatively, it is plausible that endogenous healing of large tissue defects does not parallel the cellular and molecular responses observed in fracture healing. Additional insight may have been gained by including experimental composite injury groups in which one of the defects was left untreated (e.g., treated bone defect with untreated nerve gap). Such groups would have been able to tease out whether untreated nerve defects negatively influenced bone repair, or perhaps whether delivery of BMP-2 affected nerve regeneration.

Although differences between the composite injury model and single-injury models were not observed in tissue regeneration for outcome parameters investigated here, the difference in functional deficit was quite profound. Restoration of limb function

remains a major obstacle in limb salvage following extremity trauma in human patients. Taken together with our results, this highlights the need for tissue engineering and regenerative medicine research to benchmark technologies using quantitative measures of both tissue and limb function.

CHAPTER 4

RECOVERY FROM HIND LIMB ISCHEMIA ENHANCES BMP-2-MEDIATED SEGMENTAL BONE DEFECT REPAIR IN A RAT COMPOSITE INJURY MODEL[b]

Abstract

Although severe extremity trauma is often inclusive of skeletal and vascular damage in combination, segmental bone defect repair with concomitant vascular injury has yet to be experimentally investigated. To this end, we developed a novel rat composite limb injury model by combining a critically-sized segmental bone defect with surgically-induced hind limb ischemia (HLI). Unilateral 8 mm femoral defects were created alone (BD) or in combination with HLI (BD+HLI), and all defects were treated with rhBMP-2 via a hybrid biomaterial delivery system. Based on reported clinical and experimental observations on the importance of vascular networks in bone repair, we hypothesized that HLI would impair bone regeneration. Interestingly, the BD+HLI group displayed improved radiographic bridging, and quantitative micro-CT analysis revealed enhanced bone regeneration as early as week 4 ($p<0.01$) that was sustained through week 12 ($p<0.001$) and confirmed histologically. This effect was observed in two independent studies and at two different doses of rhBMP-2. Micro-CT angiography was used to quantitatively evaluate vascular networks at week 12 in both the thigh and the

---

[b] Portions of this chapter were adapted from Uhrig BA, Boerckel JD, Willett NJ, Li MA, Huebsch N, Guldberg RE. Recovery from hind limb ischemia enhances rhBMP-2-mediated segmental bone defect repair in a rat composite injury model. Bone. 2013; [Epub ahead of print].

regenerated bone defect. No differences were found between groups in total blood vessel volume in the thigh, but clear differences in morphology were present as the BD+HLI group possessed a more interconnected network of smaller diameter vessels ($p<0.001$). Accordingly, while the overall thigh vessel volume was comparable between groups, the contributions to vessel volume based on vessel diameter differed significantly. Despite this evidence of a robust neovascular response in the thigh of the BD+HLI group, differences were not observed between groups for bone defect blood vessel volume or morphology. In total, our results demonstrate that a transient ischemic insult and the subsequent recovery response to HLI significantly enhanced BMP-2-mediated segmental bone defect repair, providing additional complexity to the relationship between vascular tissue networks and bone healing. Ultimately, a better understanding of the coupling mechanisms may reveal important new strategies for promoting bone healing.

Introduction

Vascular tissues play an intricate role in many aspects of bone physiology, including bone repair. Blood vessel invasion is a critical step in developmental skeletogenesis as the cartilaginous intermediate is converted to bone (Gerber *et al.*, 1999; Kronenberg, 2003). Skeletal repair also recapitulates much of the developmental coupling of vascular and osseous growth (Ferguson *et al.*, 1999). A commendable amount of orthopaedic research has explored the role of angiogenesis in bone formation and repair, significantly advancing our understanding of angiogenic-osteogenic crosstalk. Angiogenesis is a necessary component in bone healing (Glowacki, 1998; Carano and Filvaroff, 2003), and inhibition has experimentally been shown to disrupt both endochondral and intramembranous pathways of bone repair (Street *et al.*, 2002).

Beyond experimental results, clinical observations reinforce the importance of vasculature in bone healing. Diminished blood supply and concomitant vascular injury are clinical risk factors for delayed or nonunion fracture healing (Dickson *et al.*, 1994; Einhorn, 1995; Brinker and Bailey, 1997), while lower limb fractures with vascular injuries experience higher rates of amputation (Glass *et al.*, 2009).

The deleterious effects of impaired vascular supply or concomitant vascular insult on clinical bone repair are certainly not surprising. Beyond the obvious physiological role of oxygen and nutrient transport, vascular networks likely also function as conduits for migrating inflammatory and progenitor cells as well as soluble factors essential for modulating the molecular signaling cascades of repair. Despite such a well-established understanding of the importance of adequate vascular networks for successful bone healing, only a few studies have investigated experimental bone repair with concomitant vascular injury (Kase *et al.*, 1998; Lu *et al.*, 2007), and none have involved bone defect repair. The lack of such research models is noteworthy, as extremity trauma with substantial skeletal damage is often accompanied by insults to the surrounding vasculature, and these injuries present unique and significant complications for clinicians (Nauth *et al.*, 2011). Additionally, insufficient vascularization is an acknowledged shortcoming of status quo bone tissue engineering strategies (Muschler *et al.*, 2004; Kanczler and Oreffo, 2008), further complicating clinical treatment strategies. Continuing to unravel the complex interactions between vascular networks and bone regeneration will help to advance the design of therapeutic interventions for skeletal repair, and ultimately improve orthopaedic trauma patient treatment outcomes.

Accordingly, our aim here was to develop a rat model of composite lower limb bone and vascular trauma to serve as a test bed for evaluating technologies to improve bone regeneration, as well as provide new insights on interactions between bone healing and vascular tissues. To do so, we incorporated surgically-induced hind limb ischemia (HLI) with a well-established segmental bone defect model. Bone defects were treated using a previously reported recombinant human bone morphogenetic protein-2 (rhBMP-2) hybrid biomaterial delivery system (Boerckel *et al.*, 2011; Kolambkar *et al.*, 2011; Kolambkar *et al.*, 2011). This system has demonstrated efficacious bone regeneration, producing bone defect bridging with functional restoration. Based on reported clinical observations and experimental results, we hypothesized that HLI would impair bone regeneration in this model.

Materials and Methods

Experimental Design

The work described here consists of two independent experiments with pooled results. Thirteen-week-old female SASCO Sprague-Dawley rats (Charles River Laboratories) were designated for one of two injury model groups: 8 mm mid-femoral bone defects alone (BD) or in combination with hind limb ischemia (BD+HLI). The initial experiment consisted of n=10 per group with each bone defect receiving a 2 μg rhBMP-2 treatment dose. This dose was chosen as it was previously shown to produce consistent bridging of defects in this model (Boerckel *et al.*, 2011), but would not be so high as to overwhelm potential effects of HLI. A second experiment was performed to confirm the findings of the first study at 2 μg rhBMP-2 (n = 4 - 5 per group) as well as evaluate a lower 0.5 μg treatment dose of rhBMP-2 previously shown to be inadequate

for bone bridging (n=5 per group) (Boerckel *et al.*, 2011). Within groups, no differences were found between experiments for the 2 μg dose, thus, results have been pooled for that dose level. All procedures were reviewed and approved by the Georgia Institute of Technology Institutional Animal Care and Use Committee and the United States Army Medical Research and Materiel Command Animal Care and Use Review Office.

Surgical Procedure

Animals were anesthetized via isoflurane inhalation and received unilateral surgeries to the left hind limb. The bone defect surgery and fixation was performed as described previously (Oest *et al.*, 2007). The hind limb ischemia technique was adapted from methods previously described for mouse models (Couffinhal *et al.*, 1998; Duvall *et al.*, 2004). Briefly, the femoral artery and vein (spanning from the inguinal ligament to the popliteal bifurcation) were dissected free from associated nerves, ligated with 6-0 silk suture, and excised. Each bone defect was treated with a hybrid nanofiber mesh and RGD-functionalized alginate hydrogel rhBMP-2 delivery system previously described (Kolambkar *et al.*, 2011). The rhBMP-2 treatment dose was 2 μg per defect, except where a lower 0.5 μg dose is indicated. Subcutaneous injections of buprenorphine were given for post-op analgesia. Animals were allowed access to food and water *ad libitum*, housed in a temperature and humidity controlled environment, and maintained on a 12:12 hour light/dark cycle.

Laser Doppler Perfusion Imaging

Laser Doppler perfusion imaging (LDPI) was used to assess blood flow to the hind limb immediately following surgery and confirm successful induction of ischemia. Anesthetized animals were shave of hair on their legs, placed on a heating pad in a supine

position and imaged (moorLDI2-IR-HR, Moor Instruments). Regions of interest analyzed were the entire leg, the foot, and the thigh. To control for possible effects of ambient temperature and lighting, each data point was expressed in terms of blood flow in the operated limb as percentage of the contralateral control limb.

Radiography

Digital 2-D radiographs (Faxitron MX-20 Digital, Faxitron X-ray Corp.) were used for qualitative *in vivo* assessment of bone regeneration. Radiograph acquisition settings were 15 s exposure time at 25 kV. Radiograph imaging was performed at 2, 4, 8, and 12 weeks post-surgery. Bony bridging was evaluated in radiographs by three blinded investigators.

Microcomputed Tomography

In vivo micro-CT scans (vivaCT 40, Scanco Medical) were performed at 4, 8, and 12 weeks post-surgery to quantitatively assess 3-D bone regeneration. Legs were oriented along the z-axis and scanned with an applied electric potential of 55 kVp, a current of 109 μA, and an isometric voxel size of 38 μm. The volume of interest (VOI) for analysis was the center 5 mm (132 slices) of each defect. New mineral was segmented through application of a global threshold corresponding to 50% of native cortical bone density. A Gaussian low-pass filter was applied for noise suppression (σ = 1.2 and support = 1).

Micro-CT Angiography

At the week 12 study end-point, contrast agent-enhanced micro-CT angiography was used to quantitatively evaluate hind limb vasculature. The technique has been

previously described in detail elsewhere (Duvall *et al.*, 2004; Boerckel *et al.*, 2011). Briefly, the vasculature was cleared with physiological saline containing 0.4% papaverine hydrochloride (Sigma-Aldrich), perfusion fixed with 10% neutral buffered formalin, rinsed again with physiological saline, and finally injected with lead chromate-based radiopaque contrast agent (2 parts Microfil MV-122 : 1 part diluent, Flow Tech). Samples were stored at 4 °C overnight to allow for polymerization of the contrast agent. Hind limbs were excised and decalcified (Cal-Ex II, Fisher Scientific) over a period of 2-3 weeks under gentle agitation with routine solution changes.

Samples were oriented with the femur along the z-axis for micro-CT scanning (vivaCT 40, Scanco Medical). Two sets of scans and VOIs were used in this analysis. Initial scans were performed on the upper leg with an applied electric potential of 55 kVp, a current of 109 μA, and an isometric voxel size of 38 μm. The VOI for the initial set of scans consisted of the entirety of the cross-section of the leg spanning between the metal fixation plate components (Thigh VOI, refer to Fig. 4.7A for illustration). A second set of higher resolution scans focused on the defect region was performed with an isometric voxel size of 21 μm. The VOI for the second set of scans consisted of a cylindrical volume 5 mm in diameter that spanned the center 7 mm of the bone defect (Defect VOI, refer to Fig. 4.9A for illustration). A global threshold was applied for segmentation of vasculature and a Gaussian low-pass filter was used for noise suppression ($\sigma = 0.8$ and support = 1).

Histology

Samples designated for histology were fixed in 10% neutral buffered formalin for 48 h at 4 °C and then decalcificied (Cal-Ex II, Fisher Scientific) over a period of 2 weeks

under gentle agitation with routine solution changes. Decalcified samples were paraffin processed and embedded. Longitudinal, 5 μm-thick sections were obtained from the central region of the defect, slide mounted, and stained with hematoxylin & eosin (H&E) or Safranin-O & fast green (Saf-O).

Mechanical Testing

Explanted femora were mechanically tested to failure in torsion as previously described (Oest *et al.*, 2007). Briefly, excess soft tissue was carefully dissected from each sample, fixation hardware was removed, and femur ends were potted in custom blocks with Wood's metal (Alfa Aesar). Potted samples were mounted in torsion fixtures and rotated through failure at a ramp rate of 3 °/s (Bose ELF 3200, Bose EnduraTEC). Rotation and torque data were recorded for each sample, from which maximum torque and torsional stiffness were determined.

Data Analysis

All data are presented as mean ± standard error of the mean (SEM). Data were analyzed using analysis of variance (ANOVA) with Tukey's *post hoc* test for pairwise comparisons or unpaired t-tests, as appropriate. The significance level was a p-value < 0.05. All data analysis was performed in Minitab 15 (Minitab, Inc.) or GraphPad Prism 5 (GraphPad Software, Inc.).

Results

All operated animals tolerated the initial surgical procedure well and returned to normal activity. A small number of samples were excluded from the study due to abscess

formation at the defect, unstable fixation, or additional bone fracture (3 animals in total). Successful induction of ischemia was demonstrated in a separate experiment (Fig. 4.1).

Higher BMP-2 Dose Bone Regeneration

At the 2 μg rhBMP-2 dose, digital 2-D radiographs displayed qualitatively similar bone regeneration between groups across the 2, 4, 8, and 12 week time points examined (Fig. 4.2A). Overall, 11 of 13 defects in the BD group went on to bony bridging. In the BD+HLI group, all 15 defects achieved bridging.

Interestingly, micro-CT analysis quantitatively demonstrated a significant increase in the amount of regenerated bone for the BD+HLI group compared to BD alone (Fig. 4.2B, C). The increase was evident as early as week 4 ($p < 0.01$, 53% increase), and was sustained through week 12 ($p < 0.001$, 44% increase).

Micro-CT results were further corroborated with histological analysis performed at week 12. H&E stained tissue sections displayed qualitatively more robust bone formation in the defects of the BD+HLI group compared to BD alone (Fig. 4.3A, B). Bone formation at the periphery of the defect (along the nanofiber mesh) was similarly robust in both groups (Fig. 4.3C, F). Differences were apparent in the central region of defects, however, with the BD+HLI group possessing qualitatively more bone tissue and less fibrous tissue (Fig. 4.3D, E, G, H). In both groups, small pockets of alginate persisted at week 12. Safranin-O staining was used to assess cartilage composition in repaired defects. Small pockets of cartilage persisted in each group, but no notable differences between groups were observed (Fig. 4.4).

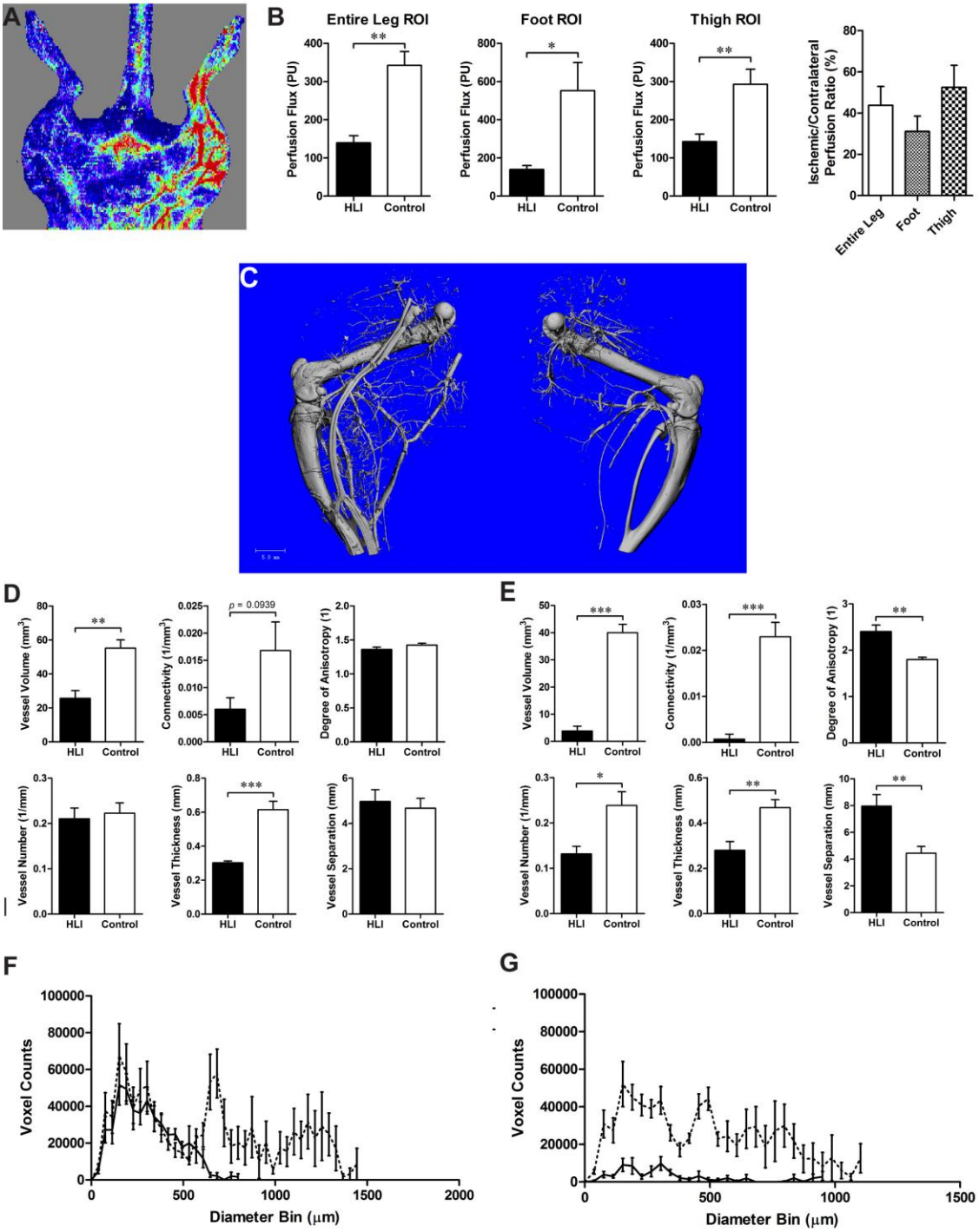

Figure 4.1. Demonstration of surgically-induced hind limb ischemia at Day 0: (A) Representative LDPI image of ischemic (left) and contralateral control (right) legs. (B) Quantified decrease in perfusion for the entire leg as well as ROIs focused on the foot and thigh. (C) Representative micro-CT angiography 3D reconstruction of ischemic (left leg, right image) and unoperated contralateral controls (right leg, left image). (D & E) Vessel volume and morphological parameters for the upper leg VOI (D) and lower leg VOI (E). (F & G) Frequency distributions of blood vessel voxel sizes for the upper leg VOI (F) and lower leg VOI (G). $*p < 0.05$, $**p < 0.01$, $***p < 0.001$. n = 5.

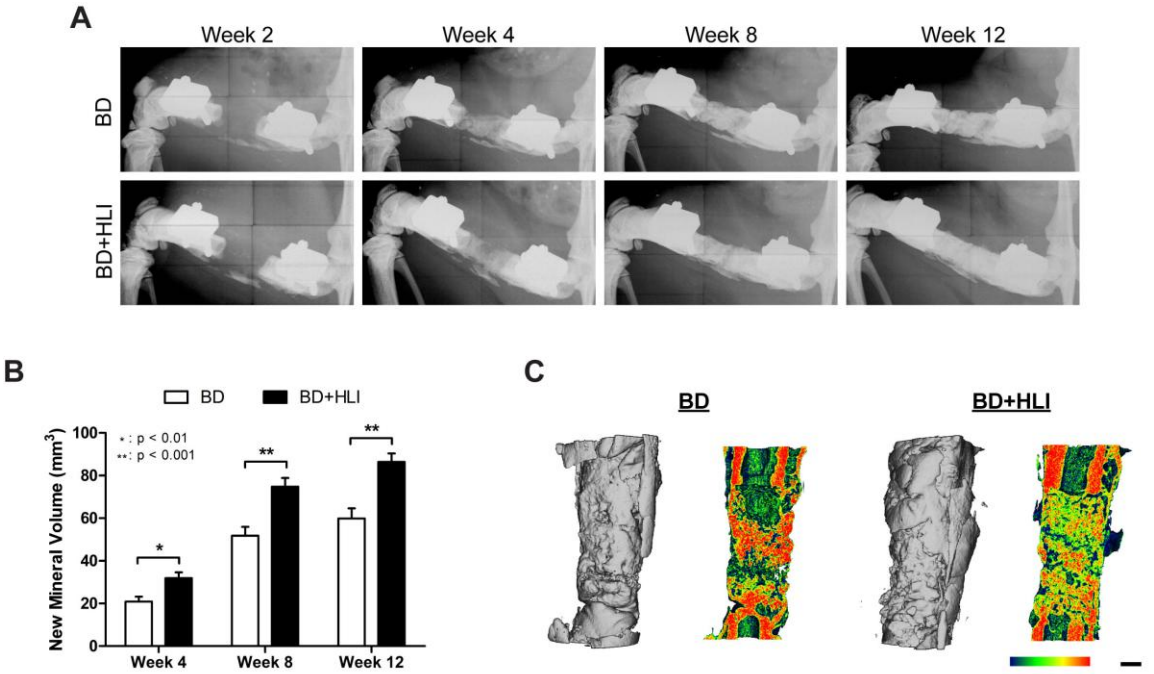

Figure 4.2. Longitudinal analysis of bone regeneration. (A) Representative digital radiographs acquired at post-surgery weeks 2, 4, 8, and 12. (B) Quantification of new mineral volume in the defect obtained from longitudinal *in vivo* micro-CT scans. (C) Representative 3D reconstructions of *ex vivo* micro-CT scans with cross-sectional mineral density maps. Native cortical bone ends have been included for reference. Scale bars: Density = 2.5 – 5 1/cm, Length = 1 mm. *: $p < 0.01$, **: $p < 0.001$. n = 13 – 15 per group.

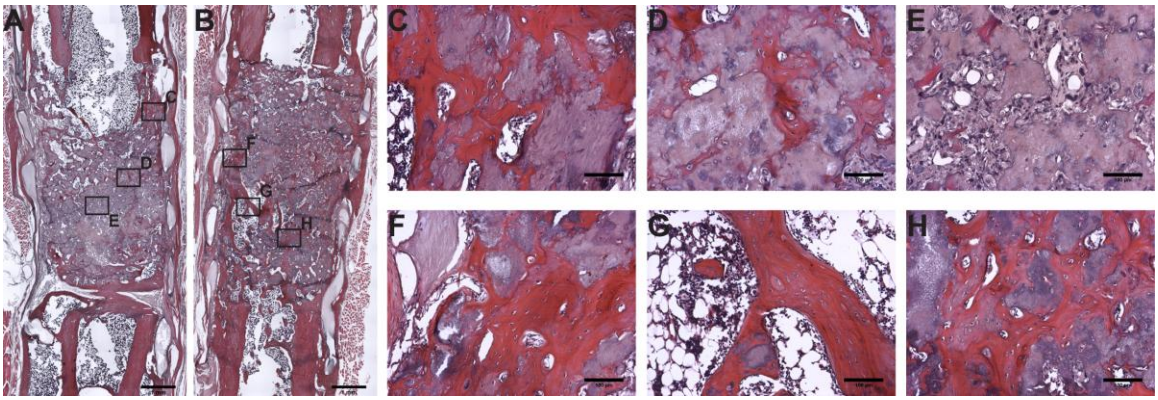

Figure 4.3. H&E histology of bone healing at 12 weeks. (A,B) Mosaic images of H&E stained mid-defect sagittal sections from the BD (A) and BD+HLI (B) groups confirmed increased bone regeneration in BD+HLI group. (C-H) Higher magnification fields from mosaic images demonstrating more robust bone formation in BD+HLI group. Magnification = 4x (A,B) and 10x (C-H). Scale bars = 1 mm (A,B) and 100 μm (C-H). Annotations: a = alginate, bm = bone marrow, ft = fibrous tissue, nb = new bone.

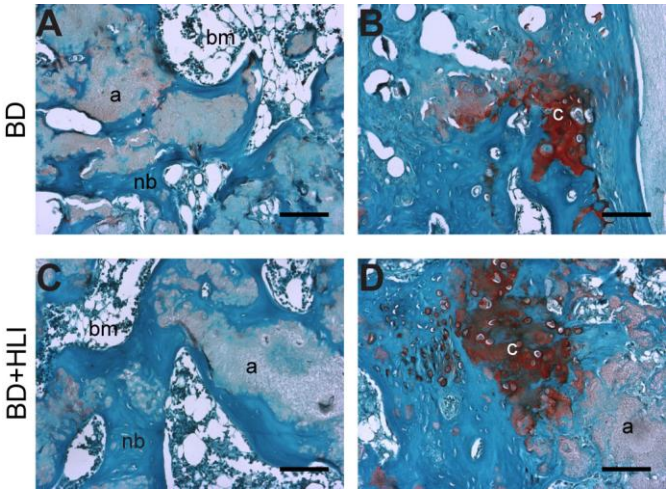

Figure 4.4. Saf-O histology of bone healing at 12 weeks. Both groups displayed new bone formation integrated with alginate hydrogel (A,C) with very few small pockets of cartilage (B,D). Magnification = 10x. Scale bars = 100 μm. Annotations: a = alginate, bm = bone marrow, c = cartilage, nb = new bone.

Torsional testing to failure was used to assess functional restoration of the regenerated bone at week 12. The BD+HLI group exhibited greater maximum torque (77% increase) and torsional stiffness (59% increase) compared to the BD group (Fig. 4.5), but differences were not statistically significant (p = 0.214 and p = 0.434, respectively). Compared to historical data of age-matched, naïve intact femur controls (maximum torque = 0.31 ± 0.04 N*m, torsional stiffness = 0.030 ± 0.003 N*m/deg, n = 6 (Kolambkar *et al.*, 2011)), the BD group achieved only 42% of maximum torque and 77% of torsional stiffness, whereas the BD+HLI group achieved 74% of maximum torque and 123% of torsional stiffness.

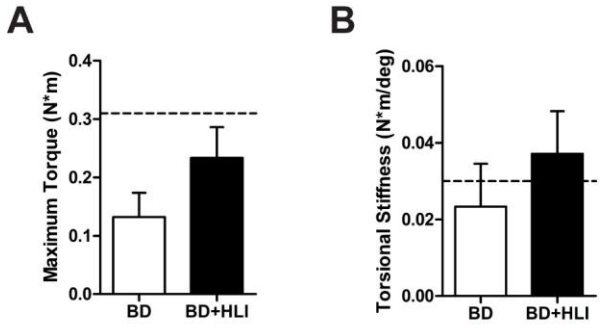

Figure 4.5. Torsional testing mechanical properties of regenerated bone at 12 weeks. (A) Maximum torque to failure and (B) torsional stiffness. Dashed lines indicate mean values for historical naïve intact controls. n = 3-4 per group.

Lower BMP-2 Dose Bone Regeneration

To further investigate these findings, an experiment was conducted using a lower 0.5 μg treatment dose of BMP-2, a dose previously demonstrated to be insufficient for consistent bridging (Boerckel *et al.*, 2011). In agreement with the findings at 2 μg dose, improved bone healing was observed in the BD+HLI group. Radiograph evaluation determined only 2 of 4 defects in the BD group achieved bony bridging; in contrast

bridging was achieved in 4 of 4 BD+HLI samples (Fig. 4.6A). Micro-CT results also showed an increase in regenerated bone volume in the BD+HLI group compared to BD alone, but did not reach statistical significance (p = 0.069 and 67% increase at week 12, Fig. 4.6A, B). Torsional testing revealed additional differences between groups (Fig. 4.6C), as the BD+HLI group displayed significantly increased maximum torque (p < 0.05, 118% increase) and a nearly 14-fold increase in torsional stiffness (p = 0.1146, 1382% increase). Compared to historical data of age-matched, naïve intact femur controls (maximum torque = 0.31 ± 0.04 N*m, torsional stiffness = 0.030 ± 0.003 N*m/deg, n = 6 (Kolambkar *et al.*, 2011)), the BD group achieved only 19% of maximum torque and 7% of torsional stiffness, whereas the BD+HLI group achieved 42% of maximum torque and 83% of torsional stiffness.

Vascular Networks

A micro-CT angiography technique was used at week 12 to quantitatively evaluate vascular volume and morphology. In the Thigh VOI (Fig. 4.7A, B), no differences in vessel volume or vessel volume fraction were evident between groups (Fig. 4.7C, D), suggesting a robust neovascular recovery response and only transient ischemia. Morphological differences were observed, however, with a more interconnected (p < 0.001) network of smaller diameter (p < 0.0001) vessels apparent in the BD+HLI group compared to BD alone (Fig. 4.7E - H). Compared to contralateral controls, both groups exhibited an approximately 60% increase in vessel volume. Both groups also showed increased vessel connectivity and number of vessels, with a decrease in vessel separation. The BD group exhibited an increase in mean vessel diameter compared to contralateral controls, while the BD+HLI group was decreased.

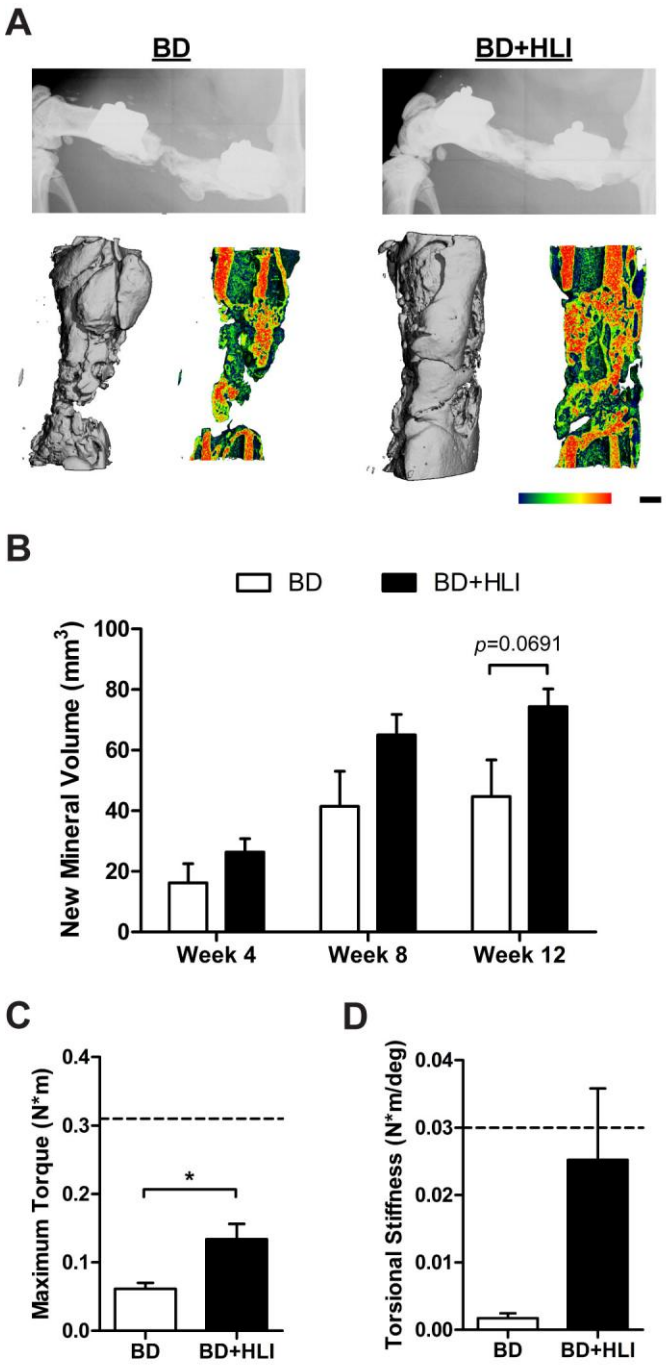

Figure 4.6. Bone repair at lower 0.5 μg rhBMP-2 dose. (A) Representative digital radiographs from week 12 and 3D micro-CT reconstructions with mineral density mapping. (B) Quantification of new mineral volume in the defect obtained from longitudinal *in vivo* micro-CT scans. (C) Maximum torque to failure and (D) torsional stiffness. Dashed lines indicate mean values for historical naïve intact controls. Scale bars: Density = 2.5 – 5 1/cm, Length = 1 mm. *: $p < 0.05$. n = 3 - 4 per group.

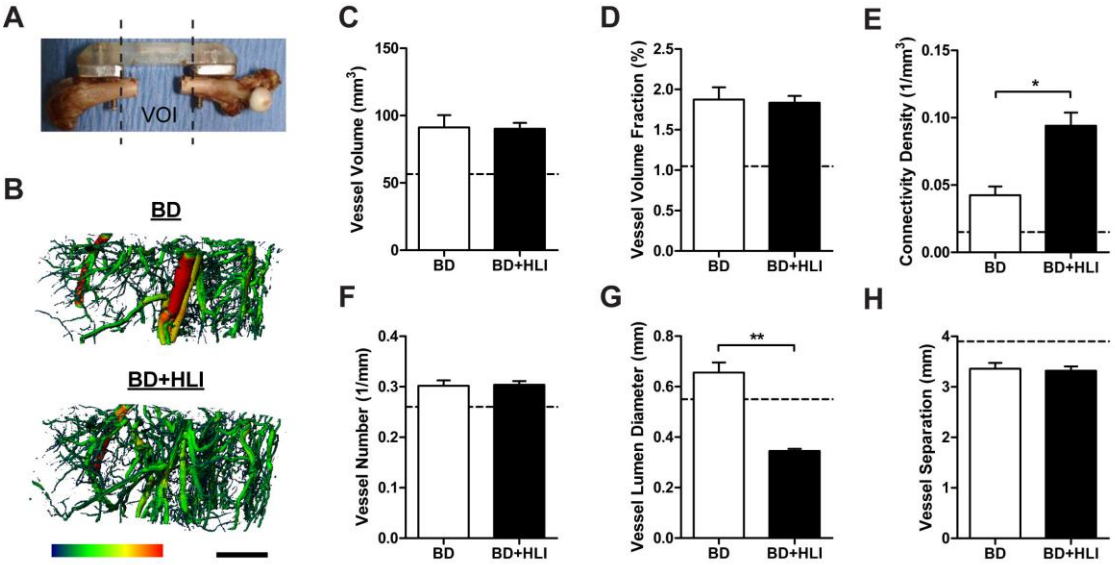

Figure 4.7. Thigh blood vessel volume and morphology at week 12. (A) Illustration of Thigh VOI. (B) Representative 3D micro-CT reconstructions with vessel diamater mapping. (C-H) Angiography parameters in the Thigh VOI: blood vessel volume (C), tissue vessel volume fraction (D), connectivity density (E), mean vessel number (F), mean vessel lumen diameter (G), and mean vessel separation (H). Dashed lines indicate mean values for contralateral controls. Scale bars: Diameter 0 – 1 mm, Length = 5 mm. *: $p < 0.001$, **: $p < 0.0001$. n = 8 per group.

Voxel count histograms provided an indication of vessel size frequency distribution. The BD+HLI group displayed a distribution skewed toward smaller diameter vessels, with an increase in vessels of luminal diameter less than ~500 μm and a lack of vessels with luminal diameter greater than ~1 mm in the BD+HLI group (Fig. 4.8A). Furthermore, while the overall vessel volume was comparable between groups, the contributions to vessel volume based on vessel diameter were significantly different between groups (Fig. 4.8B). Specifically, the BD+HLI group had a significantly greater contribution from vessels with diameters of ~200-500 μm compared to BD alone ($p < 0.005$) and significantly less contribution from vessels with diameter larger than ~1 mm ($p < 0.0001$). While contributions to vessel volume were rather uniform in the BD group (22% - 28% across the 4 bins of analysis), 75% of vessel volume in the BD+HLI group came from vessels with diameter less than ~500 μm (Fig. 4.8C).

Analysis of the Defect VOI revealed no differences between groups in terms of blood vessel volume or morphology (Fig. 4.9).

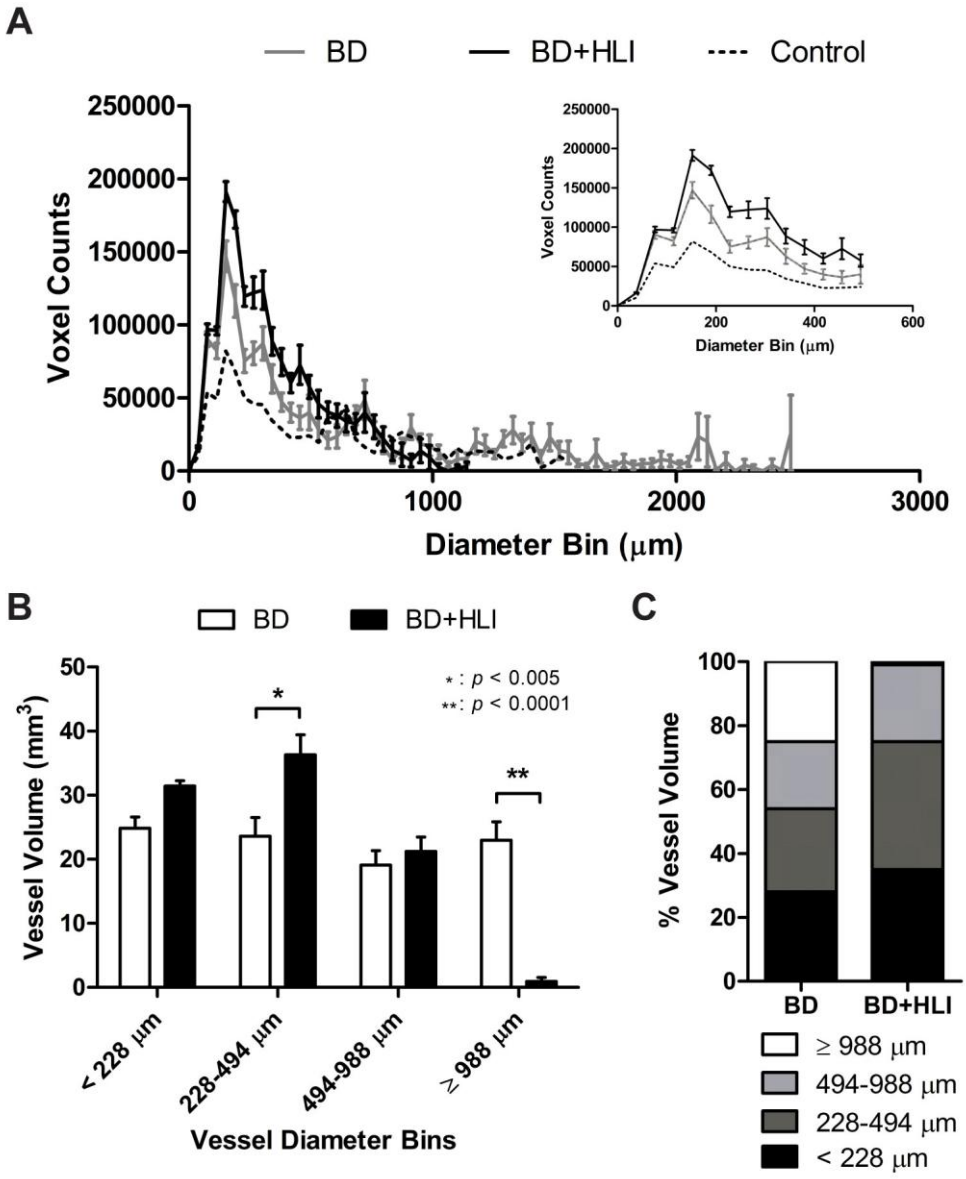

Figure 4.8. Thigh blood vessel diameter frequency distributions and contributions to vessel volume at week 12. (A) Frequency distribution of blood vessel voxel sizes from the Thigh VOI that give a representative distribution of blood vessel diameter. (Inset) Magnification of the 0 – 494 μm bins. (B) Contributions to blood vessel volume from different vessel diameter ranges. (C) Contributions to vessel volume expressed as a percent of total vessel volume. *: $p < 0.005$, **: $p < 0.0001$. n = 8 per group.

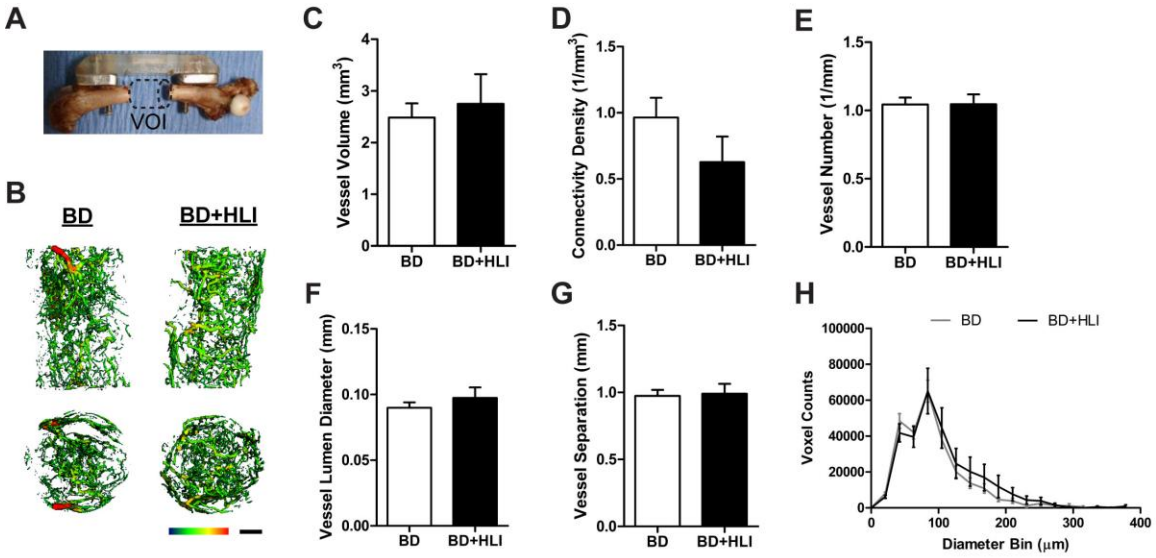

Figure 4.9. Bone defect blood vessel volume and morphology at week 12. (A) Illustration of Defect VOI. (B) Representative 3D micro-CT reconstructions with vessel diameter mapping. Side views (upper) and proximal top down views (lower) of the cylindrical volume are shown. (C-H) Angiography parameters in the Defect VOI: blood vessel volume (C), connectivity density (D), mean vessel number (E), mean vessel lumen diameter (F), mean vessel separation (G), and vessel diameter frequency distribution (H). Scale bars: Diameter 0 – 200 μm, Length = 1 mm. n = 8 per group.

Discussion

The established relationships between vascular tissues and bone repair provide compelling motivation for new research models to advance our understanding of the coupling mechanisms, as well as methods to improve treatment for orthopaedic trauma patients with concomitant vascular insults. Here we sought to address the specific lack of a small animal model of severe composite bone and vascular trauma by pairing a critically-sized mid-femoral defect with surgically-induced hind limb ischemia in the rat. Interestingly, our data did not support our original hypothesis, as recovery from transient HLI enhanced bone regeneration compared to bone defects without concomitant vascular injury. These observations were both repeatable and robust across varying levels of rhBMP-2 stimulation. Although initially unexpected, these findings are notable, and understanding the underlying mechanisms may have important implications for clinical therapeutics.

Bone regeneration and mechanical properties for the BD group here were consistent with previously published data for both the 2 μg and 0.5 μg rhBMP-2 doses (Boerckel *et al.*, 2011; Kolambkar *et al.*, 2011). Importantly, with no treatment, or vehicle alone, these defects will not heal and will progress to non-union (Oest *et al.*, 2007; Kolambkar *et al.*, 2011). One of the most interesting observations here was the transformation of the non-healing 0.5 μg rhBMP-2 dose to a healing one with concomitant HLI. In general, bone healing in the BD+HLI group was comparable with results historically observed in bone defects treated with higher rhBMP-2 doses (e.g., 2 μg similar to 5 μg; 0.5 μg similar to 1 – 2.5 μg) (Boerckel *et al.*, 2011; Kolambkar *et al.*, 2011). These historical comparisons were consistent with the results here, as both bone

regeneration and mechanical properties for the 0.5 μg BD+HLI group were comparable to those of the 2 μg BD group. This is an interesting point for future consideration given the high costs and incompletely understood (and at times negative) effects associated with current supraphysiologic doses of BMPs administered to human patients (Garrison *et al.*, 2007; Cahill *et al.*, 2009; Devine *et al.*, 2012; Even *et al.*, 2012). Furthermore, the delivery hydrogel used here provides more prolonged growth factor release kinetics than the clinical gold standard for rhBMP-2 delivery (Boerckel *et al.*, 2011; Kolambkar *et al.*, 2011), which may be important in allowing for crosstalk between vascular growth processes and bone repair. In addition, given the wide variety of physiological processes that BMP-2 has been implicated in, including blood vessel growth and remodeling (Deckers *et al.*, 2002; Langenfeld and Langenfeld, 2004), it is conceivable that in this specific model the rhBMP-2 provided an additional indirect bone healing stimulus by augmenting the vascular tissue response to ischemia. A better understanding of the coupling mechanisms involved in the model presented here may produce new therapeutic strategies that would allow for lower doses of rhBMP-2 to be used in humans without sacrificing efficacy.

One potential explanation for the enhanced bone regeneration in the BD+HLI group is a robust endogenous vascular response to ischemia. While the HLI surgical procedure was demonstrated to effectively create an initial substantial reduction in perfusion of the leg, it is understood from other work that this is a transient effect due primarily to arteriogenic growth of collateral vessels in the limb (Couffinhal *et al.*, 1998; Duvall *et al.*, 2004). Murine models of HLI are widely used in the field of vascular biology and recovery from HLI induced by femoral artery ligation has been shown to be

background strain dependent in mice, ranging from necrosis of the limb to restoration of perfusion within a few days (Helisch *et al.*, 2006). In rat models of femoral artery ligation, restoration of resting perfusion appears to possess an intermediate recovery length, having been reported at 5 -7 days (Seifert *et al.*, 1985; Corcoran *et al.*, 2009). Deficits in reserve blood flow have longer duration, extending beyond 14 days (Corcoran *et al.*, 2009), and it is unknown what influence a concomitant orthopaedic injury may have on the recovery time. As evidenced by the micro-CT angiography results, blood vessel volume was not different between groups at week 12. One limitation of the micro-CT angiography technique (as with other angiography techniques), however, is an inability to distinguish between arterial and venous supply, perhaps obscuring important insights regarding vascular networks. Vessels with luminal diameters larger than 1 mm are almost exclusively the femoral artery and vein (especially the latter). This vessel size range exhibited significantly different contributions to vessel volume between groups (25% for BD, 1% for BD+HLI). The fact that the femoral vessels were excised in the BD+HLI group, yet no differences in total blood vessel volume were observed, may suggest increased arterial blood supply to the thigh in this group. The increases in vessel volume, connectivity, number of vessels, and decrease in vessel separation in each group compared to contralateral controls is an expected wound healing response. Whereas the BD+HLI group exhibited a decrease in mean vessel lumen diameter compared to contralateral controls, the BD group actually exhibited an increase. This may be indicative of vasodilation of vessels in this group or some degree of arteriogenesis. Importantly, the results presented here provide only a single snapshot of post-injury blood vessel growth and remodeling at the week 12 end point, and do not preclude

additional differences at earlier time points. Ongoing experiments are studying vessel networks early in the healing process in order to provide additional insight into the transient response characteristics and to better interpret these results.

Post-injury vascular growth in this model likely occurs through a combination of angiogenesis and arteriogenesis. Angiogenesis is understood to be an essential component to the bone healing processes (Glowacki, 1998; Carano and Filvaroff, 2003). Previous work has demonstrated the role of hypoxia inducible transcription factor-1α (HIF-1α), an angiogenic transcription factor under inhibitory control in normoxic conditions, in coupling angiogenesis and osteogenesis during bone repair primarily through a VEGF-mediated mode of action (Wan *et al.*, 2008; Schipani *et al.*, 2009). The HLI surgery may affect tissue oxygen tension which would implicate a role for HIF-1α and VEGF in the results observed here. Endogenous VEGF is known to be essential in both intramembranous and endochondral bone healing processes, and delivery of exogenous VEGF has been shown to improve fracture and bone defect repair (Street *et al.*, 2002). VEGF may also up-regulate BMP-2 expression in vascular tissues via paracrine loops (Bouletreau *et al.*, 2002; Matsubara *et al.*, 2012) or act through direct binding with osteoblast VEGF receptors (Deckers *et al.*, 2000; Clarkin and Gerstenfeld, 2013).

Arteriogenesis offers a viable additional, if not alternative, method of augmented post-injury vascular growth. In small animal models of HLI, the upper leg is thought to primarily undergo arteriogenic growth of collateral arteries due to increased shear stress experienced by arterioles as they attempt to compensate for greater blood flow demands, whereas the lower leg primarily experiences angiogenesis in response to hypoxia

(Schaper and Scholz, 2003). This would seem to imply that although new vessel formation in the bone defect may be due to angiogenesis, arteriogenesis may be a more, relevant vascular tissue growth process in our model; however, a direct role for arteriogenesis in bone repair is not yet well-defined. In agreement with this hypothesis, recent work from Morgan *et al*. demonstrated that the vascular growth associated with distraction osteogenesis is characterized by initial arteriogenic remodeling of vessels in the surrounding skeletal muscle compartment with subsequent vessel ingrowth to the regenerating distraction space (Morgan *et al.*, 2012) .

It is also possible that HLI augments the gene expression, soluble factor availability, cellular populations mobilized to the injury site and surrounding areas, or some combination thereof. In this way, the endogenous vascular response to HLI may play more of an indirect role in enhancing the bone repair process in the BD+HLI group as opposed to exerting a direct influence. The extracellular matrix protein osteopontin is significantly up-regulated in response to HLI (Lyle *et al.*, 2012), plays a definitive role in collateral vessel development and recovery from ischemia (Duvall *et al.*, 2008), and is involved in regulating several aspects of fracture healing (Duvall *et al.*, 2007). Other growth factors associated with arteriogenesis such as platelet derived growth factor, transforming growth factor-β, fibroblast growth factor-2 (Buschmann *et al.*, 2003), have also been implicated in bone regeneration (Kempen *et al.*, 2010), and provide additional means of molecular cross-talk in these processes. At a cellular level, monocyte/macrophage invasion plays a significant role in collateral vessel growth following arterial occlusion (Arras *et al.*, 1998). Arteriogenic macrophages have been reported to be of an M2/wound-healing phenotype (Takeda *et al.*, 2011), and

macrophages may possess a capacity for osteoinductive signaling through BMP-2 secretion (Champagne *et al.*, 2002). Through such mechanisms, activation or mobilization of an augmented macrophage population due to concomitant HLI may have had downstream effects on bone repair in our model. Vascular smooth muscle cells (SMC) also play a critical cellular role in arteriogenic vessel remodeling, with phenotypic changes and proliferation initiating early in the process (Schaper and Scholz, 2003). Additionally, SMCs are considered at least partially responsible for vascular tissue calcification (Trion and van der Laarse, 2004), potentially in a process also involving macrophages (Trion and van der Laarse, 2004; Ikeda *et al.*, 2012). Pericytes, which are more commonly associated with the microvessels, may also play some role in the bone regeneration results observed here as a perivascular source of osteoprogenitor cells (Towler, 2007; Crisan *et al.*, 2008; Caplan and Correa, 2011).

Consideration should also be given to the role that the surrounding skeletal muscle envelope plays in this model, given that at the very least it is the site of extensive vascular growth and remodeling. In related work, our group recently demonstrated that volumetric muscle loss attenuated rhBMP-2-mediated segmental bone defect repair in a rat model of composite bone and skeletal muscle injury (Willett *et al.*, 2012). This effect is thought to be at least partially attributable to diminished vascular growth, but may also involve reduced availability of skeletal muscle resident osteoprogenitor cells and cytokines/growth factors involved in transmitting the necessary signaling cascades.

To our knowledge, the work here is the first to combine segmental bone defect repair with concomitant vascular injury. Two previously published models have investigated fracture healing in combination with an ischemic injury. Lu *et al*. found that

ischemia induced by femoral artery resection impaired healing of murine tibial fractures, with reduced blood vessels in and around ischemic leg fractures (Lu *et al.*, 2007). Kase *et al.* reported no differences in rat tibial fracture healing when acute ischemia/reperfusion was incorporated via tourniquet and microvascular clip application/removal (Kase *et al.*, 1998). The disparity in results from those two studies is most likely attributable to the varying degrees of ischemia induced. The model of Lu *et al.* is most similar to our own, with the inverse bone repair findings perhaps resulting from the location of orthopaedic injury, and the implications this would have on the relevant vascular growth processes. In our model, the bone defect is adjacent to the vascular injury by design in order to mimic a localized injury, whereas in the model of Lu *et al*., the fracture is further downstream of the vascular injury, perhaps producing a more hypoxic environment. The other confounding factor between the models is the rhBMP-2 delivery included here. Interestingly, in a follow-up study, Lu *et al*. found that delivery of rhBMP-7 improved ischemic fracture healing and was associated with increased tissue vascularity (Lu *et al.*, 2010).

Overall, our results did not validate our original hypothesis and suggest that this model does not recapitulate complications associated with vascular compromised clinical bone healing. This is most likely due to differences in scale of human patients versus small animal models, and the observation that the rat HLI injury induced a robust vascular response and only transient limb ischemia. However, the unexpected results of this study are important as they shed further light on the complex interactions between bone healing and vascular tissue growth. Future work to improve understanding of the underlying mechanisms could provide useful insight to exploit this interaction and guide

development of novel therapeutic strategies for challenging clinical bone healing scenarios.

Bone repair is intimately linked to vascular growth and remodeling processes. Here we describe a novel model of composite tissue trauma combining a segmental bone defect with concomitant vascular injury. Contrary to our original hypothesis, our results demonstrated that the recovery response to HLI significantly enhanced BMP-2-mediated segmental bone defect repair in this model. Despite a robust neovascular response in the thigh of the group with HLI, differences were not observed between groups for bone defect blood vessel volume and morphology. These results suggest additional mechanisms of interaction beyond the direct vascular response, perhaps inclusive of augmented cellular exchange, gene expression, soluble factor availability, or some combination thereof. In sum, the work presented here provides additional complexity to the relationship between vascular tissues and bone healing, and a better understanding of the associated coupling mechanisms may reveal important new strategies for promoting bone healing.

CHAPTER 5

EARLY VASCULAR GROWTH AND GENE EXPRESSION IN BMP-2-MEDIATED SEGMENTAL BONE DEFECT REPAIR WITH OR WITHOUT CONCOMITANT HIND LIMB ISCHEMIA

Abstract

Bone repair involves a highly coordinated orchestration of complex physiological processes, with growth of vascular networks and initiation of biological signaling cascades serving as critical early events. Previously, our group reported the interesting results of enhanced rhBMP-2-mediated bone regeneration in a rat composite injury model where a critically-sized 8 mm mid-femoral bone defect was combined with surgically-induced hind limb ischemia (BD+HLI) compared to the bone defect alone (BD). To explain these findings, we hypothesized that inclusion of HLI had coupled to the bone repair process by way of an augmented vascular tissue growth response or perturbed signaling cascades initiated in the bone defect region or surrounding skeletal muscle envelope. Laser Doppler perfusion imaging and micro-CT angiography data demonstrated a robust neovascular growth response rapidly initiated in the thigh of the BD+HLI group; however, ingrowth of blood vessels at the bone defect did not differ significantly between groups, indicating that HLI does not augment vascularization at the site of bone regeneration. Using qRT-PCR analysis, the expression of a panel of genes related to osteogenesis, vascular growth, and inflammation was investigated in the bone defect and the adjacent adductor muscle tissue. While multiple genes were upregulated compared to naïve control tissue in both the bone defect and the adductor muscle, only

minor differences in gene expression were observed between the BD and BD+HLI groups. Thus, the stimulatory effects of HLI on bone regeneration cannot be explained by gene expression alone for the genes and time points investigated here. In total, the work here provides important new insights on early vascular growth and gene expression in segmental bone defect models, but does not completely explain how recovery from HLI enhances bone regeneration. Additional future work to further elucidate mechanisms coupling the HLI response with bone repair may reveal important new strategies for promoting bone healing in challenging clinical scenarios.

Introduction

Vascular network growth and biological signaling cascades are critical early events in the progression of bone repair. Complex biological processes, beginning with the initial injury, inflammation, and hematoma formation, are orchestrated by a variety of inflammatory signaling molecules, growth and differentiation morphogens, and extracellular matrix proteins (Mehta *et al.*, 2012). Invading inflammatory cell types involved in hematoma formation are inclusive of polymorphonuclear cells, platelets, macrophages, and lymphocytes that coordinate and secrete a variety of cytokines and growth factors necessary for the initiating the proper cascade of morphogenetic events. Such factors include tumor necrosis factor-α (TNF-α), interleukins-1 and -6 (IL-1 and IL-6), receptor activator of nuclear factor kappa-B ligand (RANKL), macrophage colony stimulating factor (M-CSF), and multiple chemokines including monocyte chemotactic protein-1 (MCP-1/CCL-2) (Mountziaris and Mikos, 2008; Kolar *et al.*, 2010; Pape *et al.*, 2010). Additional secreted signaling molecules such as member of the transforming growth factor-β (TGF-β), bone morphogenetic protein (BMP), platelet derived growth

factor (PDGF), vascular endothelial growth factor (VEGF), fibroblast growth factor (FGF), insulin-like growth factor (IGF) and matrix metalloproteinase (MMP) families will then facilitate the ongoing mediation of inflammation, promote vascular growth, and initiate the recruitment of osteoprogenitors and uncommitted mesenchymal stem cells that will actively participate in bone repair (Gerstenfeld *et al.*, 2003; Schindeler *et al.*, 2008; Mehta *et al.*, 2012).

Angiogenic blood vessel ingrowth is a subsequent and necessary component in bone healing, initiating within the first few weeks of the repair process and continuing through resolution of callus remodeling (Glowacki, 1998; Carano and Filvaroff, 2003). Furthermore, targeted disruption of angiogenesis is known to impair bone healing through both the endochondral and intramembranous repair pathways (Hausman *et al.*, 2001; Street *et al.*, 2002). Given the significance of vascular support networks in bone healing outcomes, extremity trauma involving significant skeletal injuries and concomitant insults to the surrounding vasculature presents unique and significant complications for clinical management (Nauth *et al.*, 2011). Tissue engineering and regenerative medicine represent potential solutions for the current unmet clinical needs of reconstruction; however, bone tissue engineering strategies have yet to overcome the status quo limitations of poor vascularization (Muschler *et al.*, 2004; Kanczler and Oreffo, 2008).

In addition to angiogenesis, arteriogenesis – the development of collateral vessels via the growth and remodeling of preexisting arterioles – may play a role in bone healing. Recently, it was reported that arteriogenesis in the surrounding skeletal muscle precedes angiogenesis at the site of distraction osteogenesis bone repair (Morgan *et al.*, 2012).

Yet, the degree to which arteriogenesis might influence bone repair, directly or indirectly, remains unclear. In animal models of hind limb ischemia (HLI), arteriogenesis is the primary vascular growth process by which tissue blood perfusion is restored (Scholz *et al.*, 2002; Schaper and Scholz, 2003). Arteriogenesis is an inflammation driven process, brought about by an increase in fluid shear stress that results in an "activated" endothelium, prompting the production of endothelial nitric oxide synthase (eNOS) and MCP-1, as well as upregulation of endothelial cell adhesion molecules (Scholz *et al.*, 2000; Cai and Schaper, 2008). These signals combine to promote circulating monocyte extravasation into the vessel wall which initiates remodeling. Although monocytes/macrophages are required for the initiation of remodeling, vascular smooth muscle cells (VSMCs) perform most of the work load of arteriogenesis. While the key cellular mediators of arteriogenesis are known, to date, no growth factors have been identified as possessing an essential regulatory function, although the CSF, FGF, PDGF, and angiopoietin (ANG) signaling axes are thought to have potential roles (Cao *et al.*, 2003; Deindl *et al.*, 2003; Schaper and Scholz, 2003; Tressel *et al.*, 2008)

In Aim II of this thesis, we developed a novel composite tissue injury model of severe bone and vascular trauma in the rat to better understand experimentally the complex interactions between vascular tissue growth and segmental bone defect repair (Uhrig *et al.*, 2013). The model consisted of a critically-sized 8 mm mid-femoral bone defect in combination with surgically-induced hind limb ischemia. Interestingly, we observed enhanced bone regeneration in the group with HLI compared to the bone defect alone. We hypothesized that inclusion of HLI had coupled to the bone repair process by way of an augmented vascular tissue growth response or perturbed signaling cascades

initiated in the bone defect region or surrounding skeletal muscle envelope. The aim of the present work was to begin to test this hypothesis by characterizing early spatiotemporal changes in blood flow and vascular tissue growth, as well as gene expression within the bone defect and adjacent adductor muscle tissues.

Materials and Methods

Experimental Design

Thirteen-week-old female SASCO Sprague-Dawley rats (Charles River Laboratories) were designated for one of two surgical injury model groups: 8 mm mid-femoral bone defects alone (BD) or in combination with hind limb ischemia (BD+HLI). Each bone defect received a 2 μg rhBMP-2 treatment dose delivered in a hybrid nanofiber mesh and RGD-modified alginate hydrogel system previously described (Kolambkar *et al.*, 2011). This dose was chosen as it was known to produce consistent bridging of defects in the bone defect model (Boerckel *et al.*, 2011), was previously used for investigating long-term bone repair in the composite bone and vascular injury model (Uhrig *et al.*, 2013), and was unlikely to be high enough to overwhelm any effects of HLI. In some experiments a third group was included in which an additional set of BD+HLI rats were treated with alginate containing no rhBMP-2 (BD+HLI Blank). All procedures were reviewed and approved by the Georgia Institute of Technology Institutional Animal Care and Use Committee and the United States Army Medical Research and Materiel Command Animal Care and Use Review Office.

Surgical Procedure

Animals were anesthetized via isoflurane inhalation and received unilateral surgeries to the left hind limb. The bone defect surgery and fixation was performed as described previously (Oest *et al.*, 2007). Briefly, a critically-sized 8 mm bone defect was created in the mid-diaphysis of the femur and stabilized by custom-made modular internal fixation plates with the use of miniature screws. The hind limb ischemia technique was adapted from methods previously described for mouse models (Couffinhal *et al.*, 1998; Duvall *et al.*, 2004), and was performed as previously described (Uhrig *et al.*, 2013). Briefly, the femoral artery and vein (spanning from the inguinal ligament to the popliteal bifurcation) were dissected free from associated nerves, ligated with 6-0 silk suture, and excised. Each bone defect was treated with a hybrid nanofiber mesh and RGD-modified alginate hydrogel rhBMP-2 delivery system previously described (Kolambkar *et al.*, 2011). A perforated, tubular electrospun nanofiber mesh was placed into the defect region such that it enveloped the cut ends of native bone. A 150 μL volume of rhBMP-2-containing functionalized alginate hydrogel was then injected into the defect space (lumen of the nanofiber mesh). The rhBMP-2 treatment dose was 2 μg per defect, except in the case of the blank group where the injected alginate hydrogel contained no rhBMP-2. Subcutaneous injections of a sustained-release formulation of buprenorphine (ZooPharm) were given for post-op analgesia (Foley *et al.*, 2011). Animals were allowed access to food and water *ad libitum*, housed in a temperature and humidity controlled environment, and maintained on a 12:12 hour light/dark cycle.

Laser Doppler Perfusion Imaging

Laser Doppler perfusion imaging (LDPI) was used to assess blood flow to the hind limb immediately prior to surgery and at post-surgery days 1, 3, 7, and 14 (n = 5-17

per group per time point). Anesthetized animals were shaved of hair on both legs, placed on a heating pad, and imaged (moorLDI2-IR-HR, Moor Instruments). A prone position was used for imaging of the foot pad, and in a supine position for imaging of the leg. Regions of interest (ROI) analyzed were the footpad, the entire leg, and a focal adductor muscle region. To control for possible effects of ambient temperature and lighting, each data point was expressed in terms of blood flow in the operated limb as percentage of the contralateral control limb. Age-matched, unoperated control animals were also included (n = 4 per group per time point).

Radiography

Digital 2-D radiographs (Faxitron MX-20 Digital, Faxitron X-ray Corp.) were used for qualitative *in vivo* assessment of bone regeneration. Radiograph acquisition settings were 15 s exposure time at 25 kV.

Micro-CT Angiography

Contrast agent-enhanced micro-CT angiography was used to quantitatively evaluate hind limb vasculature at post-surgery day 3, 7, and 14 time points (n = 3-5 per group per time point except BD+HLI at day 3 where n = 2). The technique has been previously described in detail elsewhere (Duvall *et al.*, 2004; Boerckel *et al.*, 2011). Briefly, the vasculature was cleared with physiological saline containing 0.4% papaverine hydrochloride (Sigma-Aldrich), perfusion fixed with 10% neutral buffered formalin, rinsed again with physiological saline, and finally injected with a lead chromate-based radiopaque contrast agent (2 parts Microfil MV-122 : 1 part diluent, Flow Tech). Samples were stored at 4 °C overnight to allow for polymerization of the contrast agent.

Hind limbs were excised and decalcified (Cal-Ex II, Fisher Scientific) over a period of 2-3 weeks under gentle agitation with routine solution changes.

Samples were oriented with the femur along the z-axis for micro-CT scanning (vivaCT 40, Scanco Medical). Two sets of scans and VOIs were used in this analysis. Initial scans were performed on the upper leg with an applied electric potential of 55 kVp, a current of 109 μA, and an isometric voxel size of 38 μm. The VOI for the initial set of scans consisted of the entirety of the cross-section of the leg spanning between the metal fixation plate components (Thigh VOI, refer to Fig. 5.5C for illustration). A second set of higher resolution scans focused on the defect region was performed with an isometric voxel size of 21 μm. The VOI for the second set of scans consisted of a cylindrical volume 7 mm in diameter that spanned the center 7 mm length of the bone defect (Defect VOI, refer to Fig. 5.7C for illustration). The 7 mm diameter used for the Defect VOI was inclusive of the 5 mm diameter of nanofiber mesh and the immediately adjacent tissue extending 1 mm radially. A global threshold was applied for segmentation of vasculature and a Gaussian low-pass filter was used for noise suppression ($\sigma = 0.8$ and support = 1).

Histology

Samples designated for histology (n = 1-2 per group per time point) were fixed in 10% neutral buffered formalin for 48 h at 4 °C and then decalcified (19% EDTA) over a period of 2 weeks under gentle agitation with routine solution changes. Decalcified samples were paraffin processed and embedded. Longitudinal, 5 μm-thick sections were obtained from the central region of the defect, slide mounted, and stained with hematoxylin & eosin (H&E) or Safranin-O & Fast Green (Saf-O).

Quantiative Real-Time Reverse Transcription Polymerase Chain Reaction

Gene expression analysis was performed for post-surgery days 7, 14, and 21(n = 3-6 per group per time point) using quantitative real-time reverse transcription polymerase chain reaction (qRT-PCR). A detailed protocol can be found in Appendix A.4. Tissue samples were harvested from the bone defect region (tissue contained within nanofiber mesh) and adductor muscles using instruments cleaned with RNaseZap (Sigma-Aldrich) and were immediately placed in RNAlater reagent (Ambion). Samples were stored overnight at 4 °C and then transferred to -20 °C storage until RNA isolation. Purified RNA was obtained from homogenized tissue samples using the RNeasy Mini Kit (Qiagen) by following the manufacturer's protocol for fibrous tissues with two minor modifications: 1) homogenized samples were incubated in lysis buffer for 5 min at room temperature prior to proceeding with proteinase K incubation and 2) following proteinase K incubation, samples were transferred to QIAshredder columns (Qiagen) for centrifugation. Concentration and purity of RNA samples were determined by spectrophotometry (NanoDrop 1000, Thermo Scientific).

Synthesis of cDNA samples was performed from 500 ng of total RNA using RT^2 First Strand Kits (SABiosciences) according to manufacturer's instructions. Preliminary gene expression data was generated using commercially available rat-specific pathway-focused microarrays for osteogenesis and inflammatory cytokines & receptors (SABiosciences) on a MyiQ real-time PCR cycler (Bio-Rad). Gene expression of a selected panel of genes (Table 5.1) was then investigated using custom designed arrays (SABiosciences). Expression of each gene of interest was normalized to endogenous controls hypoxanthine phosphoribosyltransferase 1 (*Hprt1*) and ribosomal protein, large,

P1 (*Rplp1*) which were empirically selected based on their stability of expression in prelimary data. Gene expression was then normalized to control tissue from unoperated animals (femur bone and adductor muscles) using the $\Delta\Delta C_t$ method. RNA quality control was performed to test for RNA integrity, inhibitors of reverse transcription, PCR amplification, and DNA contamination. Consistency of C_t values was verified by performing linear regression on a scatter plot of technical replicates. The fitted line had a slope of 1.01 and an r^2 value of 0.97.

Table 5.1. Genes selected for custom qRT-PCR arrays

Gene Symbol	Full Name	Refseq #
Opn (Spp1)	Osteopontin	NM_012881
Col1a1	Collagen, type I, alpha 1	NM_053304
Runx2 (Cbfa1)	Runt-related transcription factor 2	NM_053470
Osx (Sp7)	Osterix	NM_181374
Rankl (Tnfsf11)	Receptor activator of nuclear factor kappa-B ligand	NM_057149
Bmp2	Bone morphogenetic protein 2	NM_017178
Pdgfb	Platelet-derived growth factor beta polypeptide	NM_031524
Igf1	Insulin-like growth factor 1	NM_178866
Vegfa	Vascular endothelial growth factor A	NM_031836
Vegfr2 (Kdr)	Vascular endothelial growth factor receptor 2	NM_013062
Fgfr1	Fibroblast growth factor receptor 1	NM_024146
Fgfr2	Fibroblast growth factor receptor 2	NM_001109892
Acta2	Smooth muscle alpha-actin	NM_031004
Mmp9	Matrix metallopeptidase 9	NM_031055
Ccl2 (Mcp1)	Chemokine (C-C motif) ligand 2	NM_031530
Cd163	CD163 molecule	NM_001107887
Ccr7	Chemokine (C-C motif) receptor 7	NM_199489
Cxcl5	Chemokine (C-X-C motif) ligand 5	NM_022214
Cxcl10 (Ip10)	Chemokine (C-X-C motif) ligand 10	NM_139089
Hprt1	Hypoxanthine phosphoribosyltransferase 1	NM_012583
Rplp1	Ribosomal protein, large, P1	NM_001007604

Data Analysis

All data are presented as mean ± standard error of the mean (SEM). Data were analyzed using two-factor analysis of variance (ANOVA) with Tukey's *post hoc* test for pairwise comparisons as appropriate. Gene expression data was transformed using Box-Cox methodology prior to statistical analysis (Box and Cox, 1964). The significance level was a p-value < 0.05. All data analysis was performed in Minitab 15 (Minitab, Inc.) or GraphPad Prism 5 (GraphPad Software, Inc.).

Results

All operated animals tolerated the initial surgical procedure well and returned to normal activity following surgery.

Early Bone Regeneration

Histological evaluation of bone regeneration at early time points supported our previously reported results (Uhrig *et al.*, 2013) that bone formation was enhanced in the BD+HLI group compared to BD alone. At day 7, no bone formation was observed within the defect for either group, but new bone had begun forming on the outside of the nanofiber mesh in the BD+HLI group (Fig. 5.1A, D). By day 14, new bone formation was evident in both groups along the outside of the nanofiber mesh, and in some perforations in the BD+HLI group (Fig. 5.1B, E). Within the defect, small pockets of chondrocytes were also found for both groups. By day 28, new bone was forming throughout the defect in both groups (Fig. 5.1C, F), but appeared qualitatively more substantial in the BD+HLI group, an observation supported by radiographs (Insets).

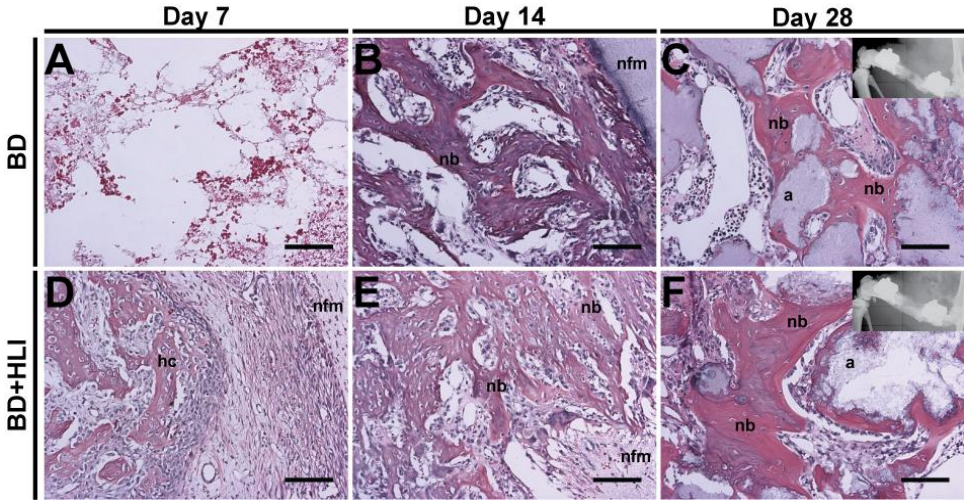

Figure 5.1. Histological evaluation of early bone regeneration. Micrographs of H&E stained sections showing progression of bone regeneration demonstrated enhanced regeneration in BD+HLI group. At day 7, no bone formation was observed within the defect for either group, but new bone had begun forming on the outside of the nanofiber mesh in the BD+HLI group (A,D). By day 14, new bone formation was evident in both groups along the outside of the nanofiber mesh, and in some perforations in the BD+HLI group (B,E). By day 28, new bone was forming throughout the defect in both groups (C,F), but appeared qualitatively more robust in the BD+HLI group, an observation supported by radiographs (Insets). Annotations: a=alginate, hc=hypertrophic chondrocytes, nb=new bone, nfm=nanofiber mesh, v=blood vessel. Scale bar=100μm. Images acquired at 10X.

Early Vascular Response

LDPI was used to evaluate blood perfusion in multiple ROIs following surgery. A sustained impairment of distal perfusion was observed in the foot pad of the operated limb in the BD+HLI group, with significantly reduced blood flow compared to the BD group at all time points investigated ($p < 0.0001$ for all time points). Initially reduced to 15% of the contralateral leg at day 1, a gradual increase in perfusion was evident for the BD+HLI group, but by day 14, foot pad perfusion had still only achieved 42% of the contralateral limb (Fig. 5.2). When examining the ROI encompassing the whole leg, the BD+HLI group displayed a significant reduction in perfusion at day 1compared to controls ($p < 0.05$, 55% of contralateral leg) but had recovered to 82% by day 3, a level that was no longer statistically significant. The BD group displayed gradually increasing perfusion as early as day 1 and peaking with a significant increase over naïve controls at day 7 ($p < 0.01$, 145% of contralateral leg). Perfusion in the BD+HLI group was significantly less than the BD group at all post-surgery time points for the leg ROI (Fig. 5.3 A, B). When evaluating an ROI focused on the adductor region of the legs, however, the BD+HLI group displayed a significant increase in perfusion compared to both the BD group and naïve controls at all post-surgery time points. Conversely, no change in adductor region perfusion was observed in the BD group compared to naïve controls (Fig. 5.3A, C). Additionally, no differences in perfusion were observed between the BD+HLI and BD+HLI Blank groups (Fig. 5.4).

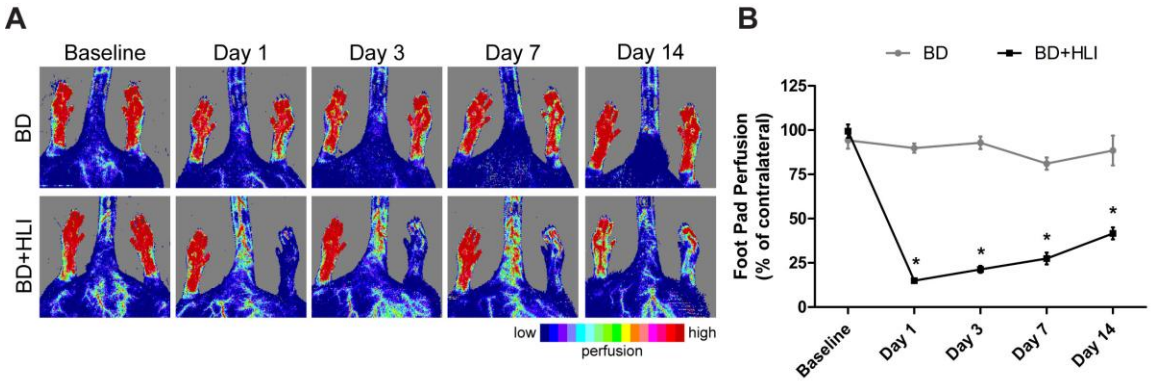

Figure 5.2. LDPI footpad analysis for BD and BD+HLI groups. (A) Representative images show the time course of changes in distal limb perfusion. (B) Quantitative analysis of footpad perfusion in the operated limb as a percent of the unoperated contralateral limb. *$p < 0.0001$ for BD vs. BD+HLI. n = 5-17 per group per time point.

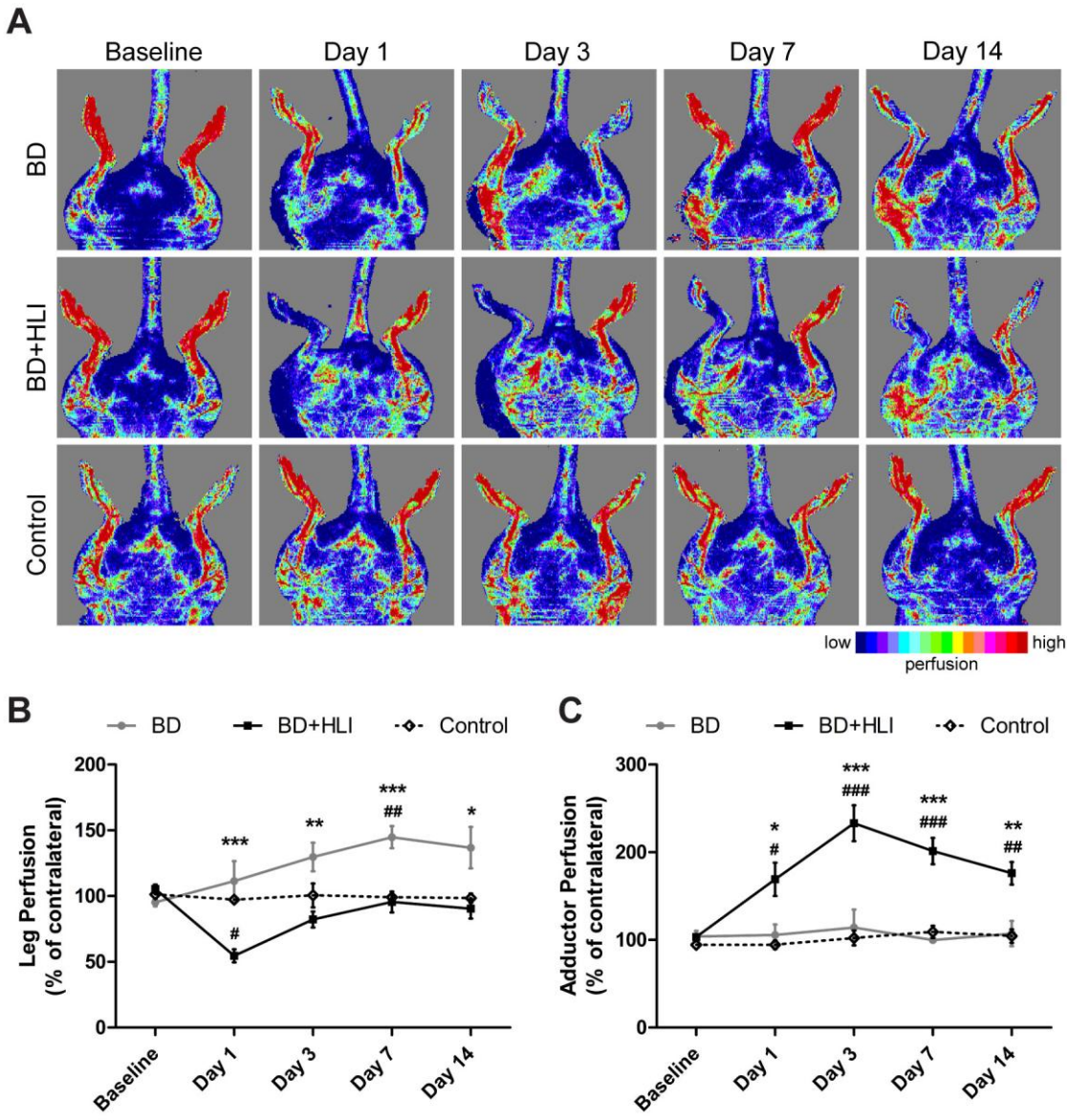

Figure 5.3. LDPI leg and adductor analysis for BD, BD+HLI, and naïve controls. (A) Representative images show the time course of changes in perfusion. (B) Quantitative analysis of perfusion in the operated limb as a percent of the unoperated contralateral limb using an ROI encompassing the whole leg. (C) Quantitative analysis of adductor perfusion in the operated limb as a percent of the unoperated contralateral limb. *$p < 0.05$ for BD vs. BD+HLI. **$p < 0.01$ for BD vs. BD+HLI. ***$p < 0.001$ for BD vs. BD+HLI. $^{\#}p < 0.05$ vs. control. $^{\#\#}p < 0.01$ vs. control. $^{\#\#\#}p < 0.001$ vs. control. n = 5-17 per group per time point except controls where n = 4.

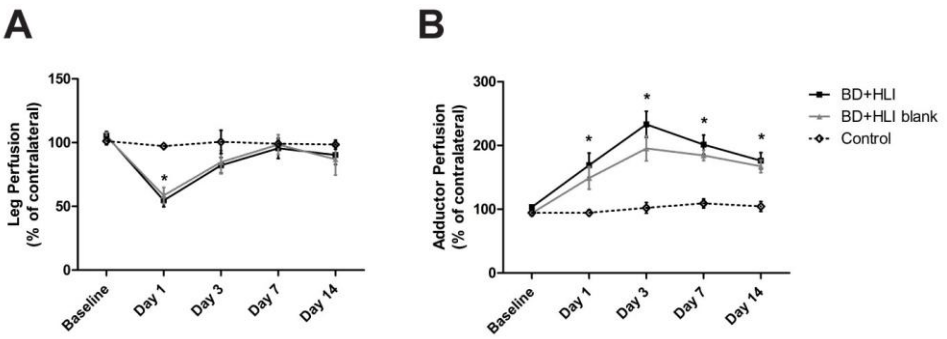

Figure 5.4. LDPI leg and adductor analysis for BD+HLI, BD+HLI Blank, and naïve controls. $^{\#}p < 0.05$ for both BD+HLI and BD+HLI Blank vs. Control. n = 5-17 per group per time point except controls where n = 4.

Micro-CT angiography was used to quantitatively evaluate vascular volume and morphology at days 3, 7, and 14 post-surgery. Collateral vessel formation in the adductor muscle tissue was evident in the BD+HLI group as early as day 3 as evidenced by newly identifiable, tortuous vessels (Fig. 5.5A, B). Vascular growth was observed in both groups with increased vessel volume in the Thigh VOI of the operated legs compared to contralateral legs at all time points. Despite the loss of the conduit femoral artery and vein, the BD+HLI group had a greater normalized blood vessel volume compared to BD alone at all 3 time points, and a statistically significant difference between these two groups ($p < 0.05$) was found in two-factor ANOVA analysis of the data (Fig 5.5C). Morphological parameters showed similar vessel connectivity, mean vessel number and mean vessel separation between groups; however, the BD+HLI group had a significant reduction in mean vessel thickness and was significantly more isotropic in orientation ($p < 0.01$, Fig. 5.6). Analysis of the Defect VOI showed similar vascular growth and morphology between groups. In both groups, vessel volume increased over time (Fig. 5.7), as did connectivity density, mean vessel number, and mean vessel thickness, with mean vessel separation and degree of anisotropy decreasing over time (Fig.5.8).

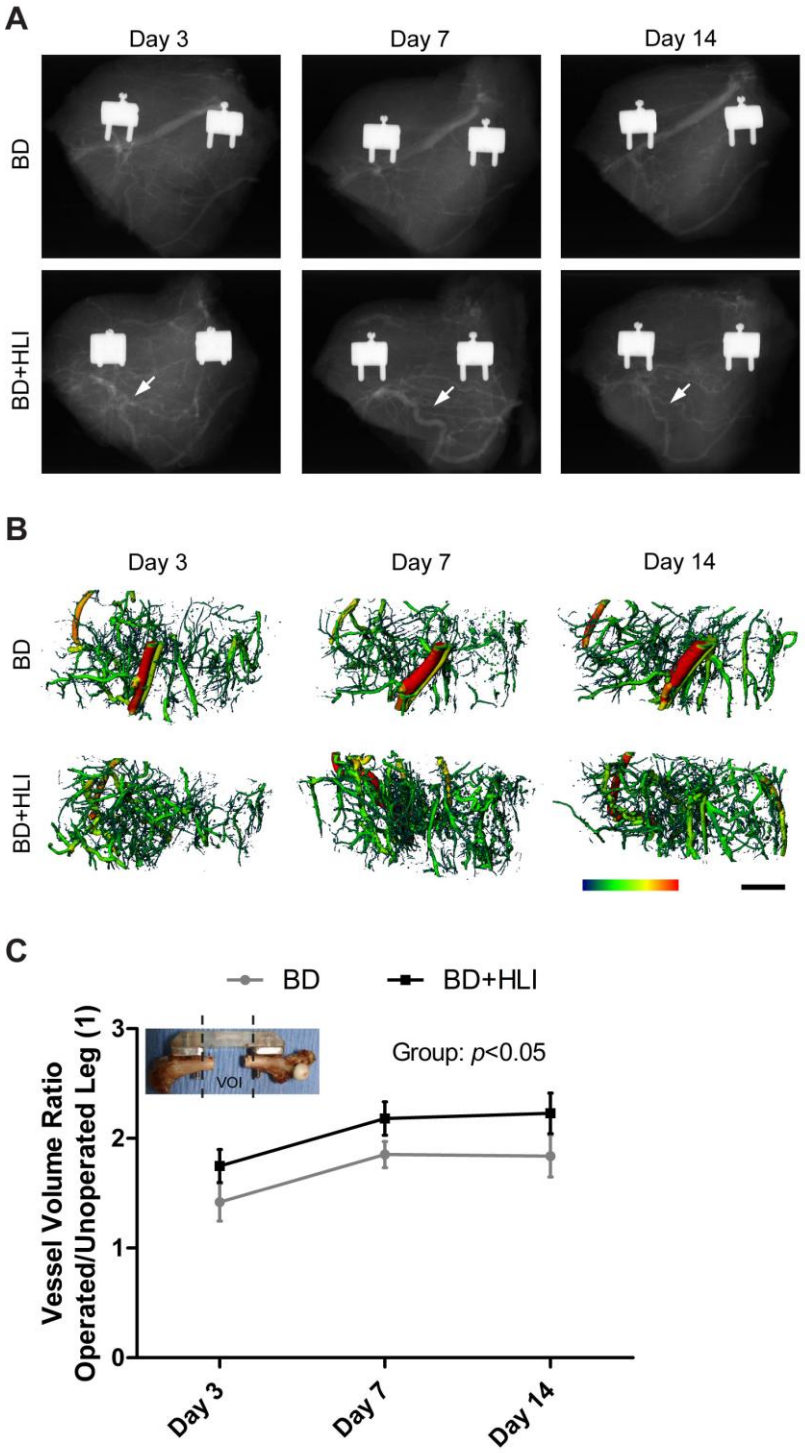

Figure 5.5. Micro-CT angiography analysis of the thigh vascular volume. (A) Representative scout view radiographs at each time point investigated. Arrows indicate collateral vessels. (B) Representative 3D micro-CT vessel reconstructions with vessel diameter mapping. Scale bars: diameter = 0-1mm, length = 5mm. (C) Quantification of vessel volume in the thigh of the operated limb normalized to the unoperated contralateral limb. n = 3-5 per group per time point except BD+HLI at day 3 where n = 2.

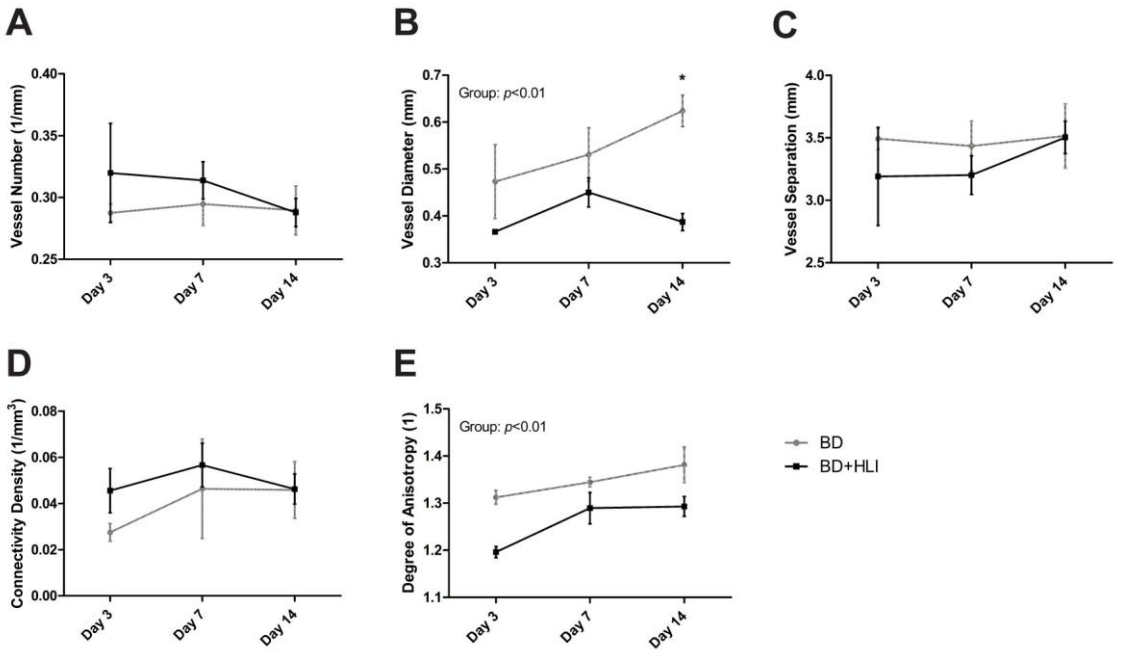

Figure 5.6. Micro-CT angiography analysis of thigh vasculature morphometry. *p<0.05 BD vs. BD+HLI. n = 3-5 per group per time point except BD+HLI at day 3 where n = 2.

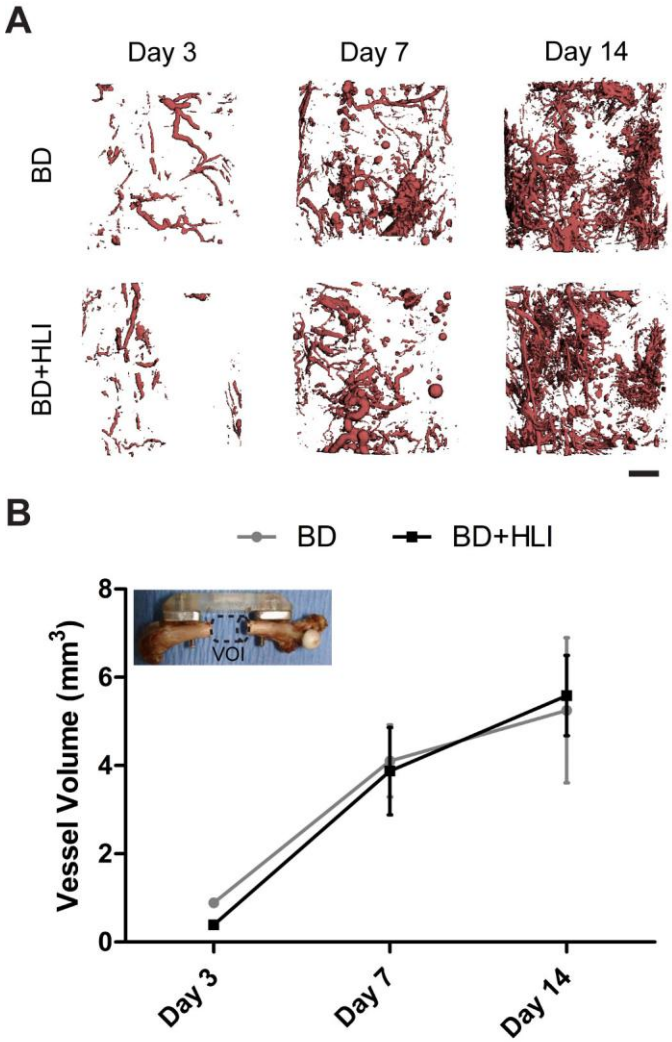

Figure 5.7. Micro-CT angiography analysis of the defect vascular volume. (A) Representative 3D micro-CT vessel reconstructions. Scale bar = 5mm. (B) Quantification of vessel volume in the defect. n = 3-5 per group per time point except BD+HLI at day 3 where n = 2.

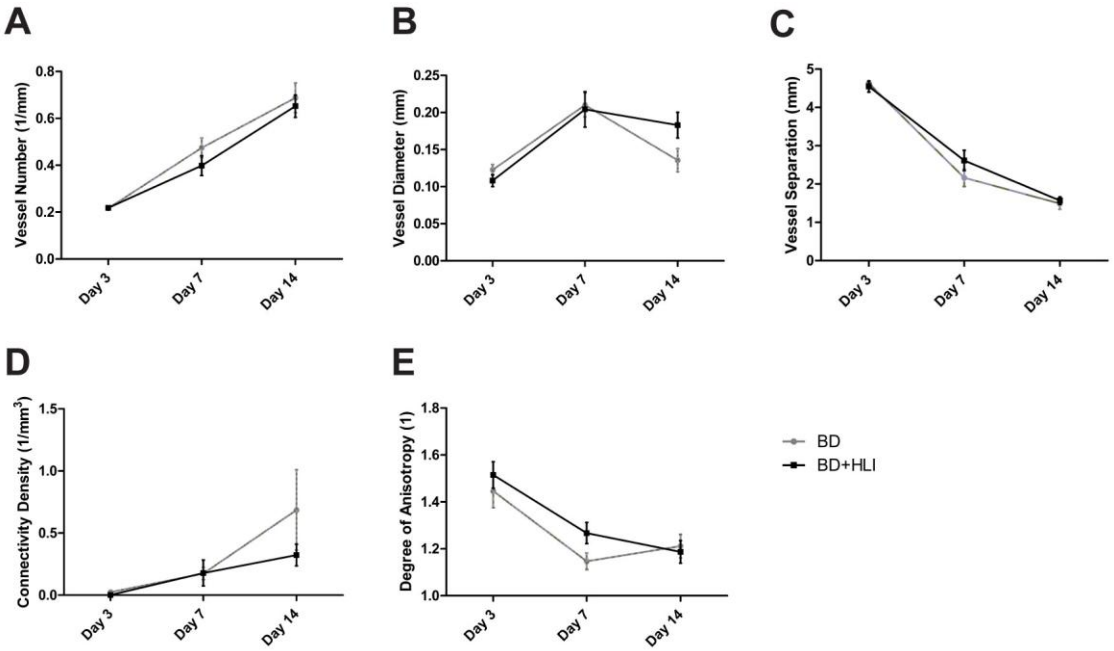

Figure 5.8. Micro-CT angiography analysis of defect vascular morphometry. n = 3-5 per group per time point except BD+HLI at day 3 where n = 2.

Histological analysis at days 7, 14, and 28 revealed notable phases in vascular ingrowth at the defect site. Quantitative angiography data from the Defect VOI was supported by histology as the vascular response progressed similarly between the BD and BD+HLI groups in the defect region and surrounding tissue. At day 7, the defect was heavily populated by erythrocytes (Fig 5.9A, D), with no clearly identifiable blood vessels within the defect space and sparse vessels along the exterior of the nanofiber mesh. More vessels were evident in the tissue adjacent to nanofiber mesh by day 14 (Fig. 5.9B, E). Vessels were found entering the nanofiber mesh at perforations and in proximity to new bone forming in the defect by day 28 (Fig. 5.9C, F).

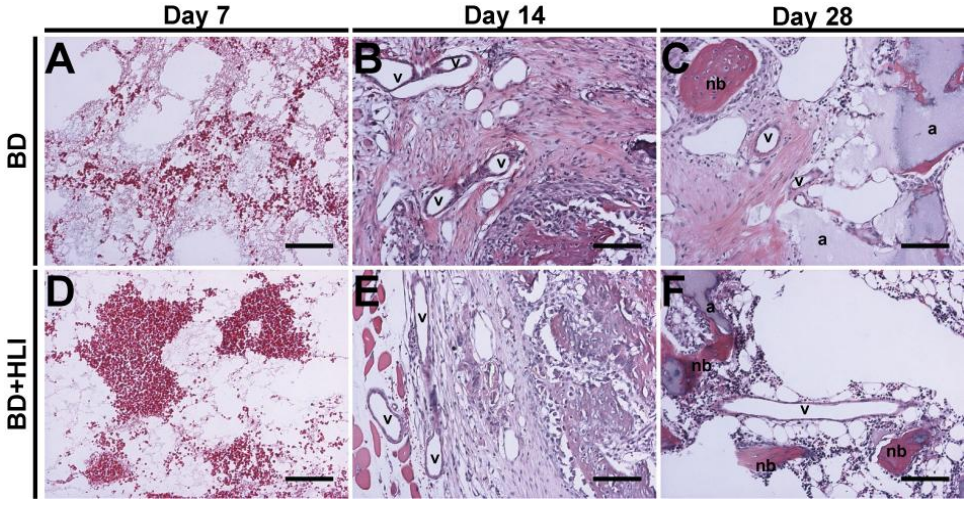

Figure 5.9. Histological evaluation of early vascular growth in the bone defect. Micrographs of H&E stained sections showed similar progression of vessel growth in both groups. At day 7, the defect was heavily populated by erythrocytes (A,D), with no clearly identifiable blood vessels within the defect space and sparse vessels along the exterior of the nanofiber mesh. More vessels were evident in the tissue adjacent to nanofiber mesh by day 14 (B,E). Vessels were found entering the nanofiber mesh at perforations and in proximity to new bone forming in the defect by day 28 (C,F) Annotations: a=alginate, nb=new bone, v=blood vessel. Scale bar=100μm. Images acquired at 10X.

Early Gene Expression in the Bone Defect Region

The time course of mRNA expression in the bone defect space was evaluated for 19 genes of interest using qRT-PCR. Interestingly, although expression of several of the genes investigated changed significantly over time and compared to control tissue, at no time point was there statistically significant differential mRNA expression between the BD and BD+HLI groups. Expression of *Opn* was highly upregulated at all time points for all groups, achieving its highest level for rhBMP-2 treated groups at day 7 with a ~60-fold increase, but never falling below a ~30-fold increase at later time points (Fig. 5.10A). Multiple genes associated with osteogenesis displayed increasing expression profiles from day 7 through day 21 for rhBMP-2 treated groups, including *Col1a1*, *Runx2*, *Osx*, *Bmp2*, and *Rankl* (Fig. 5.10B-F). By day 14, *Col1a1* expression was upregulated ~10-fold compared to controls in both the BD and BD+HLI group, and went on to even higher levels by day 21 (Fig. 5.10B). In groups receiving rhBMP-2, both *Osx* and *Runx2* expression was increased compared to controls, but the fold increases for *Osx* expression (~6-fold at day 14 and ~7- to 9-fold at day 21) were greater than those for *Runx2* (~2-fold at day 14 and ~3-fold at day 21) at the same time points (Fig. 5.10C, D). At day 7, expression of *Bmp2* was below control levels for both BD and BD+HLI groups, then steadily climbed to a ~3- to 4-fold upregulation by day 21 (Fig. 5.10E). Expression of *Rankl* was significantly increased at all time points for both rhBMP-2 treated groups compared to controls, showing ~5-fold upregulation at day 7 and reaching greater than 10-fold upregulation by day 21 (Fig. 5.10F). The temporal changes in expression of osteogenesis-related genes showed stark contrast in groups treated with rhBMP-2 compared to the group treated with blank alginate, especially for *Runx2*, *Osx*, *Bmp2*, and

Rankl where mRNA levels in the blank alginate group were significantly lower than rhBMP-2 treated groups and rarely above the 1-fold control tissue expression level (Fig. 5.10C-F).

Expression of *Igf1* and *Pdgfb* steadily increased in all groups from levels observed at day 7 (Fig. 5.10G, H). Whereas expression of *Vegfa* did not differ significantly over control levels for any group at any time point (Fig. 5.10I), *Vegfr2* mRNA expression increased from day 7 through day 21, reaching a significant increase compared to controls at day 21 (Fig. 5.10J). Both *Fgfr1* and *Fgfr2* showed increasing expression over time from their levels at day 7; however, while *Fgfr1* displayed greater fold changes relative to controls (Fig. 5.10K), *Fgfr2* showed more pronounced differences with rhBMP-2 treatment (Fig. 5.10L). Expression of *Acta2* was highly upregulated in all groups, with differing profiles (Fig. 5.10M). For the BD group, *Acta2* expression was highest at day 7 (~15-fold upregulation) before reducing to roughly half that level at day 14 (~8-fold upregulation) and remaining relatively constant between days 14 and 21 (Fig. 5.10M). The BD+HLI group exhibited a similar ~16-fold upregulation in *Acta2* at day 7 that was sustained through day 14 before falling to ~8-fold expression at day 21 (Fig. 5.10M). The blank group showed a temporal delay in maximum *Acta2* expression, possessing a ~7-fold upregulation at day 7 before going on to a ~20-fold upregulation at day 14 (Fig. 5.10M). In rhBMP-2 treated groups, expression of *Mmp9* increased over time, achieving a ~ 15-fold upregulation by day 21 while expression remained relatively unchanged in the blank group compared to controls (Fig. 5.10N).

A significant increase in expression of *Ccl2* mRNA was observed in all groups at all time points, but showed a decreasing profile from day 7 to day 21 (Fig. 5.10O). Also,

upregulation of *Ccl2* was less intense in rhBMP-2 treated groups compared to the blank alginate group (Fig. 5.10O). Expression of *Cd163* was increasing from levels at day 7 in all groups, but was downregulated at all time points compared to control levels (Fig. 5.10P). Expression of *Ccr7* was upregulated at least 2-fold at all time points, but was highest at day 7 in rhBMP-2 treated groups, whereas the blank alginate group showed highest expression at day 14 (Fig. 5.10Q). In all groups, expression of Cxcl5 was highest at day 14 (Fig. 5.10R). At all time points, *Cxcl10* expression was elevated compared to controls, achieving statistical significance for all groups at days 14 and 21 (Fig. 5.10S).

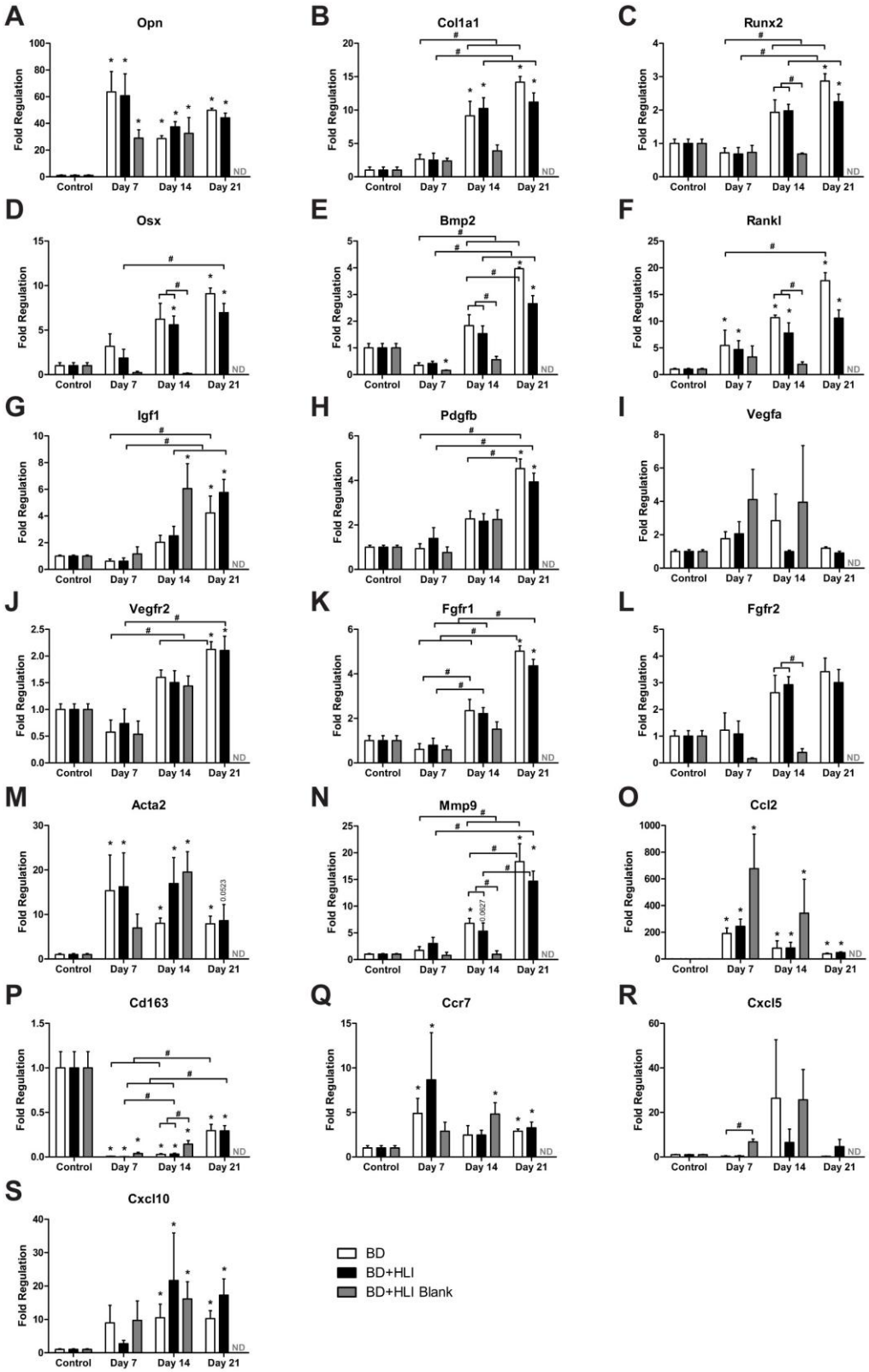

Figure 5.10. Bone defect gene expression analysis. Fold regulation normalized to levels in control tissue is shown for all genes investigated. *$p < 0.05$ vs. Control. $^{\#}p < 0.05$ as indicated. n = 3-6 per group per time point.

Early Gene Expression in the Adductor Muscle Tissue

Temporal changes in mRNA expression were also evaluated in the adductor muscles of the leg. Again, *Opn* expression was highest at day 7, with greater than 100-fold upregulation in all groups, before falling precipitously by day 14 to more modest levels on the order of 10-fold upregulation (Fig. 5.11A). Day 7 expression levels did appear slightly higher in groups with HLI compared to the BD group, but the differences were not statistically significant. Expression of *Col1a1* was significantly upregulated over controls in all groups at day 7 (~10- to 15-fold), but expression profiles differed between groups at later time points (Fig. 5.11B). While *Col1a1* expression remained elevated in the BD group through day 14 before falling at day 21, the BD+HLI group experienced a marked drop at day 14 (statistically lower expression compared to the BD group) before returning to a significantly elevated level at day 21 (Fig. 5.11B). In the blank alginate group, *Col1a1* expression fell from day 7 to day 14, but remained significantly higher than controls (Fig. 5.11B). Expression of *Runx2* mRNA was elevated at day 7, but afterward decreased over time (Fig. 5.11C). Other osteogenesis related genes *Osx*, *Bmp2*, and *Rankl* were relatively unchanged over time compared to control levels (Fig. 5.11D-F).

At day 7, expression of *Igf1* was upregulated ~2- to 3-fold in all groups, and remained at similar levels through day 21 (Fig. 5.11G). Both *Pdgfb* and *Vegfa* mRNA expression initially fell to levels below controls for all groups at day 7, but showed increased expression thereafter achieving ~2-fold upregulation by day 21 (Fig. 5.11H,I). Expression of *Vegfr2* remained relatively unchanged through day 14 compared to controls before reaching a ~3- to 4-fold upregulation at day 21 (Fig. 5.11J). Similar

expression profiles were also observed for *Fgfr1*, *Fgfr2*, and *Acta2* (Fig. 5.11K-M), but more modest 2- to 3-fold upregulation was observed for *Fgfr1* and *Fgfr2* at day 21. Expression of *Mmp9* was upregulated in all groups at day 7, but was increased more in BD and BD+HLI groups (~21-fold and ~35-fold, respectively) than the blank alginate group (~6-fold). By day 14, *Mmp9* expression had fallen substantially and was similar to controls or upregulated on the order of ~2- to 3-fold (Fig. 5.11N).

At all time points, *Ccl2* expression was elevated to at least 2-fold upregulation in all groups, but expression profiles differed between groups (Fig. 5.11O). In the BD group, the ~3-fold upregulation at day 7 climbed to ~7-fold at day 14 before falling back to 2-fold at day 21. In the BD+HLI group, a relatively consistent ~2- to 4-fold upregulation was sustained through all time points. The highest *Ccl2* expression was observed in the blank alginate group, where a 23-fold upregulation at day 7 (significantly increased compared to both rhBMP-2 treated groups) fell to 2.5-fold by day 14 (Fig. 5.11O). Expression profiles for *Cd163* and *Ccr7* also differed between groups. The BD group displayed a relatively consistent ~2-fold upregulation in *Cd163* across all time points, whereas the BD+HLI group showed more modest upregulation at days 7 and 14 before reaching its highest expression with a 3-fold upregulation at day 21 (Fig. 5.11P). Expression of *Ccr7* in the BD group was upregulated 3-fold at day 7, then achieved its highest expression with ~11-fold upregulation at day 14 before returning to a 3-fold upregulation at day 21, while the BD+HLI group sustained a ~5- to 6-fold upregulation at days 7 and 14 before increasing to a 11-fold upregulation at day 21 (Fig. 5.11Q). In the blank alginate group, expression of both *Cd163* and *Ccr7* was highest at day 7 and elevated at this time point compared to rhBMP-2 treated groups, but dropped

considerably by day 14 (Fig. 5.11P,Q). Only modest changes in Cxcl5 mRNA expression were observed over time for all groups, never rising above a 2-fold upregulation (Fig. 5.11R). The BD group exhibited slightly higher upregulation of *Cxcl10* than the BD+HLI group at all time points, but the highest expression was observed in the blank alginate group at day 7 (~20-fold upregulation) before returning to control levels by day 14 (Fig. 5.11S).

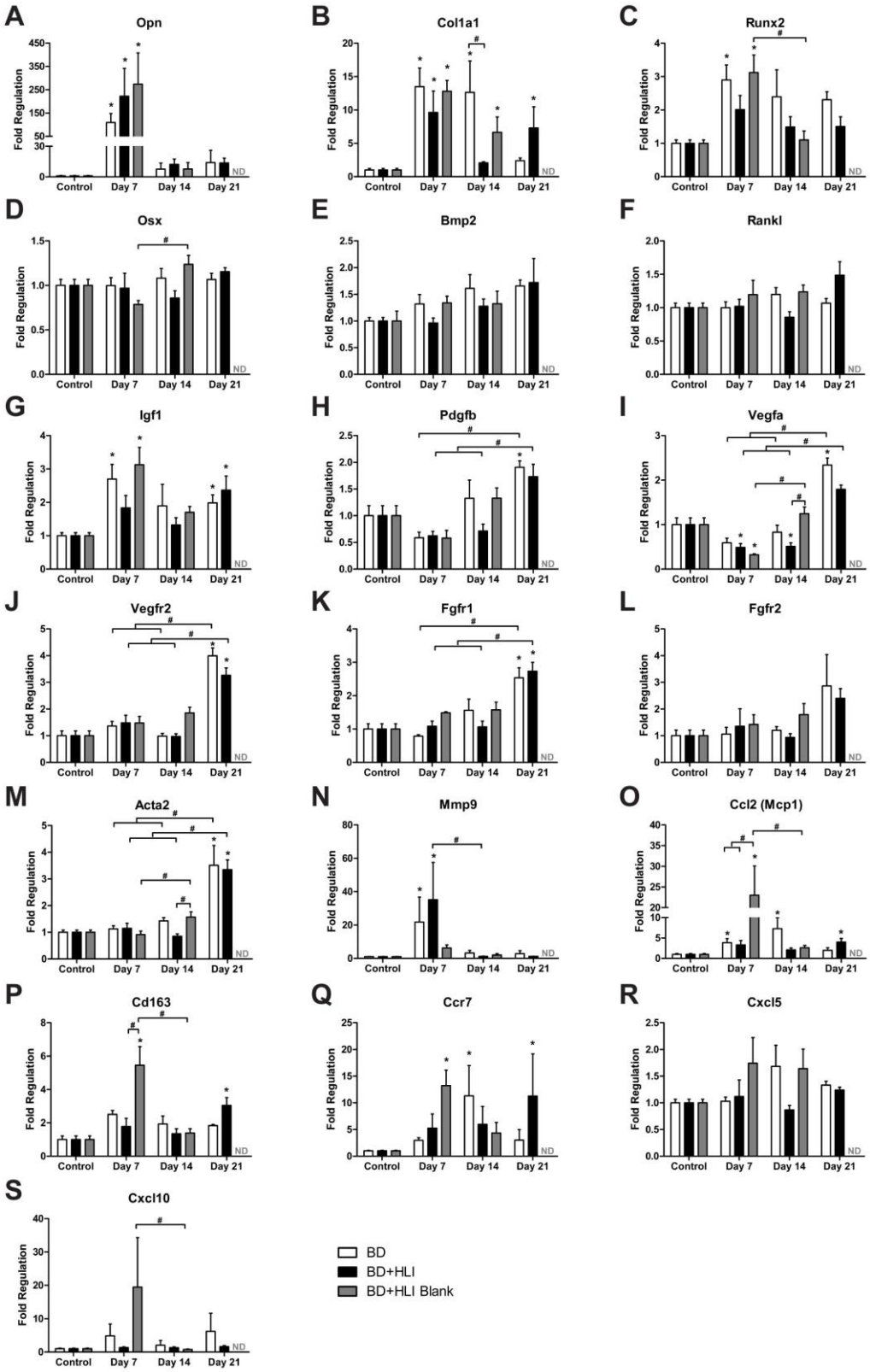

Figure 5.11. Adductor muscle gene expression analysis. Fold regulation normalized to levels in control tissue is shown for all genes investigated. *$p < 0.05$ vs. Control. $^{\#}p < 0.05$ as indicated. n = 3-6 per group per time point.

Discussion

Bone repair involves a highly coordinated orchestration of complex physiological processes, with vascular network growth and initiation of biological signaling cascades functioning as critical early events. In Aim II of this thesis, enhanced rhBMP-2-mediated bone regeneration was observed for segmental bone defects with concomitant hind limb ischemia in a rat composite injury model (Uhrig *et al.*, 2013). As an explanation for these findings, we hypothesized that inclusion of HLI stimulated the bone repair process by way of an augmented vascular tissue growth response or perturbed signaling cascades initiated in the bone defect region or surrounding skeletal muscle envelope. Here we began to test this hypothesis by investigating early spatiotemporal changes in blood flow and vascular tissue growth, as well as gene expression within the bone defect and adjacent adductor muscle tissues. Based on the results obtained, we were able to draw multiple conclusions in relation to our hypothesis. While HLI produced sustained reduction in perfusion to the distal limb, it also promoted increased vascular growth in the upper leg. Despite the enhanced vascular growth in the skeletal muscle, blood vessel growth into the regenerating defect was not affected by HLI at the time points investigated. Therefore, any effects of ischemia-induced vascular growth on bone regeneration appear to be indirect ones. Finally, the stimulatory effects of ischemia on bone regeneration cannot be explained by changes in gene expression alone, and delivery of 2 μg rhBMP-2 does not appear to strongly influence gene expression in the adductor muscle tissue for the genes and time points investigated here.

The histological results of early bone regeneration observed here support our previously reported long-term results (Uhrig *et al.*, 2013), with the BD+HLI group

exhibiting more robust bone regeneration than the BD group. Additionally, in previous work, it was demonstrated that when combined with HLI a non-healing 0.5 μg rhBMP-2 dose will produce consistent bone repair (Uhrig *et al.*, 2013). It has also been shown that with no treatment, nanofiber mesh alone, or nanofiber mesh with blank alginate, these defects will not heal and will progress to non-union (Oest *et al.*, 2007; Kolambkar *et al.*, 2011). Together, those results prompted speculation of whether the response to HLI in the absence of rhBMP-2 could promote effective bone repair. Here we demonstrated the necessity of the osteoinductive stimulus, as the BD+HLI Blank group did not display an initiation of bone regeneration via osteogenic gene expression.

The HLI surgery has been shown to effectively induce significant ischemia in the operated leg (Uhrig *et al.*, 2013), but this effect is understood to be transient, with recovery attributed primarily to arteriogenic collateral vessel growth (Couffinhal *et al.*, 1998; Duvall *et al.*, 2004). In rat models of femoral artery ligation, restoration of resting perfusion has been reported at 5 -7 days (Seifert *et al.*, 1985; Corcoran *et al.*, 2009), with deficits in reserve blood flow persisting beyond 14 days (Corcoran *et al.*, 2009). In our model, distal limb perfusion remained significantly reduced in the BD+HLI group at day 14, having only achieved 42% of the contralateral leg, with the extended delay in recovery perhaps attributable to concomitant orthopaedic injury or differences in surgical technique.

The reduction in perfusion for the BD+HLI group was less pronounced for the ROI of the entire leg, displaying a significant decrease to 55% of contralateral perfusion at day 1. By day 3, this had recovered to 82%, which was no longer statistically different from naïve controls. Conversely, the BD group showed increasing perfusion to the

operated leg beginning as early as day 1 and reaching maximal levels by day 7. Interestingly, while HLI clearly affected the perfusion to the limb, both groups displayed similar temporal changes in perfusion from their respective day 1 levels through day 14.

The rapid recovery of perfusion in the leg of the BD+HLI group appears to be attributable to the significantly increased perfusion in the region of the adductor muscles, given the sustained reduction in the distal limb. Although perfusion in the adductor ROI was unchanged at any time point for the BD group, in the BD+HLI group it was significantly increased at day 1, appeared to peak at day 3, but remained highly elevated through day 14. The marked increase in adductor ROI perfusion in the BD+HLI group was not unexpected, as arteriogenic growth of collateral vessels in the adductor muscles is the predominant restoration mechanism is small animal HLI models (Scholz *et al.*, 2002; Schaper and Scholz, 2003; Duvall *et al.*, 2004).

Delivery of 2 μg rhBMP-2 did not appear to influence perfusion in the operated limb, as evidenced by the similar temporal changes in perfusion between the BD+HLI and the BD+HLI Blank group. Importantly, interpretation of LDPI data should consider the limitations of this imaging modality. While providing useful functional assessment, the limited penetration depth precludes full characterization of limb blood perfusion. Cutaneous inflammation and wound healing may also mask possible differences.

The increased adductor perfusion observed in the BD+HLI group with LDPI was further supported by micro-CT angiography results. Collateral vessel growth was readily apparent as early as day 3 in contrast agent perfused samples from this group. These collateral vessels were potentially responsible for delivering the functional perfusion increase observed with LDPI. The collateral vessels were quantitatively captured in the

Thigh VOI analysis, and in agreement with LDPI, the BD+HLI group showed increased normalized vessel volume in the thigh compared to the BD group. Together, these results indicate a robust vascular growth response to ischemia in this model. Both groups possessed increased vascularity in the thigh of the operated leg compared to the contralateral leg; however, considering the excision of femoral vessels, the BD+HLI group exhibited vascular growth in excess of the BD group. Although this vascular growth did not produce differences in the mean vessel number parameter at the time points investigated, the BD+HLI group did possess a more isotropic network of smaller diameter vessels. One limitation of the micro-CT angiography technique (as with other angiography techniques) is the inability to distinguish between arterial and venous vessels, and perhaps resulted in a failure to detect important differences in vascular networks. For example, the BD+HLI group exhibited greater normalized vessel volume in the thigh despite excision of the femoral vessels, perhaps suggesting increased arterial blood supply. In such a scenario, the BD+HLI group may have experienced enhanced oxygenation and nutrient supply to the surrounding skeletal muscle envelope, which could contribute to the enhanced bone regeneration observed.

Although HLI produces differences in vascular network growth in the surrounding muscle tissue of the thigh, it does not appear to influence vessel growth at the defect site. Micro-CT angiography results for the Defect VOI demonstrated very similar temporal changes for vessel volume and morphological parameters for the BD and BD+HLI groups. As outlined in the methods section, the 7 mm diameter of the Defect VOI was inclusive of the 5 mm diameter of the nanofiber mesh and the immediately adjacent tissue extending radially outward a distance of 1 mm. In light of

these Defect VOI results, and given the 200 μm limit of blood oxygen diffusion (Muschler *et al.*, 2004), any effect of superior tissue oxygenation and nutrient supply in the hypothetical scenario above would seem to be an indirect one. Histological analysis was in agreement with these results, showing a similar progression of vascular ingrowth at the defect site between groups. Previously, we reported that vessel volume and morphological parameters are not different between groups at 12 weeks (Uhrig *et al.*, 2013); however, this does not preclude the possibility of differences in the time spanning the early time points investigated here and the week 12 end point.

The stimulatory effects of HLI on bone repair cannot be explained by differential gene expression alone based on the genes and time points investigated in these studies. Based on our previous findings that bone regeneration was increased in the BD+HLI group by week 4 (Uhrig *et al.*, 2013), we investigated gene expression at multiple preceding time points. Although we believe these to have been a thorough effort to identify differences between groups, temporal changes in gene expression do not proceed at discrete intervals, and differences at other time points may have gone undiscovered. Alternatively, while we attempted to capture a range of genes involved in osteogenesis, vascular growth, and inflammation, these biological processes are highly complex and the critical regulators – be those soluble signaling factors, membrane receptors, or ECM proteins – may not have been amongst the genes selected. Furthermore, given the heterogeneity of the bone defect and muscle tissue samples, qRT-PCR may not have been sensitive enough to detect changes between groups. For example, osteoprogenitors and vascular tissue cells make up only a small portion of the granulation tissue found at early time points in the defect, and in the context of the entire defect sample, may not produce

sufficiently large differences in mRNA expression. In the adductor muscles, focal gene expression analysis on vessels in the BD+HLI group undergoing arteriogenic remodeling may demonstrate differences compared to vessels from the BD group, but these effects may be lost when evaluating gene expression at the skeletal muscle tissue level.

In the bone defect, temporal changes in gene expression progressed very similarly for the BD and BD+HLI groups. As expected, in groups treated with rhBMP-2, multiple genes associated with osteogenic transcription factors, growth factors, and ECM proteins – *Runx2*, *Osx*, *Bmp2*, *Igf1*, *Pdgfb*, *Opn*, *Col1a1* – displayed increased mRNA expression over control tissue and increasing expression levels over time. Although the mature naïve femoral bone tissue possesses some degree of modeling/remodeling due to growth, it has much less activity than newly forming bone. Furthermore, in the absence of the osteoinductive rhBMP-2 stimulus, HLI and blank alginate alone were insufficient to promote osteogenic gene expression. In particular, expression of *Runx2* and *Osx*, master transcription factors for osteogenic differentiation, and *Bmp2*, a necessary morphogen required for postnatal bone healing (Tsuji *et al.*, 2006), was significantly lower in the blank alginate group than rhBMP-2-treated groups and was depressed compared to expression levels in control tissue. Additionally, *Opn* expression was significantly elevated in all groups at all time points, but was ~2x more highly upregulated at day 7 in rhBMP-2 treated groups than the blank alginate group.

Expression of genes related to vascular growth was similar between groups, with a few notable exceptions. Of all the genes investigated, *Acta2* appeared to be the most differentially regulated between groups in the bone defect region. Previous work has demonstrated a role for *Acta2* expressing cells in bone repair (Kinner *et al.*, 2002), and

these cells are believed to be osteoprogenitors of perivascular or myofibroblast lineage (Kalajzic *et al.*, 2008). Furthermore, *Acta2* is expressed by VSMCs, a cell population thought to be contributors to pathological vascular calcification (Trion and van der Laarse, 2004), that are also known to increase proliferation and migration activity during arteriogenesis (Schaper and Scholz, 2003). Thus, the prolonged duration of heightened *Acta2* expression in the BD+HLI group is thus perhaps indicative of an increased residence time of cells at the defect capable of participating in bone repair. Interestingly, *Vegfa* expression in the defect was only modestly upregulated and did not produce a statistically significant increase over the level of controls at any time for any group. Although VEGF signaling has been shown to be essential for angiogenic-osteogenic coupling and bone repair (Street *et al.*, 2002), the modest upregulation of *Vegfa* displayed here is in agreement with what has been observed in other models (Carvalho *et al.*, 2004; Lienau *et al.*, 2009; Matsubara *et al.*, 2012). The expression levels seen here are also perhaps an effect of the time points investigated, as histology showed that vessel ingrowth at the defect occurs between days 14 and 28. The mRNA expression of *Mmp9* in rhBMP-2 treated defects lends support to the possibility of additional downstream *Vegfa* expression. Matrix degradation by MMP9 is understood to precede VEGF signaling and angiogenesis during bone repair (Ferguson *et al.*, 1999; Colnot *et al.*, 2003), and in the work here *Mmp9* expression was observed to still be increasing from day 14 to day 21. In vascular growth signaling, expression of the growth factor receptors is perhaps as important, if not more so, than their respective ligands. In rhBMP-2 treated defects, expression of *Vegfr2*, the primary receptor through which VEGF signaling is mediated, as well as *Fgfr1* and *Fgfr2*, all increased over time, achieving statistical

significance versus controls or at least a 3-fold upregulation, and in the case of *Fgfr1*, achieving both. Furthermore, beyond their function in vascular growth, VEGFR2, FGFR1, and FGFR2 are also expressed as surface receptors on bone cells and implicated in bone repair processes (Du *et al.*, 2012; Clarkin and Gerstenfeld, 2013). It has also been proposed that while both FGFR1 and FGFR2 modulate signaling in osteoprogenitors cells, FGFR2 is more involved in receptor signaling for mature osteoblasts (Marie, 2003). In this study, *Fgfr1* expression in the defect was more highly upregulated compared to controls, however, *Fgfr2* was more differentially regulated in rhBMP-2 treated groups compared to the blank alginate HLI group, suggesting that in this model FGFR2 is more involved in bone healing, perhaps being indicative of further osteogenic differentiation.

The very strong upregulation of *Ccl2* observed in the defect for all groups is unsurprising given it is a key molecule in mediating inflammation, particularly monocyte/macrophage recruitment. Furthermore, inhibited CCL2 signaling through knockout of its receptor CCR2 has been implicated in delaying the progression fracture repair (Xing *et al.*, 2010). The higher levels of *Ccl2* expression in the BD+HLI Blank group relative to groups receiving rhBMP-2 may be indicative of an increased inflammatory response or prolonged resolution of inflammation at the defect site due to an insufficient osteogenic stimulus. Expression of *Ccr7* and *Cd163*, reported biomarkers of M1 (classically activated, pro-inflammatory) and M2 (alternatively activated, wound healing) macrophage phenotypes, respectively (Mokarram *et al.*, 2012), was investigated to further characterize the inflammatory response. In all groups, and at all time points, expression of *Cd163* was downregulated compared to controls, but expression was shown

to be increasing over time. Conversely, expression of *Ccr7* was upregulated at all time points, but decreased after day 7 in rhBMP-2 treated groups. Taken together, these results suggest a gradual transition from a pro-inflammatory M1 phenotype toward the wound-healing M2 phenotype. The increased *Ccr7* expression observed from day 7 to day 14 in the blank alginate group, like the *Ccl2* expression discussed above, is perhaps indicative of prolonged inflammation in this group given the lack of a sufficient osteogenic stimulus.

For the genes and time points investigated here, HLI did not appear to strongly influence gene expression in these muscles when comparing amongst experimental groups, nor did delivery of 2 μg rhBMP-2. The overall lack of differences in temporal gene expression patterns in adductor muscles with or without HLI was an unexpected observation of this study. These results are potentially explained by the muscle trauma inherent to the segmental bone defect procedure which may elicit upregulation of many of the same genes involved in the response to HLI, effectively masking any effect of the concomitant vascular injury on gene expression. This is supported by the stark differences in gene expression of all groups compared to naïve controls. Additionally, angiography results demonstrate that a significant amount of collateral vessel growth has already occurred prior to day 7; thus, the majority of differential gene expression due to HLI may have occurred earlier than the time points investigated here.

The higher levels of *Opn* expression at day 7 in HLI groups compared to controls was an expected result, as OPN has been shown to be significantly upregulated in response to HLI (Lyle *et al.*, 2012) and plays a definitive role in collateral vessel development and recovery from ischemia (Duvall *et al.*, 2008). The nearly equal increase

in *Opn* expression for the BD group was unexpected, but is not entirely surprising given the pervasive muscle trauma inherent to the segmental bone defect surgery. Although the skeletal muscle envelope is thought to contribute in multiple ways to bone repair, very little upregulation was observed for osteogenesis related transcription and growth factor genes in the adductor muscle tissue for any group. Thus, any stimulatory effect on bone repair from the surrounding skeletal muscle does not appear to be mediated at the level of osteogenic gene expression.

Expression of genes related to angiogenesis (*Vegfa*, *Vegfr2*, *Fgfr1*, and *Fgfr2*) increased over time in the adductors from their day 7 levels, as might be expected, but at most were upregulated only ~3- to 4-fold over controls. These relatively modest increases lend support to the idea that arteriogenesis rather than angiogenesis is the more relevant vascular growth process in the surrounding skeletal muscle envelope, especially at time points inside 14 days (Scholz *et al.*, 2002; Morgan *et al.*, 2012). Arteriogenesis is an inflammation driven process, with increased MCP-1 (CCL2) secretion promoting extravasation of monocytes into the vessel wall to initiate remodeling that is further carried out by VSMCs (Scholz *et al.*, 2000; Cai and Schaper, 2008). Interestingly, differential expression of *Ccl2* was not observed between the BD and BD + HLI groups. This is most likely explained by the time points analyzed, as HLI induced expression of CCL2 is highest in the adductor muscles in the first 3 days (Lee *et al.*, 2004), which is prior to the earliest time point investigated here. Although the *Ccl2* levels observed for the BD+HLI group are in agreement with those previously reported for HLI models at day 7 (Lee *et al.*, 2004), *Ccl2* expression remains elevated in the BD+HLI Blank group for reasons that are not entirely clear. No differences in mRNA expression were found

for *Mmp9*, a protein known to be involved in the matrix degradation aspects of vessel remodeling (Heil and Schaper, 2004), or *Acta2* which is highly expressed by VSMCs, the cell type most responsible for arteriogenic remodeling (Cai and Schaper, 2008). Furthermore, despite the well-established role of monocytes/macrophages in arteriogenesis, HLI did not have a clear effect on expression of *Cd163* or *Ccr7*. Although no explanation can be offered for the greater fold increases of *Cd163* and *Ccr7* expression found in the BD+HLI Blank group at day 7, these results are perhaps related to the higher level of *Ccl2* expression also observed.

Other areas yet to be tested may provide important insights for explaining the stimulatory effect of HLI recovery on rhBMP-2-mediated bone regeneration in this model. Rather than differential gene expression, augmented soluble factor bioavailability or cell populations mobilized due to the HLI response may contribute to enhanced bone repair. Monocytes/macrophages play a critical role in arteriogenesis. Increased circulating monocyte concentration and extravasation is associated with HLI (Heil *et al.*, 2002; Bergmann *et al.*, 2006), and pharmacological depletion of monocytes impairs arteriogenesis (Heil *et al.*, 2002). This could be one key difference between the experimental groups here that is yet to be studied. Increased mobilization of these cell populations may increase matrix degradation and soluble factor bioavailability (la Sala *et al.*, 2012) or otherwise augment tissue regeneration. Recent work demonstrating the essential role of macrophages in salamander limb regeneration lends supports to such a hypothesis (Godwin *et al.*, 2013). Furthermore, OPN is thought to play a role in mediating macrophage migration and adhesion (Giachelli *et al.*, 1998; Duvall *et al.*, 2008), and increased *Opn* expression in HLI animals, although not statistically

significant, may have been biologically relevant to promote differences in activity of these cell populations. Given the importance of myeloid lineage cells in the recovery from HLI, it is conceivable that in response to the ischemic insult, an additional population of bone marrow-derived progenitor cells is mobilized into the circulation. Although it is believed that the progenitor cells involved in fracture repair arise primarily from the periosteum, it would be interesting to investigate whether HLI animals contain an additional population of bone-marrow derived cells participating in bone regeneration. Endothelial progenitor cells would be an additional cell population worth investigating. Migration and neovascularization by endothelial progenitor cells is mediated by aniopoietin-2 (Kim *et al.*, 2006), a molecule reported to play a role in the recovery from HLI (Tressel *et al.*, 2008).

In total, the studies here constitute the initial work investigating how the recovery response to HLI mechanistically promotes enhanced bone regeneration in a composite injury model of bone and vascular trauma. In partial support of our hypothesis, characterization of vascular network growth determined that a robust response is rapidly initiated in the thigh following HLI. Yet despite the enhanced vascular growth in the skeletal muscle, blood vessel growth into the regenerating bone defect was not affected by HLI at the time points investigated. Therefore, any effects of ischemia-induced vascular growth on bone regeneration appear to be indirect ones. Gene expression results did not support our hypothesis, leading to the conclusion that the stimulatory effects of HLI on bone regeneration cannot be explained by differential gene expression alone for the genes and time points investigated here. Additional future work to further elucidate potential coupling mechanisms between the recovery response to ischemia and bone

repair may reveal important new strategies for promoting bone healing in challenging clinical scenarios.

CHAPTER 6

SUMMARY AND FUTURE DIRECTIONS

Overall Summary

Improving structural and functional outcomes of intervention for extremity trauma patients remains a pressing, unmet clinical need. Doing so will likely require advancing our understanding of the biological interactions between damaged tissues. While TE/RM therapeutics offer promising potential to overcome the status quo limitations of surgical reconstruction, very few products have transitioned to clinical practice. In the status quo, musculoskeletal trauma research models almost exclusively consist of single-tissue defects. While these models have an undeniable place as valuable research tools, they inherently possess limited utility for investigating therapeutic strategies for the repair of large, multi-tissue defects and afford little potential for insight into endogenous interactions between healing tissues. Models of composite tissue trauma are uniquely positioned to bridge this knowledge gap and advance the TE/RM field.

Bone tissue is known to be innervated and highly vascularized, and both tissue types are involved in bone physiology. However, the degree to which these tissue interactions influence the repair of large, multi-tissue defects remains unknown. Accordingly, the *overall objective* of this project was to investigate interactions occurring between tissues following composite limb injuries in support of the *long-term goal* to develop TE/RM therapies for improved reconstruction and functional outcomes following severe limb trauma. The *central hypothesis* of this work was that interactions

exist in the healing response of large, composite tissue deficits, and these interactions influence bone tissue regeneration and functional restoration.

To test our hypothesis, two novel rat models of composite bone and soft tissue trauma were developed. First, we characterized interactions in tissue regeneration in a composite bone and nerve injury model where a segmental bone defect was combined with a peripheral nerve gap (Aim I, Chapter 3). Interestingly, our results indicated that bone regeneration was not significantly impaired by concomitant nerve injury, nor was nerve regeneration significantly impaired by bone injury in this model. Yet despite the similar tissue regeneration observed, the composite injury group experienced a marked functional deficit in the operated limb compared to either of the single-tissue injury groups. Second, we established a model of concomitant bone and vascular extremity trauma by combining a critically-sized segmental bone defect with surgically-induced hind limb ischemia to evaluate the effects on BMP-2-mediated segmental bone defect repair (Aim II, Chapter 4). Surprisingly, our results demonstrated significantly enhanced bone regeneration in the group with ischemia compared to bone defects alone, perhaps by way of coupling to the endogenous vascular growth response to HLI. Finally, building on those results, we investigated the potential early vascular growth and gene expression mechanisms of interaction between the injury response to HLI and bone defect repair (Aim III; Chapter 5). Although HLI induced a more robust vascular growth response in the thigh, ingrowth of blood vessels at the bone defect did not differ, indicating that HLI does not directly augment vascularization at the site of bone regeneration. In addition, the expression of multiple genes related to osteogenesis, vascular growth, and inflammation were upregulated compared to naïve control tissue; however, the

stimulatory effects of HLI on bone regeneration cannot be explained by gene expression alone based on the genes and time points investigated. Taken together, this thesis presents pioneering research on a platform of small animal test-bed models of composite limb injury and has advanced our understanding of endogenous interactions that occur during the repair of concomitant bone & peripheral nerve or bone & vascular injuries.

Understanding Bone and Nerve Interactions

In Aim I (Chapter 3) of this thesis, a novel composite limb injury model of severe bone and peripheral nerve trauma was developed to assess tissue interactions during concomitant bone and nerve regeneration. To our knowledge, this was the first work on a small animal model of critically-sized bone and neural injuries. Our working hypothesis was that a composite bone and nerve injury would affect bone regeneration and limb function compared to bone injury alone. We characterized the healing response using quantitative outcome measures to assess bone regeneration and peripheral nerve regeneration, as well as tissue and overall limb function. Secondarily, we studied morphology and mechanical properties of ipsilateral and contralateral femora to test the hypothesis that the nerve injury would induce an adaptive response in intact femora.

Interestingly, although both single tissue injuries were challenging, our results did not support our hypothesis as bone regeneration was not significantly impaired by concomitant nerve injury in this model, nor was nerve regeneration significantly impaired by bone injury. Thus, alternative models may be better suited to study interactions in bone and nerve tissue regeneration. Although differences were not observed in tissue regeneration for outcome parameters investigated here, the difference in functional deficit in the injured limb was quite profound in the composite injury group compared to either

single-tissue injury group in agreement with our hypothesis. Restoration of limb function remains a major obstacle in limb salvage following extremity trauma in human patients. Taken together with our results, this highlights the need for TE/RM to benchmark technologies using quantitative measures of both tissue and limb function. Additionally, in support of our secondary hypothesis we found injury to the sciatic nerve was associated with significant changes in the morphology and mechanical properties of intact femora.

The exact mechanism responsible for the marked functional deficit observed in the composite injury group is unknown. This response may simply be a result of bone trauma compounding the loss of innervation to the lower leg. Muscle contractures in the lower limb associated with sciatic nerve transection may also contribute to the persistent functional deficit if they are unresolved or progress in severity over time. Presence of the fixation hardware may also augment the muscle contractures and contribute to an increased functional deficit. Additional experimentation including a group where the peripheral nerve gap is combined with placement of fixation hardware only (no bone defect created) might help to answer such questions. The time course for full functional restoration may also be longer than the 16 weeks of healing allotted in this work, and extending experiment duration could potentially provide additional insights. It would be an oversight to not consider the role of a physical therapy protocol (or lack thereof) in assessing functional outcomes following extremity trauma. Physical therapy is a vital component in the rehabilitation and recovery process for human patients. In this study, the lack of a physical therapy protocol may be at least partially responsible for the persistent functional deficit. Future studies incorporating physical therapy regimens may

prove incredibly insightful; however, implementation of a standardized protocol for rats would present a multitude of logistical hurdles.

Additional insight may be gained from this model by performing experiments with composite injury groups in which one of the defects is left untreated (e.g., treated bone defect with untreated nerve gap). Such groups may be able to tease out whether untreated nerve defects negatively influenced bone repair compared to those that are treated, or perhaps whether delivery of BMP-2 affected nerve regeneration. It should be noted, however, that the time-course of nerve regeneration in the model we used is such that bone repair was in all likelihood well underway by the time axons had bridged the nerve gap. In such a case, there may be little physiological difference in whether or not the nerve gap is treated or untreated, or differences would not be observed until downstream mechanical loading induced remodeling.

The absence of distinguishable interactions between bone and nerve tissue regeneration in this work was somewhat unexpected. A growing body of work continues to elucidate neurotransmitter and neuropeptide signaling pathways in the skeletal system and a neuronal arm contributing to the regulation of bone modeling and remodeling (Imai and Matsusue, 2002; Spencer *et al.*, 2004; Elefteriou, 2008). While the number of nerve fibers in bone may not be numerous, it is postulated that they function in two specific regulatory roles: 1) mediators of mechanical forces in bone and 2) a source of trophic factors necessary for bone form and function (Masi, 2012). Clinical observations of enhanced osteogenic activity in fracture patients with head injuries provide anecdotal evidence for the role of the nervous system in physiological bone healing (Perkins and Skirving, 1987; Spencer, 1987; Garland, 1988). However, it remains controversial

whether this increase in osteogenesis is an actual augmentation of fracture healing or a form of heterotopic ossification (Kushwaha and Garland, 1998; Morley *et al.*, 2005). The effect of innervation status on fracture healing has also been studied experimentally, with inconsistent conclusions. Sciatic nerve transection has been associated with both smaller, less dense fracture calluses compared to innervated controls (Aro *et al.*, 1981; Aro, 1985), and also with larger, more mineralized calluses (Nordsletten *et al.*, 1994; Hukkanen *et al.*, 1995; Madsen *et al.*, 1998). The apparent confounding fracture healing results from similar injury models is very likely explained by differences in fracture stabilization employed across the studies. Although such discrepancies preclude the ability to collectively interpret the findings with great accuracy, when taken together with clinical reports, it seems clear that concomitant neural insult is at least associated with augmented fracture healing or osteogenic response. Furthermore, in sum, the previous experimental results suggest potential modulation of fracture healing via sensory innervation feedback on fracture stability. Work from our own laboratory has investigated the role of mechanical loading on repair of segmental bone defects; early loading was shown to have deleterious effects, whereas delayed loading enhanced bone regeneration (Boerckel *et al.*, 2011; Boerckel *et al.*, 2012). Future studies of bone defect regeneration incorporating nerve injury with or without mechanical loading may help to advance our understanding of the coupling of innervation status on mechanoregulation of bone repair.

The lack of observed interactions in our work here may be a consequence of the model design. Given the close anatomical proximity of the sciatic nerve and the femur (the former running just posterior to the latter in the musculature of the hamstrings), it is

susceptible to injury in instances of lower extremity trauma that damage the femur. This relationship made it a logical choice for a trauma model. From a functional perspective, however, the two are not as closely related. The primary function of the sciatic nerve is to innervate the lower leg and foot. An inability for direct signaling between the injury sites of the femur and sciatic nerve is a potential explanation for the lack of observed healing response interactions. It may be necessary to disrupt the specific nerves responsible for innervation of the injured bone in order to observe a neuronal influence on bone healing. The previously mentioned results from experimental models of denervated tibial fracture healing support such a hypothesis (Aro *et al.*, 1981; Aro, 1985; Nordsletten *et al.*, 1994; Hukkanen *et al.*, 1995; Madsen *et al.*, 1998), as well as a recent study which showed that chemically-induced local sensory denervation was associated with impaired healing of femur fractures by way of a larger, less dense fracture callus, with a significantly decreased failure load (Apel *et al.*, 2009). Alternatively, it is plausible that endogenous healing of large tissue defects does not completely parallel the physiological responses observed in fracture healing.

Accordingly, future work could incorporate changes to the model where the specific nerves innervating the femur are transected rather than the sciatic nerve in order to examine the effect on segmental bone defect repair. A different model could also be designed where sciatic nerve transection is combined with a tibial segmental bone defect. In such a model, or even with tibial fracture healing, varying lengths of sciatic nerve gaps could be used to better understand how the time course of nerve regeneration may influence bone repair. In addition, incorporation of sciatic nerve transection in a tibial distraction osteogenesis model (Aronson *et al.*, 1997), could offer particularly unique

insights into how innervation status mediates mechanically-induced bone repair. Developing a similar composite injury model based on murine distraction osteogenesis (Jacobsen *et al.*, 2008; Wan *et al.*, 2008) would allow investigation of specific mechanistic questions using a variety of transgenic mouse lines already available.

Model selection should ultimately depend on the type of injury of interest and the scientific question under investigation. Careful consideration should also be given to the degree of load bearing allowed and whether muscle tone in surrounding tissue has been disrupted, as both may influence the healing response observed in experimental and control groups, and ultimately the interpretation of results. There also exist ethical considerations specific to rodent strain selection for peripheral nerve injury models. Differences in the degree of autotomy/autophagia (i.e., self-mutilation) have been reported amongst varying rat strains following sciatic nerve transection, ranging from a complete absence to severe complications (Carr *et al.*, 1992). Although an increasing amount of research is being devoted to studying interactions between the nervous and skeletal systems, the complexities are far from being completely understood. With proper design considerations, composite bone and nerve injury models can provide a novel avenue to explore the degree of cross-talk during tissue repair and functional restoration, as well as the specific pathways involved.

Understanding Bone and Vascular Interactions

In Aim II (Chapter 4), a novel composite tissue injury model of severe bone and vascular trauma was developed to evaluate the effects of HLI on segmental bone defect repair. To our knowledge, this was the first work on a small animal model of a critically-sized bone defect with concomitant vascular injury. Based on reported clinical and

experimental observations on the importance of vascular networks in bone repair, we hypothesized that HLI would impair bone regeneration. Interactions in tissue regeneration were clearly evident in this model, but interestingly, our results demonstrated significantly enhanced bone regeneration in the group with ischemia compared to bone defects alone. We hypothesized that the bone regeneration may be attributable to a robust endogenous vascular growth response to ischemia. Although the HLI surgical procedure was demonstrated to effectively create an initial substantial reduction in perfusion of the leg, it is understood from the work in the field of vascular biology that this is a transient effect due primarily to arteriogenic growth of collateral vessels in the limb. Indeed, despite excision of the femoral vessels, by week 12 no differences were found between in total blood vessel volume in the thigh; however, clear differences in morphology were present as HLI group possessed a more interconnected network of smaller diameter vessels. Accordingly, while the overall thigh vessel volume was comparable between groups, the contributions to vessel volume based on vessel diameter differed significantly. Yet, despite the evidence of a robust vascular growth response occurring in the thigh following ischemia, differences were not observed for bone defect blood vessel volume or morphology.

Consequently, we proposed a revised hypothesis that inclusion of HLI had coupled to the bone repair process by way of an augmented early vascular tissue growth response or perturbed signaling cascades initiated in the bone defect region or surrounding skeletal muscle envelope. In Aim III (Chapter 5), this same model was used to begin to test that hypothesis by investigating early spatiotemporal changes in blood flow and vascular tissue growth, as well as gene expression within the bone defect and

adjacent adductor muscle tissues. Although a rapid induction of vascular growth in the thigh was evident in both groups, HLI was associated with a more robust response. Ingrowth of blood vessels at the bone defect did not different significantly, however, indicating that HLI also does not augment vascularization at the site of bone regeneration at early time points. Thus, any effects of ischemia-induced vascular growth on bone regeneration are likely indirect ones. Additionally, while gene expression changed dramatically compared to naïve control tissue, based on the genes and time points investigated here, the stimulatory effects of HLI on bone regeneration could not be explained by gene expression alone. Taken together, this work suggests new, additional complexity to the coupling of bone repair with vascular growth and remodeling.

Overall, the enhanced bone regeneration observed in defects with HLI did not validate our original hypothesis of impaired healing with concomitant vascular injury, and suggests that this model does not recapitulate complications associated with vascular compromised clinical bone healing. This is most likely due to differences in scale of human patients versus small animal models, and the observation that the rat HLI injury induced a robust vascular response and only transient limb ischemia. However, the unexpected results of this study are important as they shed further light on the complex interactions between bone healing and vascular tissue growth. Furthermore, these results are an especially interesting point for future consideration given the high costs and incompletely understood (and at times negative) effects associated with current supraphysiological doses of BMPs administered to human patients (Garrison *et al.*, 2007; Cahill *et al.*, 2009; Devine *et al.*, 2012; Even *et al.*, 2012). Future work to improve understanding of the underlying mechanisms could provide useful insight to exploit this

interaction and guide development of novel therapeutic strategies for challenging clinical bone healing scenarios, and perhaps permit lower doses of rhBMP-2 to be used in humans without sacrificing efficacy.

Rapid vascular growth was evident in the thigh musculature at early time points following surgery, but was surpassed by the additional response invoked by concomitant HLI, with development of collateral vessels evident as early as post-surgery day 3. The HLI induced vascular growth produced stark differences in the morphology of thigh vasculature, resulting in more interconnected networks of smaller diameter vessels. Yet, HLI was not associated with differential vascularization of the bone defect at early time points or at the week 12 endpoint. Although when taken together these results do not preclude possible differences at intermediate time points that could be further investigated with additional experimentation, they suggest indirect coupling mechanisms for the stimulatory effect of HLI on bone regeneration rather than a direct influence on blood vessel ingrowth at the defect. Such mechanisms could perhaps be inclusive of augmented cellular exchange, gene expression, soluble factor bioavailability, or some combination thereof.

Accordingly, we investigated the expression of several genes involved in osteogenesis and vascular growth to determine whether HLI was associated with differential expression. Genes associated with inflammation were also investigated given its importance to both arteriogenesis (Cai and Schaper, 2008) and bone healing (Mountziaris and Mikos, 2008). Based on our findings that bone regeneration was increased with HLI as early as week 4, we investigated gene expression at multiple preceding time points. The overall minor effects of HLI on temporal gene expression in

both the defect region and adjacent adductor muscle tissue were unexpected. These results are perhaps indicative of the time points investigated. Although we believe these to have been a thorough effort to identify differences between groups, temporal changes in gene expression do not proceed at discrete intervals, and differences at other time points may have gone undiscovered. This is perhaps especially true with regard to the adductor muscle analysis. Angiography results show that collateral vessel development is already well underway by day 3, thus the day 7 time point may have missed much of the effects of HLI on gene expression. However, the primary focus of these studies was to characterize gene expression in the bone defect, and there was not a great deal of confidence that RNA samples of sufficient concentration and quality could be obtained from the defect prior to day 7. Accordingly, future studies could focus on additional upstream, downstream, or intermediate time points to further evaluate the effects of HLI on gene expression. Alternatively, while we attempted to capture a range of genes involved in osteogenesis, vascular growth, and inflammation, these biological processes are highly complex and the critical regulators – be those soluble signaling factors, membrane receptors, or ECM proteins – may not have been amongst the genes selected. Additional experimentation with expansion of the genes under investigation through the use of commercial microarray technology, global gene profiling (Niikura *et al.*, 2006), or transcriptome analysis (Grimes *et al.*, 2011) may provide additional insights not uncovered in the work here. Finally, given the heterogeneity of the bone defect and muscle tissue samples, qRT-PCR may not have been sensitive enough to detect the effects of HLI.

Other areas yet to be tested may provide useful insights for explaining the stimulatory effect of HLI recovery on rhBMP-2-mediated bone regeneration in this model. Rather than differential gene expression, augmented soluble factor bioavailability or cell populations mobilized due to the HLI response may contribute to enhanced bone repair. Future experiments using immunoblotting and immunohistochemistry techniques could assess whether the HLI recovery response is associated with increased circulating or localized soluble factor availability that might contribute to stimulatory effects for bone regeneration. Additionally, monocytes/macrophages are known to play a critical role in arteriogenesis. Increased circulating monocyte concentration and extravasation is associated with HLI (Heil *et al.*, 2002; Bergmann *et al.*, 2006), and could be one key difference between the experimental groups here that is yet to be studied. Increased mobilization of these cell populations might produce additional matrix degradation and soluble factor release. Furthermore, OPN is thought to play a role in mediating macrophage migration and adhesion (Giachelli *et al.*, 1998; Duvall *et al.*, 2008), and increased OPN expression in HLI animals, although not statistically significant, may have been biologically relevant to promote differences in activity of these cell populations. Experiments incorporating immunohistochemistry and flow cytometry could be performed to try and characterize the constituents of cell populations. Alternatively, experiments could be designed to perturb the activity of a certain cell population to determine the downstream effects on vascular growth and bone repair. One such experiment would be the targeted inhibition of monocyte extravasation in the HLI model via a pharmacological agent. Doing so would impair arteriogenesis, affording the opportunity to evaluate potential deleterious effects on bone regeneration.

Given the importance of myeloid lineage cells in the recovery from hind limb ischemia, it is conceivable that in response to the ischemic insult, an additional population of bone marrow-derived progenitor cells is mobilized into the circulation. Although it is believed that the progenitor cells involved in fracture repair arise primarily from the periosteum, it would be interesting to investigate whether HLI animals contain an additional population of bone-marrow derived cells participating in bone regeneration. Again, immunohistochemistry and flow cytometry could be two tools used to probe such questions. Bone marrow transplant studies could also be one potential way to evaluate such an effect. In these studies, bone marrow cells from labeled donors (e.g., GFP or Rosa26-lacZ) would be transplanted into irradiated wild type rats, and vice versa. After a suitable recovery period, surgery would be performed as usual and the relative contributions of bone-marrow derived cells could be assessed histologically.

In the work performed here, one limitation of the micro-CT angiography technique (as with other angiography techniques) is the inability to distinguish between arterial and venous supply, perhaps resulting in a failure to identify important insights for vascular networks. The recovery response to HLI produced rapid vascular growth in the thigh as demonstrated by comparable or increased blood vessel volume even at early time points despite the femoral vessels having been excised. This enhanced vascular growth may suggest increased arterial blood supply. In such a scenario, recovery from HLI may have resulted in superior oxygenation and nutrient supply to the surrounding skeletal muscle envelope, which could contribute to bone repair. Future work incorporating direct measurement of tissue oxygen levels or techniques to discriminate between arterial and venous structures may help to better interpret these results. Immunohistochemistry

techniques could provide some degree of insight on the latter, but are imperfect means for discerning vessel function and are unable to differentiate between patent and non-patent vessels. Additionally, LDPI was used here as a functional measure of blood perfusion, but while providing useful data points, the limited penetration depth of this imaging modality precludes full characterization of limb blood perfusion, and cutaneous inflammation and wound healing likely bias the data to some degree that is unrepresentative of tissue perfusion. When coupled with micro-CT angiography, a compelling evaluation of vascularity can be inferred, but an ability to acquire direct, longitudinal measurements of blood flow at the defect and in surrounding tissue would advance our understanding of the bone regeneration process.

One particularly intriguing future question prompted by the work here is whether the mechanisms associated with enhanced bone regeneration are a local effect or a systemic one. To probe this question, an experiment could be conducted where the HLI surgery is performed on the contralateral limb from the bone defect surgery. Were the effect to be demonstrated to be systemic, additional analysis would need to be performed to examine how the cellular constituents and soluble factor composition differed between groups with ischemia and groups without. A systemic effect would be particularly interesting from a clinical perspective, as it may be more readily translational.

Transitioning the bone and vascular injury used here to a murine model could provide useful insights in the future. Previously, others have shown that HLI will produce deleterious effects on tibial fracture healing in a mouse model (Lu *et al.*, 2007). It would be interesting to determine what effect concomitant HLI would have on murine femoral fracture healing or segmental bone defect repair. Were enhanced bone repair

results to be observed in femoral bone healing as they were in the work here, it would seem to further implicate the differences in vascular processes and tissue oxygenation between the upper and lower limb. Furthermore, a wide variety of transgenic knockout mice are already available to researchers. Coupling this model with transgenic knockout mice would allow for more specific mechanistic probing. Conversely, developing a large animal model of composite bone and vascular injury may better represent the size scale of humans and recapitulate complications associated with vascular compromised clinical bone healing. Such a model would provide a better platform to investigate the underlying mechanisms of impaired bone healing with concomitant vascular injury, as well as a suitable test bed to evaluate therapeutics designed to improve outcomes in healing challenged scenarios. In a similar vein, through collaboration with Dr. Dietmar Hutmacher at the Queensland University of Technology in Brisbane, Australia, an ovine tibial defect model is currently being used to evaluate the efficacy of the hybrid alginate/nanofiber mesh system in defects of a similar size to those presented clinically.

Beyond additional work using *in vivo* models, *in vitro* systems may be able to improve interpretation of the work presented here and further elucidate the mechanisms of interaction. The initial trigger for arteriogenesis is thought to be the "activated" endothelium produced as pre-existing collateral vessels are exposed to increased fluid shear stress in an attempt to compensate for arterial occlusions (Buschmann and Schaper, 1999). A series of *in vitro* experiments could be designed to begin to investigate how this activated endothelium may couple to bone repair. Conditioned media could be collected from endothelial cell cultures exposed to a normal level of oscillatory shear stress, high oscillatory shear stress, or no flow control. This conditioned media could then be used to

treat osteoblast or mesenchymal stem cell cultures to determine potential osteogenic effects. Osteogenic culture media would serve as a positive control. Another experiment could be performed to evaluate the chemotactic effects of the conditioned media. To do so, cell culture transwell inserts could be seeded with mesenchymal stem cells or hematopoietic stem cells with varying conditioned media samples in the lower reservoirs. After an allotted culture period, samples would be fixed and migration assessed.

Overall, the sparse amount of published experimental work on bone repair with concomitant vascular injury is surprising given the known clinical complications and poor healing outcomes for patients with these injuries. Accordingly, this is a clear area for future investigation to advance our understanding of this complex relationship and to develop TE/RM therapies to improve patient outcomes. As with all *in vivo* research, selection of the appropriate animal model for the desired objectives is paramount. Rat and mouse models present attractive choices for composite bone and vascular tissue trauma research for a variety of reasons, but consideration should be given to the specific limitations of models in these species. Undoubtedly, small animal composite injury models are more representative of clinical trauma conditions than their single-tissue injury counterparts, and are capable of providing new insight on interactions between vascular growth and osteogenesis beyond the scope of normal bone healing. However, interpretation of data from small animal models must take into consideration the robust neovascularization response in these species and differences in mass transport due to reduced size scale. This may be of particular importance when developing therapies to overcome the increased clinical challenges associated with diminished blood supply. Evaluation of therapeutic strategies in models where revascularization is not a limiting

factor is unlikely to reveal positive effects. Location of the orthopaedic injury is another important consideration. Bones of the lower leg have substantially decreased surrounding skeletal muscle mass; consequently, they are likely more susceptible to local tissue ischemia, and healing may be more strongly influenced by concomitant vascular injury.

Bone repair is intimately linked to vascular growth and remodeling. With sufficient consideration given to experimental design and intrinsic limitations, animal models of composite bone and vascular injuries offer a unique platform to obtain valuable insight for bone repair in instances with compromised vasculature, to advance our understanding of the complex mechanisms coupling vascular growth to bone repair, and ultimately improve outcomes for clinical patients.

Onward Toward Full Limb Regeneration

Ultimately, achieving the potential of TE/RM therapeutics will involve harnessing the regenerative potential of endogenous mechanisms – identifying the minimal intervention necessary to achieve maximum therapeutic benefit. Doing so will require a more advanced understanding of the interactions between healing tissues than is currently possessed. The overwhelming majority of musculoskeletal trauma models currently used for evaluating new TE/RM therapeutics consist of single-tissue defects. Although indispensible research tools, such models inherently possess limited utility for investigating strategies for the repair of large, multi-tissue defects and afford only little potential for insight into endogenous interactions between healing tissues. Models of composite tissue trauma are uniquely positioned to bridge this knowledge gap and advance the TE/RM field. This is because even in instances when composite injury

models fall short of recreating clinical conditions, as occurred with the bone-vascular injury model presented here, the additional intrinsic complexity affords potential for elucidating new insights.

As with all *in vivo* research, selection of the appropriate animal model for the research questions of interest is paramount. Considerations specific to bone-nerve and bone-vascular injury models have been previously discussed in this document. In general, the ramifications of species selection should be considered when designing research questions and when interpreting experimental results. Furthermore, location of the musculoskeletal injury should be carefully considered due to anatomical and physiological differences between the upper and lower portion of extremities. For effective comparisons of therapeutics, the model must present a challenging tissue defect in which a regenerative intervention is required for full recovery. In all models, quantitative outcome measures should be included for evaluation of tissue regeneration and composition, with three-dimensional analysis whenever possible. When evaluating therapeutics, functional assessments should be performed for the regenerated tissue, with comparisons made to intact or autograft controls. Additionally, when practical, outcome measures should be included to evaluate the degree of functional restoration in the limb *in vivo*.

The models covered in this project are primarily representative of controlled injuries to just two tissue types (although the surgical procedures possess inherent damage to muscle, fascia, and cutaneous tissues). While these models are undeniably more representative of clinical conditions than their single-tissue injury counterparts, the most accurate model of extremity trauma would be inclusive of bone, skeletal muscle,

vascular, neural, and adipocutaneous injuries. Such models would certainly present their own set of limitations, however, most notably the feasibility of implementation. As a step in that direction, ongoing work in our lab has focused on a composite injury model of a segmental bone defect in combination with volumetric muscle loss. The skeletal muscle envelope surrounding bones houses the peripheral nervous system as well as the vasculature of the circulatory system, and thus, volumetric muscle loss invokes injury to both tissue types in addition to the muscle tissue damaged. Findings from this model confirmed the hypothesis that volumetric muscle loss would impair bone regeneration (Willett *et al.*, 2012). Interactions between skeletal muscle and the bones it envelopes extend beyond physiologic biomechanical stimuli. Initial studies have identified skeletal muscle as a source of vascular supply to intact and healing bone, as well as a possible reservoir of soluble factors and progenitor cells capable of participating in, and influencing the outcome of, bone healing (Fig. 6.1).

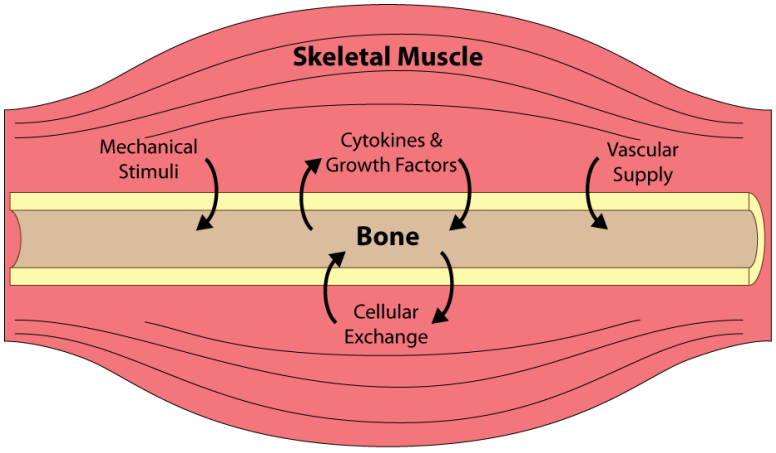

Figure 6.1. Mechanisms of interaction between bone and skeletal muscle. The skeletal muscle envelope of bones provides contraction-induced mechanical stimuli due to its physiological function, but also serves as a source of vascular supply, soluble factors, and cellular exchange.

However, the mechanisms of interaction associated with volumetric muscle loss may also be inclusive of those previously discussed for bone-neural and bone-vascular tissues. Beyond preclinical mammalian models, additional future insight may be obtained from ongoing work in vertebrate species such as salamanders that possess the inherent capacity to regenerate entire limbs (Brockes and Kumar, 2005; Nacu and Tanaka, 2011) (Fig. 6.2).

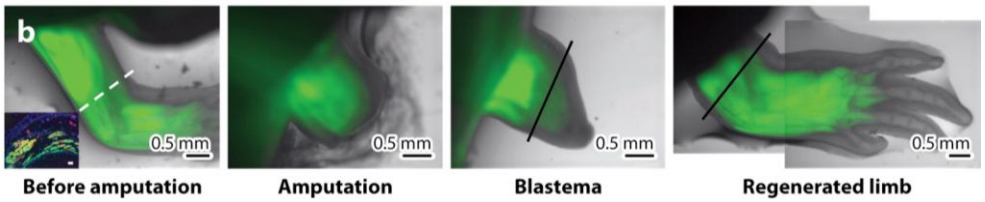

Figure 6.2. Entire limb regeneration demonstrated by salamanders. Adapted from Nacu and Tanaka, 2011.

Moving forward, successful leverage of models of composite tissue limb trauma will advance the understanding of tissue repair biology, and ultimately, may produce new therapeutic interventions for limb salvage and reconstruction that improve outcomes for extremity trauma patients.

APPENDIX A

PROTOCOLS

A.1 Segemental Bone Defect Surgery

Materials

Autoclave on Trays

- surgery drill
- surgery saw
- saw hex tool
- # 65 uncoated drill bits
- 5.5 x 12 x 0.4 mm micro oscillator saw blade
- scalpel handles
- curved hemostats
- needle holders/suture cutters
- small sharp scissors
- blunt scissors to cut drapes
- pickups (brown-adson forceps)
- small pointed forceps (both curved and straight)
- russian forceps
- wound clip applicator
- retractors
- fixation plate holding c-clamp

- miniature screws, #00-90, ¼" length (JI Morris Part No. P000120CE125)
- miniature screws, #000-120, 1/8" length (JI Morris Part No. P0090CE250)
- fixation plate assemblies (1 polysulfone and 2 steel components per assembly)
- miniature screw drivers (both larger and smaller tips)

Autoclave separately in pouches

- sterile bowls
- hoses for pneumatic drill/saw
- wound clips
- surgery lamp handles

Other Materials

- 4-0 vicryl suture
- #10 scalpel blades
- sterile 4x4 gauze
- small sterile drapes packs
- sterile half-drapes for surgery table
- sterile table drape for side table with tools
- surgical gowns
- sterile gloves
- glass bead sterilizer
- sterile water for rinsing tools
- sterile water (or saline) for irrigation
- sterile needles for irrigation

- sterile 10 ml syringes for irrigation
- scaffolds and biologics as necessary
- sterile bowls
- hoses for pneumatic drill/saw
- wound clips
- surgery lamp handles

Procedure

1. All personnel should wear scrubs, masks, head caps, and booties to ensure sterile environment.
2. Surgeons and sterile assistants should scrub in.
3. After scrubbing in, sterile personnel should assemble surgery tables making care to ensure a sterile surgical field. Non-sterile personnel assist in opening packaging.
4. Position glass bead sterilizer and turn on.
5. Position the circulating water bed and turn on to pre-warm for surgery. Cover with a sterile drape.
6. Animal prep can begin when surgeons are adequately close to operating. Care should be taken to minimize the time that animals are anesthetized.
7. Transfer a properly prepared rat to the surgery table. Insert the rat's nose into the nose cone, and straighten the tail so that it is not in contact with the feet of the animal.
8. Non-sterile personnel should hold each foot/toes with forceps to allow sterile personnel to wrap the feet with ioban.

9. Cut a hole in a sterile drape and position over the rat such that only the leg and surgical site are exposed.
10. Verify that fixation plate assemblies are constructed prior to beginning operation.
11. Make a skin incision on the anterior side of the leg. The incision should be roughly 25-30 mm and run approximately from the knee to the lower abdomen near the most caudally located nipple. Retract the skin. Additional skin retraction can be achieved by dissecting the skin away from underlying fascia.
12. It may be necessary to make an incision in the adipose tissue below the skin as well, especially at the more proximal end of the skin incision.
13. Using blunt dissection with a hemostat, separate the quadriceps muscle on the anteriolateral side of the femur. There should be a visible split in the muscle bundles that can serve as a guide. Be careful to avoid the femoral artery and other large blood vessels on the medial side of the quadriceps.
14. Loosen and retract the soft tissues from around the femur. Muscle tissue must be separated from the defect area to allow for accurate fixation plate placement.
15. As necessary, make small incisions in the musclulature to extend the opening created by blunt dissection and expose the femur for placement of fixation hardware.
16. Place the fixation plate on the anteriolateral side of the femur. This surface of the bone should be relatively flat and accommodate the plate placement well.
17. Secure the fixation plate in place with the c-clamp. After verifying correct plate placement, tighten the c-clamp prior to drilling. Be careful not to over-tighten the c-clamp, as this can lead to plate failure or bone fracture.

18. Drill through the bone using the screw holes on the plate as a guide. Start on the distal end and insert one screw, making sure that it is fully seated. If desired, the plate placement can be re-examined after insertion of the first screw to allow for adjustment if necessary.
19. Drill on the proximal end and drive one screw in the same manner.
20. Drill holes and drive the remaining two screws and remove the c-clamp.
21. Squirt a small amount of sterile water or saline onto the bone to serve as cooling fluid for making the saw cuts.
22. Make bone cuts using the oscillating saw at positions indicated by plate notches. Cuts should be made perpendicular to the long axis of the femur and parallel to each other.
23. Remove the segment of the femur and flush the defect site to remove any debris and residual bone chips.
24. Implant scaffolds and biologics as necessary.
25. Close the soft tissues with 4-0 vicryl suture.
26. Appose the skin incision and apply wound clips for closure.
27. When surgery is complete, non-sterile personnel can transfer the animal from the table and begin post-operative care.

A.2 Hind Limb Ischemia Surgery

Materials

Autoclave on Trays

- scalpel handles
- curved hemostats
- needle holders/suture cutters
- small sharp scissors
- blunt scissors to cut drapes
- pickups (brown-adson forceps)
- small pointed forceps (both curved and straight)
- fine dissecting Dumont forceps
- russian forceps
- wound clip applicator
- retractors

Autoclave separately in pouches

- sterile bowls
- wound clips
- surgery lamp handles

Other Materials

- 4-0 vicryl suture
- 6-0 silk suture

- #10 scalpel blades
- sterile 2x2 and 4x4 gauze
- sterile Q-tips
- small sterile drapes packs
- sterile half-drapes for surgery table
- sterile table drape for side table with tools
- surgical gowns
- sterile gloves
- glass bead sterilizer
- sterile water for rinsing tools
- sterile water (or saline) for irrigation
- sterile needles for irrigation
- sterile 10 ml syringes for irrigation
- scaffolds and biologics as necessary

Procedure

1. All personnel should wear scrubs, masks, head caps, and booties to ensure sterile environment.
2. Surgeons and sterile assistants should scrub in.
3. After scrubbing in, sterile personnel should assemble surgery tables making care to ensure a sterile surgical field. Non-sterile personnel assist in opening packaging.
4. Position glass bead sterilizer and turn on.

5. Position the circulating water bed and turn on to pre-warm for surgery. Cover with a sterile drape.
6. Animal prep can begin when surgeons are adequately close to operating. Care should be taken to minimize the time that animals are anesthetized.
7. Transfer a properly prepared rat to the surgery table. Insert the rat's nose into the nose cone, and straighten the tail so that it is not in contact with the feet of the animal.
8. Non-sterile personnel should hold each foot/toes with forceps to allow sterile personnel to wrap the feet with ioban.
9. Cut a hole in a sterile drape and position over the rat such that only the leg and surgical site are exposed.
10. Make a skin incision on the anterior side of the leg. The incision should be roughly 25-30 mm and run approximately from the knee to the lower abdomen near the most caudally located nipple. Retract the skin. Additional skin retraction can be achieved by dissecting the skin away from underlying fascia.
11. Locate femoral vessels and dissect away connective tissue.
12. Using fine Dumont forceps, carefully dissect the femoral artery and vein away from the associated nerves.
13. Ligate the femoral artery and vein at the level of the inguinal ligament using 6-0 silk suture. This is the most proximal ligation.
14. Ligate the femoral artery and vein just proximal to the popliteal bifurcation. This is the most distal ligation.
15. Two additional ligations are made at major arterial branch points.

16. Excise the length of the femoral artery and vein between the proximal and distal ligations, taking care to not cut any nerves. If necessary, the distance between the proximal and distal ligations can be measured prior to excision.
17. Irrigate the surgical field with saline.
18. If bone defect surgery is not necessary, proceed to wound closure.
19. Appose the skin incision and apply wound clips for closure.
20. When surgery is complete, non-sterile personnel can transfer the animal from the table and begin post-operative care.

A.3 Contrast Agent Vascular Perfusion

Materials

- 0.9% normal saline
- 0.4% (m/v) papaverine hydrochloride (Sigma-Aldrich) in 0.9% saline (vasodilator)
- Microfil MV-122 kit (yellow color lead chromate compound) (http://www.flowtech-inc.com)
- 10% neutral buffered formalin
- properly labeled waste bottles for formalin waste
- 1 pair small surgical scissors, 1 pair large scissors, 2 hemostats, 1 small curved pair of forceps, additional instruments by personal preference
- 18 gauge (green) 2" long catheter (Terumo SurFlo)
- needles
- 1ml slip tip and 30ml luer lock syringes
- peristaltic pump
- peristaltic pump tubing (Cole-Parmer Masterflex 96410-16)
- small tubing for connecting pump tubing to catheter (Cole-Parmer 95802-02)
- male and female luer lock connectors as needed
- diaper pads
- 50ml conicals for mixing Microfil and harvesting legs
- gauze and cotton swabs
- 2-0 needle-less suture
- Super glue

Procedure

1. Set up the peristaltic pump, check the flow, and bleed all air out of the line using the saline solution. You may have to start flow by siphoning the saline through the tubing using a syringe.
2. Induce anesthesia at 5% isoflurane in an induction chamber.
3. Switch animal over to the face mask at 2% isoflurane.
4. Check for pedal withdrawal reflex using the toe pinch. When this reflex is not observed, the animal has reached a deep surgical plane and the procedure can begin.
5. Using needles, pin animals hands and feet to styrofoam. Legs should be as straight as possible.
6. Using scissors, cut transversely through the skin & muscles just below the xyphoid process of the rib cage to expose the diaphragm.
7. Gently cut the diaphragm away from the rib cage, taking care not to puncture the heart or underlying vessels. Administration of isoflurane can be discontinued once the diaphragm has been cut.
8. Cut through the rib cage to allow opening of the chest cavity. A large hemostat can be used to help keep the chest cavity open by clamping to xyphoid and positioning the instrument as necessary.
9. Carefully dissect the heart free of the connective tissue holding it to the rib cage.
10. Using small blunt tip forceps, pass a piece of 2-0 suture behind the aorta.
11. While the heart is still pumping, insert the 18g catheter into the left ventricle (apex of the heart). Blood should begin to back out of the catheter.

12. After penetrating the wall of the LV, carefully back the needle and advance the soft catheter into the ascending aorta. Note the position of the catheter relative to the first branch of the aorta. During perfusion, the catheter tip should not be in this branch. It should be short of the branch or passed beyond the branch.
13. Using a single loop with the 2-0 suture, constrict the aorta around the catheter within its lumen to prevent back-flow later in the perfusion process. Optionally, place a small amount of super glue at the insertion point at the apex of the heart for additional stability.
14. Attach the connection tubing to the catheter, making sure to minimize any air in the tubing.
15. Cut the inferior vena cava.
16. Immediately, turn on the pump, pefusing with saline ~25-50 ml
17. Perfuse with ~100 ml of papaverine solution. The liver should blanche quite quickly. Skin can carefully be cut away on the leg for "windows" to inspect perfusion of the hind limbs. Kidneys can be inspected to evaluate perfusion, also.
18. Clear with ~25-50 ml of saline. It may be necessary to continue to run saline for the vessels to clear.
19. Perfuse with 10% NBF ~150-250 ml. Perfusion volume is an estimate. The goal is to perfuse until the extremities are fully fixed. Inflation of the lungs is an indicator of backflow in the system. After ~100 ml, one may observe relative inflation of the GI system, which is not abnormal.
20. Clear with Saline ~25-50 ml

21. Mix MV-122 with diluent in a 50 ml conical tube. Then, add catalyst, mix, and immediately transfer to a 30 ml syringe for injection. Exhaust as much air as possible from the syringe before attaching to tubing.
22. Switch luer-lock connector from pump tubing to syringe, being careful to minimize induction of air to the system. Slowly perfuse the animal manually, taking care not to let the catheter back out.
23. Store animal in 4C refrigerator overnight to allow the microfil to polymerize.
24. Remove the hindlimbs and immersion fix (generally only a few days).
25. MicroCT scan to get composite image of bone and vasculature.
26. Decalcify hindlimbs in Cal-Ex II for 2 weeks. Use only gentle agitation, if any. Strong agitation will shake polymerized microfil out of the vessels.
27. MicroCT scan to get vasculature alone.

A.4 RNA Sample Purification from Animal Tissue

This protocol is a modification of the Qiagen protocol for the RNEasy Fibrous Tissue Mini Kit. It is recommended to review their handbook prior to beginning RNA purification.

Determining the Correct Amount of Starting Material

It is essential to use the correct amount of tissue in order to obtain optimal RNA yield and purity. With the RNeasy Fibrous Tissue Mini Kit, a maximum of 30 mg tissue can generally be processed. For most tissues, the RNA binding capacity of the RNeasy spin column and the lysing capacity of Buffer RLT and proteinase K will not be exceeded by this amount. Average RNA yields from various tissues are given in the Qiagen handbook. For more homogeneous sampling, starting material in excess of 30 mg tissue can be used (with appropriate scale up of RLT buffer), but after lysis step, only 300 µl should be used for downstream steps. The remainder of the homogenized tissue lysate can be stored at –70°C for several months.

Do not overload the RNeasy spin column, as this will significantly reduce RNA yield and quality.

Weighing tissue is the most accurate way to quantify the amount of starting material. As a guide, a 3 mm cube (27 mm3) of most animal tissues weighs 25–35 mg.

Important Points Before Starting

- If using RNeasy Fibrous Tissue Kits for the first time, read “Important Notes” from Qiagen handbook
- If working with RNA for the first time, read Appendix A from Qiagen handbook

- Since the RNase-inactivating Buffer RLT must be diluted to permit proteinase K digestion, this protocol should not be used for tissues rich in RNases, such as pancreas or intestine per Qiagen.
- Fresh, frozen, or RNAlater stabilized tissues can be used. If freezing tissues, flashfreeze in liquid nitrogen and immediately transfer to –70°C, where they can be stored for several months. Do not allow tissues to thaw during weighing or handling prior to disruption in Buffer RLT. Homogenized tissue lysates from step 4 can also be stored at –70°C for several months. Incubate frozen lysates at 37°C in a water bath until completely thawed and salts are dissolved before continuing with step 5. Avoid prolonged incubation, which may compromise RNA integrity.
- Do not vortex reconstituted DNase I. DNase I is especially sensitive to physical denaturation. Mixing should only be carried out by gently inverting the tube.
- Buffer RLT may form a precipitate upon storage. If necessary, redissolve by warming, and then place at room temperature (15–25°C).
- Buffer RLT and Buffer RW1 contain a guanidine salt and are therefore not compatible with disinfecting reagents containing bleach.
- Unless otherwise indicated, perform all steps of the procedure at room temperature. During the procedure, work quickly.
- Perform all centrifugation steps at 20–25°C. Ensure that the centrifuge does not cool below 20°C.

Things to Do Before Starting

- β-Mercaptoethanol (β-ME) must be added to Buffer RLT before use. Add 10 µl β-ME per 1 ml Buffer RLT. Dispense in a fume hood and wear appropriate

protective clothing. Buffer RLT containing β-ME can be stored at room temperature for up to 1 month.

Alternatively, add 20 µl of 2 M dithiothreitol (DTT) per 1 ml Buffer RLT. The stock solution of 2 M DTT in water should be prepared fresh, or frozen in single-use aliquots. Buffer RLT containing DTT can be stored at room temperature for up to 1 month.

- Rotor stator homogenizer must be cleaned before use if it will be used for generating homogenized tissue lysates. It should be thoroughly wiped down with RNaseZAP and thoroughly rinsed with ethanol then water.
- Buffer RPE is supplied as a concentrate. Before using for the first time, add 4 volumes of ethanol (96–100%) as indicated on the bottle to obtain a working solution.
- If on column DNase digestion will be performed, prepare DNase I stock solution before using the RNase-Free DNase Set for the first time. Dissolve the lyophilized DNase I (1500 Kunitz units) in 550 µl of the RNasefree water provided in the RNase-Free DNase Set box. To avoid loss of DNase I, do not open the vial. Inject RNase-free water into the vial using an RNase-free needle and syringe. Mix gently by inverting the vial. Do not vortex.
- For long-term storage of DNase I, remove the stock solution from the glass vial, divide it into single-use aliquots, and store at –20°C for up to 9 months. Thawed aliquots can be stored at 2–8°C for up to 6 weeks. Do not refreeze the aliquots after thawing.

Procedure

1. Heat a water bath or heating block to 55°C for proteinase K digestion in step 6.
2. If working with tissues that are notstabilized in RNAlater RNA Stabilization Reagent, place the tubes on dry ice.

3. Excise the tissue sample from the animal or remove it from storage. Determine theamount of tissue. Do not use more than 30 mg (as noted above, exceptions apply for the amount of initial tissue, but more than 30 mg worth of lysed tissue should not be used downstream of the lysis step). Proceed immediately to RLT buffer addition in step 4.

   Weighing tissue is the most accurate way to determine the amount.

   If the tissue sample was stored in RNAlater RNA Stabilization Reagent, remove it from the reagent using forceps and be sure to remove any crystals that may have formed.

   RNA in harvested tissues is not protected until the tissues are treated with RNAlater RNA Stabilization Reagent, flash-frozen, or disrupted and homogenized in step 4. Frozen tissues should not be allowed to thaw during handling. The relevant procedures should be carried out as quickly as possible.

4. Place the tissue in a suitably sized vessel. Add 300 µl Buffer RLT (add additional RLT buffer if tissue sample for lysis is in excess of 30 mg).

   Generally, round-bottomed tubes allow more efficient disruption and homogenization than conical-bottomed tubes. Qiagen 2 ml collection tubes (PCR clean) and BD polystyrene 5 ml tubes (not-PCR clean) have both been successfully used.

5. Disrupt the tissue and homogenize the lysate using the rotor stator homogenizer.

   See “Disrupting and homogenizing starting material” in Qiagen handbook, for more details on disruption and homogenization.

Note: Ensure that β-ME is added to Buffer RLT before use (see "Things to do before starting").

Note: Incomplete homogenization leads to significantly reduced RNA yields and can cause clogging of the RNeasy spin column.

Place the tip of the homogenizer into the vessel and operate at 50-75% full speed until the lysate is uniformly homogeneous (usually 1 or 2 bouts of ~20 s).

Note: Between samples, the homogenizer should be cleaned to avoid cross-contamination. Wipe down with RNaseZAP, followed by rinses of PCR clean water, ethanol, and water again. Excess fluid remaining on homogenizer should be dabbed away with a KimWipe to avoid dilution of RLT buffer.

6. Incubate homogenized lysate samples at RT for 5 min.
7. Add 590 µl RNase-free water to each 300 µl lysate. Then add 10 µl proteinase K solution, and mix thoroughly by pipetting.
8. Incubate on heat block at 55°C for 10 min.
9. Pipette each sample to two Qiashredder columns (450 µl in each). Centrifuge at 20–25°C for 5 min at 12,000 x g.
10. Pipet the supernatant (approximately 900 µl) into a new 1.5 ml or 2 ml microcentrifuge tube (not supplied).

    Avoid transferring any of the pellet. If this is unavoidable, a small amount of pelleted debris may be carried over without affecting the RNeasy procedure. If any film is present on top of supernatant (rare after having used Qiashredder column), hold the pipet tip under the thin layer or film on top of the supernatant, if

present. This layer will usually adhere to the outside of the pipet tip and should not be transferred.

11. Add 0.5 volumes (450 µl) of ethanol (96–100%) to the cleared lysate. Mix well by pipetting. Do not centrifuge.

    Precipitates may be visible after addition of ethanol. This does not affect the procedure.

12. Transfer 700 µl of the sample, including any precipitate that may have formed, to an RNeasy Mini spin column placed in a 2 ml collection tube. Close the lid gently, and centrifuge at 20–25°C for 15 s at 8000 x g (10,000 rpm). Discard the flowthrough in proper recepticle.

    Reuse the collection tube in step 13.

13. Repeat step 10 using the remainder of the sample. Discard the flow-through.

    Reuse the collection tube in step 14.

14. Add 350 µl Buffer RW1 to the RNeasy spin column. Close the lid gently, and centrifuge at 20–25°C for 15 s at 8000 x g (10,000 rpm) to wash the membrane. Discard the flow-through.

    Reuse the collection tube in step 15.

    Optional: If on-column DNase digestion is not desired, add 700 µl Buffer RW1 instead, centrifuge for 15 s at 8000 x g, and discard the flow-through* (but not the collection tube). Proceed to step 18.

15. Add 10 µl DNase I stock solution to 70 µl Buffer RDD. Mix by gently inverting the tube, and centrifuge briefly to collect residual liquid from the sides of the tube.

Note: DNase I is especially sensitive to physical denaturation. Mixing should only be carried out by gently inverting the tube. Do not vortex.

16. Add the DNase I incubation mix (80 µl) directly to the RNeasy spin column membrane, and place on the benchtop (20–30°C) for 15 min.

    Note: Be sure to add the DNase I incubation mix directly to the RNeasy spin column membrane. DNase digestion will be incomplete if part of the mix sticks to the walls or the O-ring of the spin column.

17. Add 350 µl Buffer RW1 to the RNeasy spin column. Close the lid gently, and centrifuge for 15 s at 8000 x g (10,000 rpm) at 20–25°C. Discard the flowthrough.

    Reuse the collection tube in step 18.

18. Add 500 µl Buffer RPE to the RNeasy spin column. Close the lid gently, and centrifuge at 20–25°C for 15 s at 8000 x g (10,000 rpm) to wash the membrane. Discard the flow-through.

    Reuse the collection tube in step 19.

    Note: Buffer RPE is supplied as a concentrate. Ensure that ethanol is added to Buffer RPE before use (see "Things to do before starting").

19. Add 500 µl Buffer RPE to the RNeasy spin column. Close the lid gently, and centrifuge at 20–25°C for 2 min at 8000 x g (10,000 rpm) to wash the membrane.

    The long centrifugation dries the spin column membrane, ensuring that no ethanol is carried over during RNA elution. Residual ethanol may interfere with downstream reactions.

Note: After centrifugation, carefully remove the RNeasy spin column from the collection tube so that the column does not contact the flow-through. Otherwise, carryover of ethanol will occur.

20. Optional: Place the RNeasy spin column in a new 2 ml collection tube, and discard the old collection tube with the flow-through. Close the lid gently, and centrifuge at full speed for 1 min.

    Perform this step to eliminate any possible carryover of Buffer RPE, or if residual flow-through remains on the outside of the RNeasy spin column after step 19.

21. Place the RNeasy spin column in a new 1.5 ml collection tube (Eppendorf). Add 30–50 µl RNase-free water directly to the RNeasy spin column membrane. Close the lid gently. Allow to rest for 1 min prior to centrifugation. To elute the RNA, centrifuge for 1 min at 8000 x g (10,000 rpm) at 20–25°C.
22. Optional: Repeat step 21 using another 30–50 µl RNase-free water, or using the eluate from step 21 (if high RNA concentration is required). Reuse the collection tube from step 21. If the expected RNA yield is >30 µg, there is no need to repeat step 19.If using the eluate from step 19, the RNA yield will be 15–30% less than that obtained using a second volume of RNase-free water, but the final RNA concentration will be higher.
23. Use spectrophotometer to determine RNA sample concentration and purity.
24. Store RNA samples at -80°C until ready to proceed to downstream applications.

REFERENCES

Alsberg E, Kong HJ, Hirano Y, Smith MK, Albeiruti A, Mooney DJ. 2003, Regulating bone formation via controlled scaffold degradation, *J Dent Res*, **82**: 903-908

Apel PJ, Crane D, Northam CN, Callahan M, Smith TL, Teasdall RD. 2009, Effect of selective sensory denervation on fracture-healing: an experimental study of rats, *J Bone Joint Surg Am*, **91**: 2886-2895

Araldi E, Schipani E. 2010, Hypoxia, HIFs and bone development, *Bone*, **47**: 190-196

Aro H. 1985, Effect of nerve injury on fracture healing. Callus formation studied in the rat, *Acta Orthop Scand*, **56**: 233-237

Aro H, Eerola E, Aho AJ. 1985, Development of nonunions in the rat fibula after removal of periosteal neural mechanoreceptors, *Clin Orthop Relat Res*: 292-299

Aro H, Eerola E, Aho AJ, Penttinen R. 1981, Healing of experimental fractures in the denervated limbs of the rat, *Clin Orthop Relat Res*: 211-217

Aronson J, Shen XC, Skinner RA, Hogue WR, Badger TM, Lumpkin CK, Jr. 1997, Rat model of distraction osteogenesis, *J Orthop Res*, **15**: 221-226

Arras M, Ito WD, Scholz D, Winkler B, Schaper J, Schaper W. 1998, Monocyte activation in angiogenesis and collateral growth in the rabbit hindlimb, *J Clin Invest*, **101**: 40-50

Asaumi K, Nakanishi T, Asahara H, Inoue H, Takigawa M. 2000, Expression of neurotrophins and their receptors (TRK) during fracture healing, *Bone*, **26**: 625-633

Ballica R, Valentijn K, Khachatryan A, Guerder S, Kapadia S, Gundberg C, Gilligan J, Flavell RA, Vignery A. 1999, Targeted expression of calcitonin gene-related peptide to osteoblasts increases bone density in mice, *J Bone Miner Res*, **14**: 1067-1074

Beamish JA, He P, Kottke-Marchant K, Marchant RE. 2010, Molecular regulation of contractile smooth muscle cell phenotype: implications for vascular tissue engineering, *Tissue Eng Part B Rev*, **16**: 467-491

Bergmann CE, Hoefer IE, Meder B, Roth H, van Royen N, Breit SM, Jost MM, Aharinejad S, Hartmann S, Buschmann IR. 2006, Arteriogenesis depends on circulating monocytes and macrophage accumulation and is severely depressed in op/op mice, *Journal of leukocyte biology*, **80**: 59-65

Bernard GW, Shih C. 1990, The osteogenic stimulating effect of neuroactive calcitonin gene-related peptide, *Peptides*, **11**: 625-632

Bjurholm A, Kreicbergs A, Brodin E, Schultzberg M. 1988, Substance P- and CGRP-immunoreactive nerves in bone, *Peptides*, **9**: 165-171

Boerckel JD, Kolambkar YM, Dupont KM, Uhrig BA, Phelps EA, Stevens HY, Garcia AJ, Guldberg RE. 2011, Effects of protein dose and delivery system on BMP-mediated bone regeneration, *Biomaterials*, **32**: 5241-5251

Boerckel JD, Kolambkar YM, Stevens HY, Lin AS, Dupont KM, Guldberg RE. 2011, Effects of in vivo mechanical loading on large bone defect regeneration, *J Orthop Res*,

Boerckel JD, Kolambkar YM, Stevens HY, Lin AS, Dupont KM, Guldberg RE. 2012, Effects of in vivo mechanical loading on large bone defect regeneration, *J Orthop Res*, **30**: 1067-1075

Boerckel JD, Uhrig BA, Willett NJ, Huebsch N, Guldberg RE. 2011, Mechanical regulation of vascular growth and tissue regeneration in vivo, *Proc Natl Acad Sci U S A*, **108**: E674-680

Boes M, Kain M, Kakar S, Nicholls F, Cullinane D, Gerstenfeld L, Einhorn TA, Tornetta P, 3rd. 2006, Osteogenic effects of traumatic brain injury on experimental fracture-healing, *J Bone Joint Surg Am*, **88**: 738-743

Bosse MJ, MacKenzie EJ, Kellam JF, Burgess AR, Webb LX, Swiontkowski MF, Sanders RW, Jones AL, McAndrew MP, Patterson BM, McCarthy ML, Travison TG, Castillo RC. 2002, An analysis of outcomes of reconstruction or amputation after leg-threatening injuries, *N Engl J Med*, **347**: 1924-1931

Bouletreau PJ, Warren SM, Spector JA, Peled ZM, Gerrets RP, Greenwald JA, Longaker MT. 2002, Hypoxia and VEGF up-regulate BMP-2 mRNA and protein expression in microvascular endothelial cells: implications for fracture healing, *Plast Reconstr Surg*, **109**: 2384-2397

Box GE, Cox DR. 1964, An analysis of transformations, *Journal of the Royal Statistical Society. Series B (Methodological)*: 211-252

Bozkurt A, Deumens R, Scheffel J, O'Dey DM, Weis J, Joosten EA, Fuhrmann T, Brook GA, Pallua N. 2008, CatWalk gait analysis in assessment of functional recovery after sciatic nerve injury, *J Neurosci Methods*, **173**: 91-98

Bozkurt A, Scheffel J, Brook GA, Joosten EA, Suschek CV, O'Dey DM, Pallua N, Deumens R. 2011, Aspects of static and dynamic motor function in peripheral nerve regeneration: SSI and CatWalk gait analysis, *Behav Brain Res*, **219**: 55-62

Brain SD, Williams TJ, Tippins JR, Morris HR, MacIntyre I. 1985, Calcitonin gene-related peptide is a potent vasodilator, *Nature*, **313**: 54-56

Brinker MR, Bailey DE, Jr. 1997, Fracture healing in tibia fractures with an associated vascular injury, *J Trauma*, **42**: 11-19

Brockes JP, Kumar A. 2005, Appendage regeneration in adult vertebrates and implications for regenerative medicine, *Science*, **310**: 1919-1923

Bruick RK, McKnight SL. 2001, A conserved family of prolyl-4-hydroxylases that modify HIF, *Science*, **294**: 1337-1340

Buie HR, Campbell GM, Klinck RJ, MacNeil JA, Boyd SK. 2007, Automatic segmentation of cortical and trabecular compartments based on a dual threshold technique for in vivo micro-CT bone analysis, *Bone*, **41**: 505-515

Burgess AR, Dischinger PC, O'Quinn TD, Schmidhauser CB. 1995, Lower extremity injuries in drivers of airbag-equipped automobiles: clinical and crash reconstruction correlations, *J Trauma*, **38**: 509-516

Buschmann I, Heil M, Jost M, Schaper W. 2003, Influence of inflammatory cytokines on arteriogenesis, *Microcirculation*, **10**: 371-379

Buschmann I, Schaper W. 1999, Arteriogenesis Versus Angiogenesis: Two Mechanisms of Vessel Growth, *News in physiological sciences : an international journal of physiology produced jointly by the International Union of Physiological Sciences and the American Physiological Society*, **14**: 121-125

Cahill KS, Chi JH, Day A, Claus EB. 2009, Prevalence, complications, and hospital charges associated with use of bone-morphogenetic proteins in spinal fusion procedures, *JAMA : the journal of the American Medical Association*, **302**: 58-66

Cai W, Schaper W. 2008, Mechanisms of arteriogenesis, *Acta biochimica et biophysica Sinica*, **40**: 681-692

Cao R, Brakenhielm E, Pawliuk R, Wariaro D, Post MJ, Wahlberg E, Leboulch P, Cao Y. 2003, Angiogenic synergism, vascular stability and improvement of hind-limb ischemia by a combination of PDGF-BB and FGF-2, *Nat Med*, **9**: 604-613

Caplan AI, Correa D. 2011, PDGF in bone formation and regeneration: new insights into a novel mechanism involving MSCs, *J Orthop Res*, **29**: 1795-1803

Carano RA, Filvaroff EH. 2003, Angiogenesis and bone repair, *Drug Discov Today*, **8**: 980-989

Carmeliet P. 2000, Mechanisms of angiogenesis and arteriogenesis, *Nat Med*, **6**: 389-395

Carr MM, Best TJ, Mackinnon SE, Evans PJ. 1992, Strain differences in autotomy in rats undergoing sciatic nerve transection or repair, *Ann Plast Surg*, **28**: 538-544

Carvalho RS, Einhorn TA, Lehmann W, Edgar C, Al-Yamani A, Apazidis A, Pacicca D, Clemens TL, Gerstenfeld LC. 2004, The role of angiogenesis in a murine tibial model of distraction osteogenesis, *Bone*, **34**: 849-861

Champagne CM, Takebe J, Offenbacher S, Cooper LF. 2002, Macrophage cell lines produce osteoinductive signals that include bone morphogenetic protein-2, *Bone*, **30**: 26-31

Clarkin CE, Gerstenfeld LC. 2013, VEGF and bone cell signalling: an essential vessel for communication?, *Cell biochemistry and function*, **31**: 1-11

Clements IP, Kim YT, English AW, Lu X, Chung A, Bellamkonda RV. 2009, Thin-film enhanced nerve guidance channels for peripheral nerve repair, *Biomaterials*, **30**: 3834-3846

Colnot C, Thompson Z, Miclau T, Werb Z, Helms JA. 2003, Altered fracture repair in the absence of MMP9, *Development*, **130**: 4123-4133

Corcoran HA, Smith BE, Mathers P, Pisacreta D, Hershey JC. 2009, Laser Doppler imaging of reactive hyperemia exposes blood flow deficits in a rat model of experimental limb ischemia, *Journal of cardiovascular pharmacology*, **53**: 446-451

Couffinhal T, Silver M, Zheng LP, Kearney M, Witzenbichler B, Isner JM. 1998, Mouse model of angiogenesis, *Am J Pathol*, **152**: 1667-1679

Crisan M, Yap S, Casteilla L, Chen CW, Corselli M, Park TS, Andriolo G, Sun B, Zheng B, Zhang L, Norotte C, Teng PN, Traas J, Schugar R, Deasy BM, Badylak S, Buhring HJ, Giacobino JP, Lazzari L, Huard J, Peault B. 2008, A perivascular origin for mesenchymal stem cells in multiple human organs, *Cell stem cell*, **3**: 301-313

Deckers MM, Karperien M, van der Bent C, Yamashita T, Papapoulos SE, Lowik CW. 2000, Expression of vascular endothelial growth factors and their receptors during osteoblast differentiation, *Endocrinology*, **141**: 1667-1674

Deckers MM, van Bezooijen RL, van der Horst G, Hoogendam J, van Der Bent C, Papapoulos SE, Lowik CW. 2002, Bone morphogenetic proteins stimulate angiogenesis through osteoblast-derived vascular endothelial growth factor A, *Endocrinology*, **143**: 1545-1553

DeFranco MJ, Lawton JN. 2006, Radial nerve injuries associated with humeral fractures, *J Hand Surg Am*, **31**: 655-663

Deindl E, Buschmann I, Hoefer IE, Podzuweit T, Boengler K, Vogel S, van Royen N, Fernandez B, Schaper W. 2001, Role of ischemia and of hypoxia-inducible genes in arteriogenesis after femoral artery occlusion in the rabbit, *Circ Res*, **89**: 779-786

Deindl E, Hoefer IE, Fernandez B, Barancik M, Heil M, Strniskova M, Schaper W. 2003, Involvement of the fibroblast growth factor system in adaptive and chemokine-induced arteriogenesis, *Circ Res*, **92**: 561-568

Deschaseaux F, Sensebe L, Heymann D. 2009, Mechanisms of bone repair and regeneration, *Trends Mol Med*, **15**: 417-429

Deumens R, Jaken RJ, Marcus MA, Joosten EA. 2007, The CatWalk gait analysis in assessment of both dynamic and static gait changes after adult rat sciatic nerve resection, *J Neurosci Methods*, **164**: 120-130

Devine JG, Dettori JR, France JC, Brodt E, McGuire RA. 2012, The use of rhBMP in spine surgery: is there a cancer risk?, *Evidence-based spine-care journal*, **3**: 35-41

Dickson K, Katzman S, Delgado E, Contreras D. 1994, Delayed unions and nonunions of open tibial fractures. Correlation with arteriography results, *Clin Orthop Relat Res*: 189-193

Dodla MC, Bellamkonda RV. 2008, Differences between the effect of anisotropic and isotropic laminin and nerve growth factor presenting scaffolds on nerve regeneration across long peripheral nerve gaps, *Biomaterials*, **29**: 33-46

Du X, Xie Y, Xian CJ, Chen L. 2012, Role of FGFs/FGFRs in skeletal development and bone regeneration, *Journal of cellular physiology*, **227**: 3731-3743

Ducy P, Amling M, Takeda S, Priemel M, Schilling AF, Beil FT, Shen J, Vinson C, Rueger JM, Karsenty G. 2000, Leptin inhibits bone formation through a hypothalamic relay: a central control of bone mass, *Cell*, **100**: 197-207

Duvall CL, Taylor WR, Weiss D, Guldberg RE. 2004, Quantitative microcomputed tomography analysis of collateral vessel development after ischemic injury, *Am J Physiol Heart Circ Physiol*, **287**: H302-310

Duvall CL, Taylor WR, Weiss D, Wojtowicz AM, Guldberg RE. 2007, Impaired angiogenesis, early callus formation, and late stage remodeling in fracture healing of osteopontin-deficient mice, *J Bone Miner Res*, **22**: 286-297

Duvall CL, Weiss D, Robinson ST, Alameddine FM, Guldberg RE, Taylor WR. 2008, The role of osteopontin in recovery from hind limb ischemia, *Arterioscler Thromb Vasc Biol*, **28**: 290-295

Einhorn TA. 1995, Enhancement of fracture-healing, *J Bone Joint Surg Am*, **77**: 940-956

Einhorn TA. 1998, The cell and molecular biology of fracture healing, *Clin Orthop Relat Res*: S7-21

Elefteriou F. 2008, Regulation of bone remodeling by the central and peripheral nervous system, *Arch Biochem Biophys*, **473**: 231-236

Even J, Eskander M, Kang J. 2012, Bone morphogenetic protein in spine surgery: current and future uses, *J Am Acad Orthop Surg*, **20**: 547-552

Fang TD, Salim A, Xia W, Nacamuli RP, Guccione S, Song HM, Carano RA, Filvaroff EH, Bednarski MD, Giaccia AJ, Longaker MT. 2005, Angiogenesis is required for successful bone induction during distraction osteogenesis, *J Bone Miner Res*, **20**: 1114-1124

Ferguson C, Alpern E, Miclau T, Helms JA. 1999, Does adult fracture repair recapitulate embryonic skeletal formation?, *Mech Dev*, **87**: 57-66

Ferland CE, Laverty S, Beaudry F, Vachon P. 2011, Gait analysis and pain response of two rodent models of osteoarthritis, *Pharmacol Biochem Behav*, **97**: 603-610

Foley PL, Liang H, Crichlow AR. 2011, Evaluation of a sustained-release formulation of buprenorphine for analgesia in rats, *Journal of the American Association for Laboratory Animal Science : JAALAS*, **50**: 198-204

Forsythe JA, Jiang BH, Iyer NV, Agani F, Leung SW, Koos RD, Semenza GL. 1996, Activation of vascular endothelial growth factor gene transcription by hypoxia-inducible factor 1, *Mol Cell Biol*, **16**: 4604-4613

Frenkel SR, Guerra LA, Mitchell OG, Singh IJ. 1990, Nerve growth factor in skeletal tissues of the embryonic chick, *Cell Tissue Res*, **260**: 507-511

Frymoyer JW, Pope MH. 1977, Fracture healing in the sciatically denervated rat, *J Trauma*, **17**: 355-361

Garland DE. 1988, Clinical observations on fractures and heterotopic ossification in the spinal cord and traumatic brain injured populations, *Clin Orthop Relat Res*: 86-101

Garrison KR, Donell S, Ryder J, Shemilt I, Mugford M, Harvey I, Song F. 2007, Clinical effectiveness and cost-effectiveness of bone morphogenetic proteins in the non-healing of fractures and spinal fusion: a systematic review, *Health technology assessment*, **11**: 1-150, iii-iv

Gerber HP, Vu TH, Ryan AM, Kowalski J, Werb Z, Ferrara N. 1999, VEGF couples hypertrophic cartilage remodeling, ossification and angiogenesis during endochondral bone formation, *Nat Med*, **5**: 623-628

Gerstenfeld LC, Cho TJ, Kon T, Aizawa T, Cruceta J, Graves BD, Einhorn TA. 2001, Impaired intramembranous bone formation during bone repair in the absence of tumor necrosis factor-alpha signaling, *Cells Tissues Organs*, **169**: 285-294

Gerstenfeld LC, Cho TJ, Kon T, Aizawa T, Tsay A, Fitch J, Barnes GL, Graves DT, Einhorn TA. 2003, Impaired fracture healing in the absence of TNF-alpha signaling: the role of TNF-alpha in endochondral cartilage resorption, *J Bone Miner Res*, **18**: 1584-1592

Gerstenfeld LC, Cullinane DM, Barnes GL, Graves DT, Einhorn TA. 2003, Fracture healing as a post-natal developmental process: molecular, spatial, and temporal aspects of its regulation, *J Cell Biochem*, **88**: 873-884

Giachelli CM, Lombardi D, Johnson RJ, Murry CE, Almeida M. 1998, Evidence for a role of osteopontin in macrophage infiltration in response to pathological stimuli in vivo, *Am J Pathol*, **152**: 353-358

Glass GE, Pearse MF, Nanchahal J. 2009, Improving lower limb salvage following fractures with vascular injury: a systematic review and new management algorithm, *J Plast Reconstr Aesthet Surg*, **62**: 571-579

Glowacki J. 1998, Angiogenesis in fracture repair, *Clin Orthop Relat Res*: S82-89

Godwin JW, Pinto AR, Rosenthal NA. 2013, Macrophages are required for adult salamander limb regeneration, *Proc Natl Acad Sci U S A*,

Grills BL, Schuijers JA, Ward AR. 1997, Topical application of nerve growth factor improves fracture healing in rats, *J Orthop Res*, **15**: 235-242

Grimes R, Jepsen KJ, Fitch JL, Einhorn TA, Gerstenfeld LC. 2011, The transcriptome of fracture healing defines mechanisms of coordination of skeletal and vascular development during endochondral bone formation, *J Bone Miner Res*, **26**: 2597-2609

Grundnes O, Reikeras O. 1993, The importance of the hematoma for fracture healing in rats, *Acta Orthop Scand*, **64**: 340-342

Haegerstrand A, Dalsgaard CJ, Jonzon B, Larsson O, Nilsson J. 1990, Calcitonin gene-related peptide stimulates proliferation of human endothelial cells, *Proc Natl Acad Sci U S A*, **87**: 3299-3303

Haller A (1763). Experimentorum de ossium formatione. Opera minora. Lausanne, Fancisci Grasset. **2**.

Hamers FP, Lankhorst AJ, van Laar TJ, Veldhuis WB, Gispen WH. 2001, Automated quantitative gait analysis during overground locomotion in the rat: its application to spinal cord contusion and transection injuries, *J Neurotrauma*, **18**: 187-201

Hausman MR, Schaffler MB, Majeska RJ. 2001, Prevention of fracture healing in rats by an inhibitor of angiogenesis, *Bone*, **29**: 560-564

Heil M, Schaper W. 2004, Influence of mechanical, cellular, and molecular factors on collateral artery growth (arteriogenesis), *Circ Res*, **95**: 449-458

Heil M, Ziegelhoeffer T, Pipp F, Kostin S, Martin S, Clauss M, Schaper W. 2002, Blood monocyte concentration is critical for enhancement of collateral artery growth, *Am J Physiol Heart Circ Physiol*, **283**: H2411-2419

Heil M, Ziegelhoeffer T, Wagner S, Fernandez B, Helisch A, Martin S, Tribulova S, Kuziel WA, Bachmann G, Schaper W. 2004, Collateral artery growth (arteriogenesis) after experimental arterial occlusion is impaired in mice lacking CC-chemokine receptor-2, *Circ Res*, **94**: 671-677

Helisch A, Wagner S, Khan N, Drinane M, Wolfram S, Heil M, Ziegelhoeffer T, Brandt U, Pearlman JD, Swartz HM, Schaper W. 2006, Impact of mouse strain differences in innate hindlimb collateral vasculature, *Arterioscler Thromb Vasc Biol*, **26**: 520-526

Holbrook TL, Anderson JP, Sieber WJ, Browner D, Hoyt DB. 1999, Outcome after major trauma: 12-month and 18-month follow-up results from the Trauma Recovery Project, *J Trauma*, **46**: 765-771; discussion 771-763

Hukkanen M, Konttinen YT, Santavirta S, Nordsletten L, Madsen JE, Almaas R, Oestreicher AB, Rootwelt T, Polak JM. 1995, Effect of sciatic nerve section on neural ingrowth into the rat tibial fracture callus, *Clin Orthop Relat Res*, **311**: 247-257

Hukkanen M, Konttinen YT, Santavirta S, Paavolainen P, Gu XH, Terenghi G, Polak JM. 1993, Rapid proliferation of calcitonin gene-related peptide-immunoreactive nerves during healing of rat tibial fracture suggests neural involvement in bone growth and remodelling, *Neuroscience*, **54**: 969-979

Hunter J (1794). A Treatise on the Blood, Inflammation, and Gun-Shot Wounds. London, G. Nicol.

Hurrell DJ. 1937, The Nerve Supply of Bone, *J Anat*, **72**: 54-61

Ikeda K, Souma Y, Akakabe Y, Kitamura Y, Matsuo K, Shimoda Y, Ueyama T, Matoba S, Yamada H, Okigaki M, Matsubara H. 2012, Macrophages play a unique role in the plaque calcification by enhancing the osteogenic signals exerted by vascular smooth muscle cells, *Biochemical and biophysical research communications*, **425**: 39-44

Imai S, Matsusue Y. 2002, Neuronal regulation of bone metabolism and anabolism: calcitonin gene-related peptide-, substance P-, and tyrosine hydroxylase-containing nerves and the bone, *Microsc Res Tech*, **58**: 61-69

Isner JM. 2000, Tissue responses to ischemia: local and remote responses for preserving perfusion of ischemic muscle, *J Clin Invest*, **106**: 615-619

Ito WD, Arras M, Scholz D, Winkler B, Htun P, Schaper W. 1997, Angiogenesis but not collateral growth is associated with ischemia after femoral artery occlusion, *Am J Physiol*, **273**: H1255-1265

Ito WD, Arras M, Winkler B, Scholz D, Schaper J, Schaper W. 1997, Monocyte chemotactic protein-1 increases collateral and peripheral conductance after femoral artery occlusion, *Circ Res*, **80**: 829-837

Jacobsen KA, Al-Aql ZS, Wan C, Fitch JL, Stapleton SN, Mason ZD, Cole RM, Gilbert SR, Clemens TL, Morgan EF, Einhorn TA, Gerstenfeld LC. 2008, Bone formation during distraction osteogenesis is dependent on both VEGFR1 and VEGFR2 signaling, *J Bone Miner Res*, **23**: 596-609

Kalajzic Z, Li H, Wang LP, Jiang X, Lamothe K, Adams DJ, Aguila HL, Rowe DW, Kalajzic I. 2008, Use of an alpha-smooth muscle actin GFP reporter to identify an osteoprogenitor population, *Bone*, **43**: 501-510

Kanczler JM, Oreffo RO. 2008, Osteogenesis and angiogenesis: the potential for engineering bone, *European cells & materials*, **15**: 100-114

Kase T, Skjeldal S, Nordsletten L, Reikeras O. 1998, Healing of tibial fractures is not impaired after acute hindlimb ischemia in rats, *Arch Orthop Trauma Surg*, **117**: 273-276

Kempen DH, Creemers LB, Alblas J, Lu L, Verbout AJ, Yaszemski MJ, Dhert WJ. 2010, Growth factor interactions in bone regeneration, *Tissue Eng Part B Rev*, **16**: 551-566

Kempen DH, Lu L, Heijink A, Hefferan TE, Creemers LB, Maran A, Yaszemski MJ, Dhert WJ. 2009, Effect of local sequential VEGF and BMP-2 delivery on ectopic and orthotopic bone regeneration, *Biomaterials*, **30**: 2816-2825

Kim KL, Shin IS, Kim JM, Choi JH, Byun J, Jeon ES, Suh W, Kim DK. 2006, Interaction between Tie receptors modulates angiogenic activity of angiopoietin2 in endothelial progenitor cells, *Cardiovascular research*, **72**: 394-402

Kim YT, Haftel VK, Kumar S, Bellamkonda RV. 2008, The role of aligned polymer fiber-based constructs in the bridging of long peripheral nerve gaps, *Biomaterials*, **29**: 3117-3127

Kinner B, Gerstenfeld LC, Einhorn TA, Spector M. 2002, Expression of smooth muscle actin in connective tissue cells participating in fracture healing in a murine model, *Bone*, **30**: 738-745

Kolambkar YM, Boerckel JD, Dupont KM, Bajin M, Huebsch N, Mooney DJ, Hutmacher DW, Guldberg RE. 2011, Spatiotemporal delivery of bone morphogenetic protein enhances functional repair of segmental bone defects, *Bone*, **49**: 485-492

Kolambkar YM, Dupont KM, Boerckel JD, Huebsch N, Mooney DJ, Hutmacher DW, Guldberg RE. 2011, An alginate-based hybrid system for growth factor delivery in the functional repair of large bone defects, *Biomaterials*, **32**: 65-74

Kolar P, Schmidt-Bleek K, Schell H, Gaber T, Toben D, Schmidmaier G, Perka C, Buttgereit F, Duda GN. 2010, The early fracture hematoma and its potential role in fracture healing, *Tissue Eng Part B Rev*, **16**: 427-434

Kondo H, Nifuji A, Takeda S, Ezura Y, Rittling SR, Denhardt DT, Nakashima K, Karsenty G, Noda M. 2005, Unloading induces osteoblastic cell suppression and osteoclastic cell activation to lead to bone loss via sympathetic nervous system, *J Biol Chem*, **280**: 30192-30200

Koopmans GC, Deumens R, Honig WM, Hamers FP, Steinbusch HW, Joosten EA. 2005, The assessment of locomotor function in spinal cord injured rats: the importance of objective analysis of coordination, *J Neurotrauma*, **22**: 214-225

Kronenberg HM. 2003, Developmental regulation of the growth plate, *Nature*, **423**: 332-336

Kushwaha VP, Garland DG. 1998, Extremity fractures in the patient with a traumatic brain injury, *J Am Acad Orthop Surg*, **6**: 298-307

la Sala A, Pontecorvo L, Agresta A, Rosano G, Stabile E. 2012, Regulation of collateral blood vessel development by the innate and adaptive immune system, *Trends Mol Med*, **18**: 494-501

Langenfeld EM, Langenfeld J. 2004, Bone morphogenetic protein-2 stimulates angiogenesis in developing tumors, *Molecular cancer research : MCR*, **2**: 141-149

Le AX, Miclau T, Hu D, Helms JA. 2001, Molecular aspects of healing in stabilized and non-stabilized fractures, *J Orthop Res*, **19**: 78-84

Lee CW, Stabile E, Kinnaird T, Shou M, Devaney JM, Epstein SE, Burnett MS. 2004, Temporal patterns of gene expression after acute hindlimb ischemia in mice: insights into the genomic program for collateral vessel development, *Journal of the American College of Cardiology*, **43**: 474-482

Levy AP, Levy NS, Wegner S, Goldberg MA. 1995, Transcriptional regulation of the rat vascular endothelial growth factor gene by hypoxia, *J Biol Chem*, **270**: 13333-13340

Li J, Ahmad T, Spetea M, Ahmed M, Kreicbergs A. 2001, Bone reinnervation after fracture: a study in the rat, *J Bone Miner Res*, **16**: 1505-1510

Lienau J, Schell H, Duda GN, Seebeck P, Muchow S, Bail HJ. 2005, Initial vascularization and tissue differentiation are influenced by fixation stability, *J Orthop Res*, **23**: 639-645

Lienau J, Schmidt-Bleek K, Peters A, Haschke F, Duda GN, Perka C, Bail HJ, Schutze N, Jakob F, Schell H. 2009, Differential regulation of blood vessel formation between standard and delayed bone healing, *J Orthop Res*, **27**: 1133-1140

Long H, Ahmed M, Ackermann P, Stark A, Li J. 2010, Neuropeptide Y innervation during fracture healing and remodeling. A study of angulated tibial fractures in the rat, *Acta orthopaedica*, **81**: 639-646

Lu C, Miclau T, Hu D, Marcucio RS. 2007, Ischemia leads to delayed union during fracture healing: a mouse model, *J Orthop Res*, **25**: 51-61

Lu C, Xing Z, Yu YY, Colnot C, Miclau T, Marcucio RS. 2010, Recombinant human bone morphogenetic protein-7 enhances fracture healing in an ischemic environment, *J Orthop Res*, **28**: 687-696

Luo F, Wariaro D, Lundberg G, Blegen H, Wahlberg E. 2002, Vascular growth factor expression in a rat model of severe limb ischemia, *J Surg Res*, **108**: 258-267

Lyle AN, Joseph G, Fan AE, Weiss D, Landazuri N, Taylor WR. 2012, Reactive oxygen species regulate osteopontin expression in a murine model of postischemic neovascularization, *Arterioscler Thromb Vasc Biol*, **32**: 1383-1391

Mach DB, Rogers SD, Sabino MC, Luger NM, Schwei MJ, Pomonis JD, Keyser CP, Clohisy DR, Adams DJ, O'Leary P, Mantyh PW. 2002, Origins of skeletal pain: sensory and sympathetic innervation of the mouse femur, *Neuroscience*, **113**: 155-166

MacKenzie EJ, Bosse MJ, Pollak AN, Webb LX, Swiontkowski MF, Kellam JF, Smith DG, Sanders RW, Jones AL, Starr AJ, McAndrew MP, Patterson BM, Burgess AR, Castillo RC. 2005, Long-term persistence of disability following severe lower-limb trauma. Results of a seven-year follow-up, *J Bone Joint Surg Am*, **87**: 1801-1809

MacKenzie EJ, Jones AS, Bosse MJ, Castillo RC, Pollak AN, Webb LX, Swiontkowski MF, Kellam JF, Smith DG, Sanders RW, Jones AL, Starr AJ, McAndrew MP, Patterson BM, Burgess AR. 2007, Health-care costs associated with amputation or reconstruction of a limb-threatening injury, *J Bone Joint Surg Am*, **89**: 1685-1692

Mackinnon SE, Dellon AL, O'Brien JP. 1991, Changes in nerve fiber numbers distal to a nerve repair in the rat sciatic nerve model, *Muscle Nerve*, **14**: 1116-1122

Madsen JE, Hukkanen M, Aune AK, Basran I, Moller JF, Polak JM, Nordsletten L. 1998, Fracture healing and callus innervation after peripheral nerve resection in rats, *Clin Orthop Relat Res*, **351**: 230-240

Marie PJ. 2003, Fibroblast growth factor signaling controlling osteoblast differentiation, *Gene*, **316**: 23-32

Masi L. 2012, Crosstalk between the brain and bone, *Clinical cases in mineral and bone metabolism : the official journal of the Italian Society of Osteoporosis, Mineral Metabolism, and Skeletal Diseases*, **9**: 13-16

Masini BD, Waterman SM, Wenke JC, Owens BD, Hsu JR, Ficke JR. 2009, Resource utilization and disability outcome assessment of combat casualties from Operation Iraqi Freedom and Operation Enduring Freedom, *J Orthop Trauma*, **23**: 261-266

Matsubara H, Hogan DE, Morgan EF, Mortlock DP, Einhorn TA, Gerstenfeld LC. 2012, Vascular tissues are a primary source of BMP2 expression during bone formation induced by distraction osteogenesis, *Bone*, **51**: 168-180

Matsumoto T, Kuroda R, Mifune Y, Kawamoto A, Shoji T, Miwa M, Asahara T, Kurosaka M. 2008, Circulating endothelial/skeletal progenitor cells for bone regeneration and healing, *Bone*, **43**: 434-439

Mehta M, Schmidt-Bleek K, Duda GN, Mooney DJ. 2012, Biomaterial delivery of morphogens to mimic the natural healing cascade in bone, *Advanced drug delivery reviews*, **64**: 1257-1276

Midrio M, Corsi A, Granata AL. 1968, Early effects of nerve section on the blood flow of skeletal muscle, *Am J Physiol*, **214**: 287-293

Miller DL, Ortega S, Bashayan O, Basch R, Basilico C. 2000, Compensation by fibroblast growth factor 1 (FGF1) does not account for the mild phenotypic defects observed in FGF2 null mice, *Mol Cell Biol*, **20**: 2260-2268

Miller JD, McCreadie BR, Alford AI, Hankenson KD, Goldstein SA (2007). Form and Function of Bone. Orthopaedic Basic Science: Foundations of Clinical Practice. T. A. Einhorn, R. J. O'Keefe and J. A. Buckwalter. Rosemont, IL, American Academy of Orthopaedic Surgeons**:** 129-159.

Mizuno K, Mineo K, Tachibana T, Sumi M, Matsubara T, Hirohata K. 1990, The osteogenetic potential of fracture haematoma. Subperiosteal and intramuscular transplantation of the haematoma, *Journal of Bone and Joint Surgery-British Volume*, **72**: 822-829

Mokarram N, Merchant A, Mukhatyar V, Patel G, Bellamkonda RV. 2012, Effect of modulating macrophage phenotype on peripheral nerve repair, *Biomaterials*, **33**: 8793-8801

Morgan EF, Hussein AI, Al-Awadhi BA, Hogan DE, Matsubara H, Al-Alq Z, Fitch J, Andre B, Hosur K, Gerstenfeld LC. 2012, Vascular development during distraction osteogenesis proceeds by sequential intramuscular arteriogenesis followed by intraosteal angiogenesis, *Bone*, **51**: 535-545

Morley J, Marsh S, Drakoulakis E, Pape HC, Giannoudis PV. 2005, Does traumatic brain injury result in accelerated fracture healing?, *Injury*, **36**: 363-368

Mountziaris PM, Mikos AG. 2008, Modulation of the inflammatory response for enhanced bone tissue regeneration, *Tissue Eng Part B Rev*, **14**: 179-186

Muschler GF, Nakamoto C, Griffith LG. 2004, Engineering principles of clinical cell-based tissue engineering, *J Bone Joint Surg Am*, **86-A**: 1541-1558

Nacu E, Tanaka EM. 2011, Limb regeneration: a new development?, *Annu Rev Cell Dev Biol*, **27**: 409-440

Nagao M, Feinstein TN, Ezura Y, Hayata T, Notomi T, Saita Y, Hanyu R, Hemmi H, Izu Y, Takeda S, Wang K, Rittling S, Nakamoto T, Kaneko K, Kurosawa H, Karsenty G, Denhardt DT, Vilardaga JP, Noda M. 2011, Sympathetic control of bone mass regulated by osteopontin, *Proc Natl Acad Sci U S A*, **108**: 17767-17772

Nauth A, McKee MD, Einhorn TA, Watson JT, Li R, Schemitsch EH. 2011, Managing bone defects, *J Orthop Trauma*, **25**: 462-466

Niikura T, Hak DJ, Reddi AH. 2006, Global gene profiling reveals a downregulation of BMP gene expression in experimental atrophic nonunions compared to standard healing fractures, *J Orthop Res*, **24**: 1463-1471

Nordsletten L, Madsen JE, Almaas R, Rootwelt T, Halse J, Konttinen YT, Hukkanen M, Santavirta S. 1994, The neuronal regulation of fracture healing. Effects of sciatic nerve resection in rat tibia, *Acta Orthop Scand*, **65**: 299-304

O'Brien ER, Garvin MR, Stewart DK, Hinohara T, Simpson JB, Schwartz SM, Giachelli CM. 1994, Osteopontin is synthesized by macrophage, smooth muscle, and endothelial cells in primary and restenotic human coronary atherosclerotic plaques, *Arteriosclerosis and thrombosis : a journal of vascular biology / American Heart Association*, **14**: 1648-1656

Oest ME, Dupont KM, Kong HJ, Mooney DJ, Guldberg RE. 2007, Quantitative assessment of scaffold and growth factor-mediated repair of critically sized bone defects, *J Orthop Res*, **25**: 941-950

Owens BD, Kragh JF, Jr., Macaitis J, Svoboda SJ, Wenke JC. 2007, Characterization of extremity wounds in Operation Iraqi Freedom and Operation Enduring Freedom, *J Orthop Trauma*, **21**: 254-257

Owens BD, Kragh JF, Jr., Wenke JC, Macaitis J, Wade CE, Holcomb JB. 2008, Combat wounds in operation Iraqi Freedom and operation Enduring Freedom, *J Trauma*, **64**: 295-299

Pape HC, Marcucio R, Humphrey C, Colnot C, Knobe M, Harvey EJ. 2010, Trauma-induced inflammation and fracture healing, *J Orthop Trauma*, **24**: 522-525

Peng H, Wright V, Usas A, Gearhart B, Shen HC, Cummins J, Huard J. 2002, Synergistic enhancement of bone formation and healing by stem cell-expressed VEGF and bone morphogenetic protein-4, *J Clin Invest*, **110**: 751-759

Perkins R, Skirving AP. 1987, Callus formation and the rate of healing of femoral fractures in patients with head injuries, *Journal of Bone and Joint Surgery-British Volume*, **69**: 521-524

Rensen SS, Doevendans PA, van Eys GJ. 2007, Regulation and characteristics of vascular smooth muscle cell phenotypic diversity, *Netherlands heart journal : monthly journal of the Netherlands Society of Cardiology and the Netherlands Heart Foundation*, **15**: 100-108

Richter M, Pape HC, Otte D, Krettek C. 2005, Improvements in passive car safety led to decreased injury severity--a comparison between the 1970s and 1990s, *Injury*, **36**: 484-488

Robling AG, Castillo AB, Turner CH. 2006, Biomechanical and molecular regulation of bone remodeling, *Annu Rev Biomed Eng*, **8**: 455-498

Rushton WA. 1951, A theory of the effects of fibre size in medullated nerve, *J Physiol*, **115**: 101-122

Sample SJ, Behan M, Smith L, Oldenhoff WE, Markel MD, Kalscheur VL, Hao Z, Miletic V, Muir P. 2008, Functional adaptation to loading of a single bone is neuronally regulated and involves multiple bones, *J Bone Miner Res*, **23**: 1372-1381

Santavirta S, Konttinen YT, Nordstrom D, Makela A, Sorsa T, Hukkanen M, Rokkanen P. 1992, Immunologic studies of nonunited fractures, *Acta Orthop Scand*, **63**: 579-586

Schaper W, Scholz D. 2003, Factors regulating arteriogenesis, *Arterioscler Thromb Vasc Biol*, **23**: 1143-1151

Schindeler A, McDonald MM, Bokko P, Little DG. 2008, Bone remodeling during fracture repair: The cellular picture, *Seminars in cell & developmental biology*, **19**: 459-466

Schipani E, Maes C, Carmeliet G, Semenza GL. 2009, Regulation of osteogenesis-angiogenesis coupling by HIFs and VEGF, *J Bone Miner Res*, **24**: 1347-1353

Scholz D, Ito W, Fleming I, Deindl E, Sauer A, Wiesnet M, Busse R, Schaper J, Schaper W. 2000, Ultrastructure and molecular histology of rabbit hind-limb collateral artery growth (arteriogenesis), *Virchows Archiv : an international journal of pathology*, **436**: 257-270

Scholz D, Ziegelhoeffer T, Helisch A, Wagner S, Friedrich C, Podzuweit T, Schaper W. 2002, Contribution of arteriogenesis and angiogenesis to postocclusive hindlimb perfusion in mice, *Journal of molecular and cellular cardiology*, **34**: 775-787

Seifert FC, Banker M, Lane B, Bagge U, Anagnostopoulos CE. 1985, An evaluation of resting arterial ischemia models in the rat hind limb, *The Journal of cardiovascular surgery*, **26**: 502-508

Serre CM, Farlay D, Delmas PD, Chenu C. 1999, Evidence for a dense and intimate innervation of the bone tissue, including glutamate-containing fibers, *Bone*, **25**: 623-629

Shen X, Wan C, Ramaswamy G, Mavalli M, Wang Y, Duvall CL, Deng LF, Guldberg RE, Eberhart A, Clemens TL, Gilbert SR. 2009, Prolyl hydroxylase inhibitors increase neoangiogenesis and callus formation following femur fracture in mice, *J Orthop Res*, **27**: 1298-1305

Sherman MS. 1963, The Nerves of Bone, *Journal of Bone and Joint Surgery-American Volume*, **45**: 522-528

Shi YC, Baldock PA. 2012, Central and peripheral mechanisms of the NPY system in the regulation of bone and adipose tissue, *Bone*, **50**: 430-436

Shim SS, Copp DH, Patterson FP. 1966, Bone blood flow in the limb following complete sciatic nerve section, *Surg Gynecol Obstet*, **123**: 333-335

Siemionow M, Andreasen T, Chick L, Lister G. 1994, Effect of muscle flap denervation on flow hemodynamics: a new model for chronic in vivo studies, *Microsurgery*, **15**: 891-894

Smadja DM, Bieche I, Silvestre JS, Germain S, Cornet A, Laurendeau I, Duong-Van-Huyen JP, Emmerich J, Vidaud M, Aiach M, Gaussem P. 2008, Bone morphogenetic proteins 2 and 4 are selectively expressed by late outgrowth endothelial progenitor cells and promote neoangiogenesis, *Arterioscler Thromb Vasc Biol*, **28**: 2137-2143

Spencer GJ, Hitchcock IS, Genever PG. 2004, Emerging neuroskeletal signalling pathways: a review, *FEBS Lett*, **559**: 6-12

Spencer RF. 1987, The effect of head injury on fracture healing. A quantitative assessment, *Journal of Bone and Joint Surgery-British Volume*, **69**: 525-528

Spyridopoulos I, Luedemann C, Chen D, Kearney M, Murohara T, Principe N, Isner JM, Losordo DW. 2002, Divergence of angiogenic and vascular permeability signaling by VEGF: inhibition of protein kinase C suppresses VEGF-induced angiogenesis, but promotes VEGF-induced, NO-dependent vascular permeability, *Arterioscler Thromb Vasc Biol*, **22**: 901-906

Stewart R, Goldstein J, Eberhardt A, Chu GT, Gilbert S. 2011, Increasing vascularity to improve healing of a segmental defect of the rat femur, *J Orthop Trauma*, **25**: 472-476

Street J, Bao M, deGuzman L, Bunting S, Peale FV, Jr., Ferrara N, Steinmetz H, Hoeffel J, Cleland JL, Daugherty A, van Bruggen N, Redmond HP, Carano RA, Filvaroff EH. 2002, Vascular endothelial growth factor stimulates bone repair by promoting angiogenesis and bone turnover, *Proc Natl Acad Sci U S A*, **99**: 9656-9661

Street J, Winter D, Wang JH, Wakai A, McGuinness A, Redmond HP. 2000, Is human fracture hematoma inherently angiogenic?, *Clin Orthop Relat Res*: 224-237

Sullivan CJ, Doetschman T, Hoying JB. 2002, Targeted disruption of the Fgf2 gene does not affect vascular growth in the mouse ischemic hindlimb, *Journal of applied physiology*, **93**: 2009-2017

Takeda Y, Costa S, Delamarre E, Roncal C, Leite de Oliveira R, Squadrito ML, Finisguerra V, Deschoemaeker S, Bruyere F, Wenes M, Hamm A, Serneels J,

Magat J, Bhattacharyya T, Anisimov A, Jordan BF, Alitalo K, Maxwell P, Gallez B, Zhuang ZW, Saito Y, Simons M, De Palma M, Mazzone M. 2011, Macrophage skewing by Phd2 haplodeficiency prevents ischaemia by inducing arteriogenesis, *Nature*, **479**: 122-126

Takeshita S, Zheng LP, Brogi E, Kearney M, Pu LQ, Bunting S, Ferrara N, Symes JF, Isner JM. 1994, Therapeutic angiogenesis. A single intraarterial bolus of vascular endothelial growth factor augments revascularization in a rabbit ischemic hind limb model, *J Clin Invest*, **93**: 662-670

Towler DA. 2007, Vascular biology and bone formation: hints from HIF, *J Clin Invest*, **117**: 1477-1480

Tressel SL, Kim H, Ni CW, Chang K, Velasquez-Castano JC, Taylor WR, Yoon YS, Jo H. 2008, Angiopoietin-2 stimulates blood flow recovery after femoral artery occlusion by inducing inflammation and arteriogenesis, *Arterioscler Thromb Vasc Biol*, **28**: 1989-1995

Trion A, van der Laarse A. 2004, Vascular smooth muscle cells and calcification in atherosclerosis, *American heart journal*, **147**: 808-814

Trueta J. 1963, The Role of the Vessels in Osteogenesis, *Journal of Bone and Joint Surgery-British Volume*, **45**: 402-418

Tsuji K, Bandyopadhyay A, Harfe BD, Cox K, Kakar S, Gerstenfeld L, Einhorn T, Tabin CJ, Rosen V. 2006, BMP2 activity, although dispensable for bone formation, is required for the initiation of fracture healing, *Nature genetics*, **38**: 1424-1429

Uhrig BA, Boerckel JD, Willett NJ, Li MT, Huebsch N, Guldberg RE. 2013, Recovery from hind limb ischemia enhances rhBMP-2-mediated segmental bone defect repair in a rat composite injury model, *Bone*,

Urist MR. 1965, Bone: formation by autoinduction, *Science*, **150**: 893-899

Ushiku C, Adams DJ, Jiang X, Wang L, Rowe DW. 2010, Long bone fracture repair in mice harboring GFP reporters for cells within the osteoblastic lineage, *J Orthop Res*, **28**: 1338-1347

Vandeputte C, Taymans JM, Casteels C, Coun F, Ni Y, Van Laere K, Baekelandt V. 2010, Automated quantitative gait analysis in animal models of movement disorders, *BMC Neurosci*, **11**: 92

Vogelaar CF, Vrinten DH, Hoekman MF, Brakkee JH, Burbach JP, Hamers FP. 2004, Sciatic nerve regeneration in mice and rats: recovery of sensory innervation is followed by a slowly retreating neuropathic pain-like syndrome, *Brain Res*, **1027**: 67-72

Wallace AL, Draper ER, Strachan RK, McCarthy ID, Hughes SP. 1994, The vascular response to fracture micromovement, *Clin Orthop Relat Res*: 281-290

Wan C, Gilbert SR, Wang Y, Cao X, Shen X, Ramaswamy G, Jacobsen KA, Alaql ZS, Eberhardt AW, Gerstenfeld LC, Einhorn TA, Deng L, Clemens TL. 2008, Activation of the hypoxia-inducible factor-1alpha pathway accelerates bone regeneration, *Proc Natl Acad Sci U S A*, **105**: 686-691

Wang Y, Neumann M, Hansen K, Hong SM, Kim S, Noble-Haeusslein LJ, Liu J. 2011, Fluoxetine increases hippocampal neurogenesis and induces epigenetic factors but does not improve functional recovery after traumatic brain injury, *J Neurotrauma*, **28**: 259-268

Wang Y, Wan C, Deng L, Liu X, Cao X, Gilbert SR, Bouxsein ML, Faugere MC, Guldberg RE, Gerstenfeld LC, Haase VH, Johnson RS, Schipani E, Clemens TL. 2007, The hypoxia-inducible factor alpha pathway couples angiogenesis to osteogenesis during skeletal development, *J Clin Invest*, **117**: 1616-1626

Whiteside GT, Boulet JM, Sellers R, Bunton TE, Walker K. 2006, Neuropathy-induced osteopenia in rats is not due to a reduction in weight born on the affected limb, *Bone*, **38**: 387-393

Willett NJ, Li MT, Uhrig BA, Boerckel JD, Huebsch N, Lundgren TL, Warren GL, Guldberg RE. 2012, Attenuated Human Bone Morphogenetic Protein-2-Mediated Bone Regeneration in a Rat Model of Composite Bone and Muscle Injury, *Tissue engineering. Part C, Methods*,

Wu S, Wu X, Zhu W, Cai WJ, Schaper J, Schaper W. 2010, Immunohistochemical study of the growth factors, aFGF, bFGF, PDGF-AB, VEGF-A and its receptor (Flk-1) during arteriogenesis, *Molecular and cellular biochemistry*, **343**: 223-229

Xing Z, Lu C, Hu D, Yu YY, Wang X, Colnot C, Nakamura M, Wu Y, Miclau T, Marcucio RS. 2010, Multiple roles for CCR2 during fracture healing, *Disease models & mechanisms*, **3**: 451-458

Yazar S, Lin CH, Wei FC. 2004, One-stage reconstruction of composite bone and soft-tissue defects in traumatic lower extremities, *Plast Reconstr Surg*, **114**: 1457-1466

Yu YY, Lieu S, Lu C, Colnot C. 2010, Bone morphogenetic protein 2 stimulates endochondral ossification by regulating periosteal cell fate during bone repair, *Bone*, **47**: 65-73

Zhang F, Qiu T, Wu X, Wan C, Shi W, Wang Y, Chen JG, Wan M, Clemens TL, Cao X. 2009, Sustained BMP signaling in osteoblasts stimulates bone formation by promoting angiogenesis and osteoblast differentiation, *J Bone Miner Res*, **24**: 1224-1233